letnik/volume **52** - št./no. **12/06** - str./pp. **783-886**
Ljubljana, dec./Dec. 2006, zvezek/issue **500**

STROJNIŠKI VESTNIK
JOURNAL OF MECHANICAL ENGINEERING

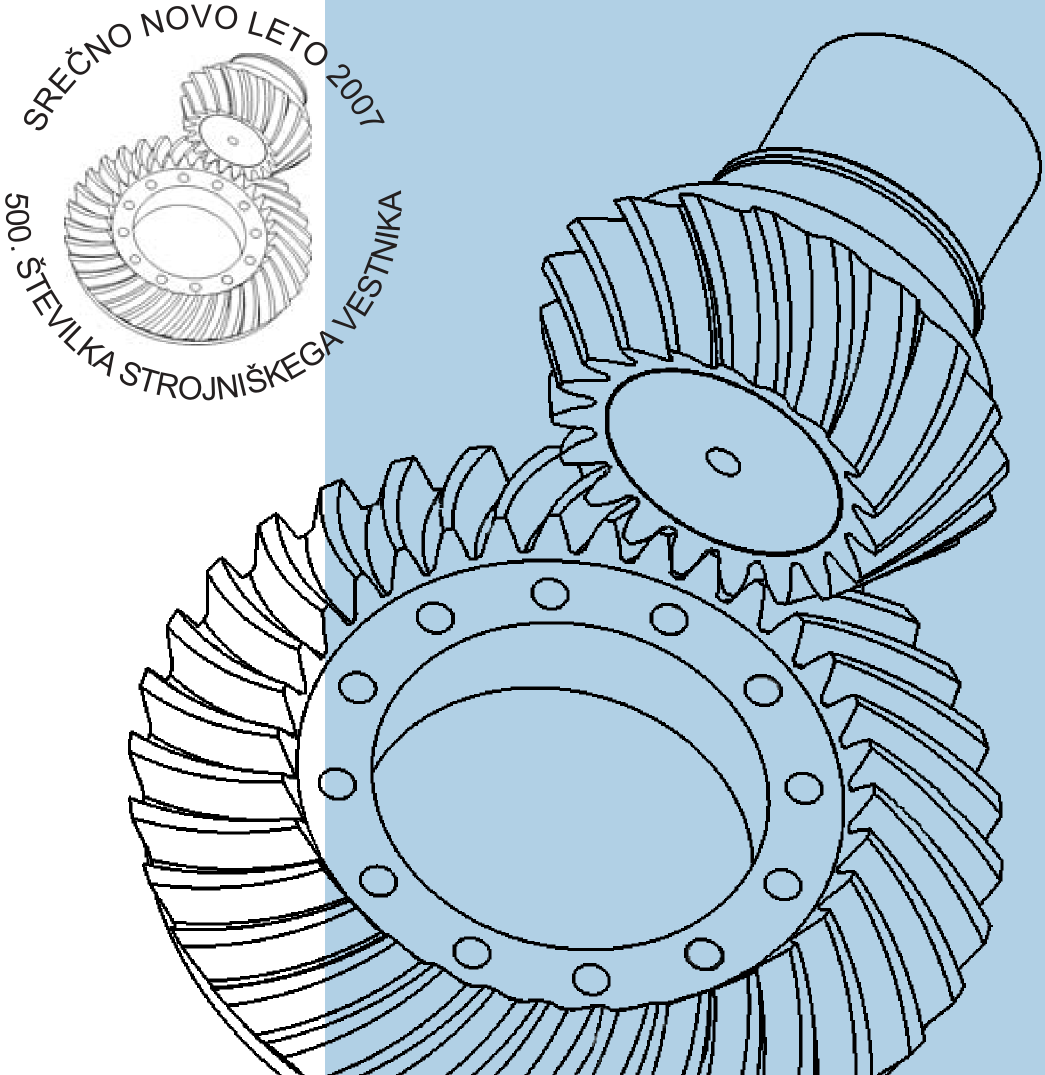

cena 800 SIT

ISSN 0039-2480

Vsebina - Contents

Strojniški vestnik - Journal of Mechanical Engineering
letnik - volume 52, (2006), številka - number 12
Ljubljana, december - December 2006
ISSN 0039-2480

Izhaja mesečno - Published monthly

Uvodnik - Editorial

500. številka (zvezek) Strojniškega vestnika - 500th issue of the Journal of Mechanical Engineering

Kmalu bo minilo 52 let od izida 1. številke Strojniškega vestnika, kar smo proslavili 24.3.2005. Najprej je izhajal 4-krat na leto, kasneje 6-krat na leto in sedaj 1-krat mesečno. Poletna številka je iz praktičnih vzrokov dvojna. Tako se je nabralo 500 številk (zvezkov) Strojniškega vestnika. V zadnjih nekaj letih so tri tematske izdaje (energetika, konstrukterstvo, tehnologija) in preostale, ki so mešane, saj avtorjev po končani presoji (doma in v tujini) ne želimo pustiti predolgo čakati. Ker je tujih avtorjev vedno več, je Izdajateljski svet sklenil, da znanstvene prispevke tujih avtorjev lahko tiskamo samo v angleškem jeziku (s slovenskim povzetkom).

Pomemben dejavnik izhajanja Strojniškega vestnika je denarna pomoč Javne agencije za raziskovalno dejavnost Republike Slovenije, ki nam je za naslednja leta (2006 do 2008) odobrila približno polovico potrebnih sredstev. Preostalo zbiramo iz prispevkov tematskih številk, vedno bolj redkih oglasov, naročnin ter pokrivanja primanjkljaja s strani izdajateljev (predvsem obeh fakultet).

V naslednjem letu čaka slovensko strojništvo izvedba Bolonjske prenove univerzitetnih učnih programov. Uredništvo Strojniškega vestnika pričakuje od vodstev obeh Fakultet za strojništvo v Ljubljani in Mariboru, da po odobritvi novih učnih programov na Svetu za visoko šolstvo Slovenije z objavo teh programov ovrže dvome, da gre le za preobleko dosedanjih učnih programov v nove kalupe, temveč za nov in drugačen način izobraževanja.

Urednik
prof.dr. Andro Alujevič

Very soon it will be 52 years since the first issue of the Journal of Mechanical Engineering was published, an event we already celebrated on 24 March 2005. The journal was originally published 4 times a year, later this was increased to 6 times a year, and now the journal is published every month; although for practical reasons a double issue appears in the summer. In total there have been 500 issues. In recent years, three thematic issues - power, design, and technology - have been printed, the remaining issues being composed of mixed papers, thus enabling the publication of papers as soon as possible after an external and internal review procedure. Due to the abundance of foreign papers, the Publishing Council decided to allow the presentation of these papers in English only (with a translated Slovenian summary).

An important contribution to publishing the Journal of Mechanical Engineering is that made by the Slovenian Research Agency. The agency will be providing approximately one half of the required funding for the period 2006 to 2008. The rest of the costs are covered by fees for thematic issues, occasional adverts, subscriptions and contributions from the Founders and Publishers (mainly the two faculties).

In the coming year the national mechanical engineering teaching is to be subject to an assessment based on the Bologna agreement. The Editorial Board of the Journal of Mechanical Engineering expects that the two faculties of mechanical engineering, in Ljubljana and in Maribor, after the approval by the National Higher Education Board, will publish new programmes relating to this new and different way of providing education in Slovenia.

Editor
Prof. Dr. Andro Alujevič

Strojniški vestnik - Journal of Mechanical Engineering 52(2006)12, 785-816
UDK - UDC 624.074.4:539.3/.4
Izvirni znanstveni članek - Original scientific paper (1.01)

Preskok sistema plitve osnosimetrične bimetalne lupine z uporabo nelinearne teorije

Snap-through of the System for a Shallow Axially symmetric Bimetallic Shell using Non-linear Theory

Marko Jakomin[1] - Franc Kosel[2] - Milan Batista[3] - Tadej Kosel[2]
([1]Primorski inštitut za naravoslovne in tehnične vede, Koper; [2]Fakulteta za strojništvo, Ljubljana;
[3]Fakulteta za pomorstvo in promet, Portorož)

V prispevku obravnavamo napetostne, deformacijske in stabilnostne razmere pri tankih, osnosimetričnih plitvih bimetalnih lupinah. Po teoriji drugega reda, ki upošteva ravnotežje sil na deformiranem telesu, podajamo model z matematičnim opisom geometrije sistema, premikov, napetosti in termoelastičnih deformacij. Enačbe temeljijo na teoriji velikih premikov. Kot primer predstavljamo rezultate za krogelne lupine, ki jih aproksimiramo s parabolično funkcijo. Poleg prosto položenih lupin obravnavamo tudi vrtljivo in konzolno vpete lupine ter lupine, ki so poleg segrevanja obremenjene tudi s silo v temenu. Deformacijsko krivuljo in temperaturo preskoka računamo numerično z nelinearno strelsko metodo.

(Ključne besede: lupine bimetalne, obremenitve toplotne, preskok sistema, teorija velikih premikov)

The paper deals with the stresses, strains and buckling conditions in thin, axially symmetric, shallow, bimetallic shells. Based on third-order theory, which takes into account the equilibrium state of the forces and moments that are acting on the deformed system, the paper presents a model with a mathematical description of the geometry of the system, the stresses, the thermoelastic strains and the displacements. The mathematical formulation is based on the theory of large displacements. As an example, the results for spherical, shallow shells are shown, approximated by a parabolic function. Besides simple roller-supported shells, also simple bearing-supported shells and clamped shells are discussed. The shells are loaded with temperature and/or a concentrated load acting at the top. The displacement state and the snap-through temperature are calculated numerically using a non-linear method.

(Keywords: bimetallic shell, thermal loads, stability, snap-through of the system, large displacement theory)

0 UVOD

Pospešen razvoj strojnih znanosti v zadnjih stoletjih je omogočil izdelavo različnih naprav, od razmeroma preprostih mehanizmov pa vse do zelo zapletenih strojnih naprav, ki jih človeštvo uporablja v tehnično tehnološkem postopku preoblikovanja materialnih dobrin. Čeprav so sodobne naprave po obliki, namenu in zgradbi med seboj zelo različne, pa se zaradi pomembnosti nemotenega in zanesljivega delovanja ter njihove vrednosti izraža zahteva po njihovi zaščiti pred različnimi preobremenitvami. Posebej pri strojih, ki spreminjajo eno obliko energije v drugo ter se pri tem segrevajo, je potrebno poskrbeti za zanesljivo zaščito pred toplotno

0 INTRODUCTION

The development of mechanical sciences over the centuries has enabled the production of various devices, from relatively simple devices to very complex mechanical appliances, which are used in the technical-technological process of remodelling the material goods. Although modern devices differ greatly in shape, purpose and structure, they – for the sake of their unobstructed and reliable functioning – all require protection from various forms of overloading. This is particularly so for machines that transform one type of energy into another, warming up during the process, thus requiring real protection against excessive temperature over-loading. For this preobremenitvijo. S tem namenom v naprave vgrajujemo elemente, ki opravljajo funkcijo "toplotne varovalke", tako da stroj izklopijo takoj, ko posamezen del doseže največjo še dopustno temperaturo. Zaradi zanesljivosti delovanja so se pri zaščiti pred toplotno preobremenitvijo uveljavili črtni in ploskovni bimetalni konstrukcijski elementi, katerih delovanje sloni na znanem fizikalnem dejstvu, da se telesa s povečevanjem temperature raztezajo. Idealno homogena telesa se širijo in krčijo izotropno.

V primeru bimetalnih teles, ki so izdelana iz dveh materialov z različnima temperaturnima razteznostnima koeficientoma, pa deformacije zaradi temperaturnih sprememb ne bodo več izotropne. V prispevku želimo poiskati in matematično formulirati funkcijsko zvezo med temperaturo, napetostjo in premiki bimetala. Ta zveza je med drugim odvisna tudi od geometrijskih značilk bimetala, saj se, npr. črtni bimetalni konstrukcijski elementi v primerjavi s ploskovnimi, na temperaturne spremembe različno odzivajo. Za prakso so predvsem pomembne razlike v stabilnostnih razmerah. Plitve bimetalne lupine imajo lastnost, da pri določeni temperaturi pridejo v indiferentno stanje, kar vodi v pojav, ki je v literaturi znan pod pojmom preskok sistema.

1 GEOMETRIJA SISTEMA

Na sliki 1 je predstavljena osrednja ploskev tanke bimetalne vrtilno simetrične lupine. Osnosimetrična oblika lupine nastane z vrtenjem neke funkcije okoli ordinatne osi. Obliko nedeformirane osnosimetrične lupine v Lagrangevem koordinatnem sistemu torej določa funkcija $y = y(x)$.

Zaradi spremembe temperature se lupina deformira v novo obliko, ki jo določa funkcija $Y = Y(X)$ v Eulerjevem koordinatnem sistemu. Tudi ta oblika je osnosimetrična v predpostavljenem homogenem temperaturnem polju, zaradi česar se mehanske veličine v odvisnosti od kota φ ne spreminjajo. Vektor premika $\vec{u}$ v naravnem koordinatnem sistemu (ψ,φ,r_ψ) poljubne točke P na osrednji ploskvi določa točko P'.
Torej:

purpose, elements that function as "heat cut-out" devices are installed, disconnecting the appliance as soon as a particular part reaches the maximum permissible temperature. Because of their reliability in functioning as protection from heat over-loading, linear and plane bimetallic structural elements are often used in these devices. Their working is based on the known physical fact that bodies expand with increasing temperature. Ideally, however, homogeneous objects expand and shrink in an isotropic manner.

In the case of bimetallic bodies, which are made of two materials with different linear expansion coefficients, however, the deformations due to temperature changes will no longer be isotropic. In this paper we try to find and mathematically formulate the functional connection between the temperature, the strain and the displacements of a bimetal. This connection, among other things, also depends on the bimetal's geometrical characteristics as, for instance, the linear bimetallic structural elements in comparison with the plane elements react differently to temperature changes. For practical purposes, above all, the differences in the stability conditions are important. Shallow bimetallic shells have the property that at a certain temperature they change to an indifferent state, which leads to a phenomenon known in the literature as a "snap-through of a system".

1 GEOMETRY OF THE SYSTEM

Fig. 1 shows the flexible, middle plane, of a thin, bimetallic rotationally symmetrical shell. The axially symmetric form of the shell is a result of the rotation of a function around the ordinate axis. The shape of undeformed axially symmetric shells in the Lagrange coordinate system is thus determined by the function $y = y(x)$.

Because of the change in temperature, the shell will deform into new shape, determined by the function $Y = Y(X)$ in the Euler coordinate system. This shape is axially symmetric too, providing that at each point the bimetallic shell is exposed to the same temperature change. The axially symmetric bimetallic shell within a homogeneous temperature field, however, represents an axially symmetric loading example, and because of this the physical magnitudes depending on the angle φ remain unchanged. The displacement of an optional point P on the middle plane of the shell to the point P' is determined by the displacement vector $\vec{u}$ in the natural coordinate system. Therefore:

$$\frac{\partial}{\partial\varphi}(\ ) = 0, \qquad \vec{u}\left(\psi,\varphi,r_\psi\right) = (u,v,w)$$

Ker je problem osnosimetrične narave, $v=0$, lahko tudi pišemo:

The displacement state is axially symmetric, so we can also write:

$$\vec{u}=(u,0,w) \quad (1).$$

Osrednja ploskev lupine je določena z enačbo $r_\psi = r_\psi(\psi)$, zaradi česar je vektor premika $\vec{u}$ funkcija kota ψ: $\vec{u}=\vec{u}(\psi)$. Opazujmo premike na tanki bimetalni osnosimetrični lupini v homogenem temperaturnem polju (sl. 1), ki je v temenu obremenjena s silo $\vec{F}_k$.

Zaradi temperaturne obremenitve se točka P, ki ima na nedeformirani lupini lego $P(x,y(x))$, premakne v lego P' s koordinatama $P'(X,Y(X))$. Premik točke P v točko P' določimo z enačbo (1), ki jo v ravnini (ψ,r_ψ) lahko tudi pišemo $\vec{u}=(u,w)$.

Zveza med Eulerjevim $(X,Y(X))$ in Lagrangevim $(x,y(x))$ koordinatnim sistemom je (sl. 1):

The middle plan is determined by the equation $r\psi = r\psi(\psi)$. Consequently, the displacement vector $\vec{u}$ is the function of angle ψ: $\vec{u}=\vec{u}(\psi)$. Let us observe the displacement state of a thin bimetallic axially symmetric shell in a homogeneous temperature field, Fig. 1, loaded at the top with the force $\vec{F}_k$.

Because of the temperature load, the point $P(x,y(x))$ on the undeformed shell will move to the point $P'(X,Y(X))$. The shifting of point P to the point P' is determined by Equation (1), which in the plane $(\psi,r\psi)$ can also be written as $\vec{u}=(u,w)$.

The relationship between the Euler $(X,Y(X))$ and Lagrange $(x,y(x))$ coordinates is, Fig. 1:

$$\vec{X}=\vec{x}+\vec{u}$$

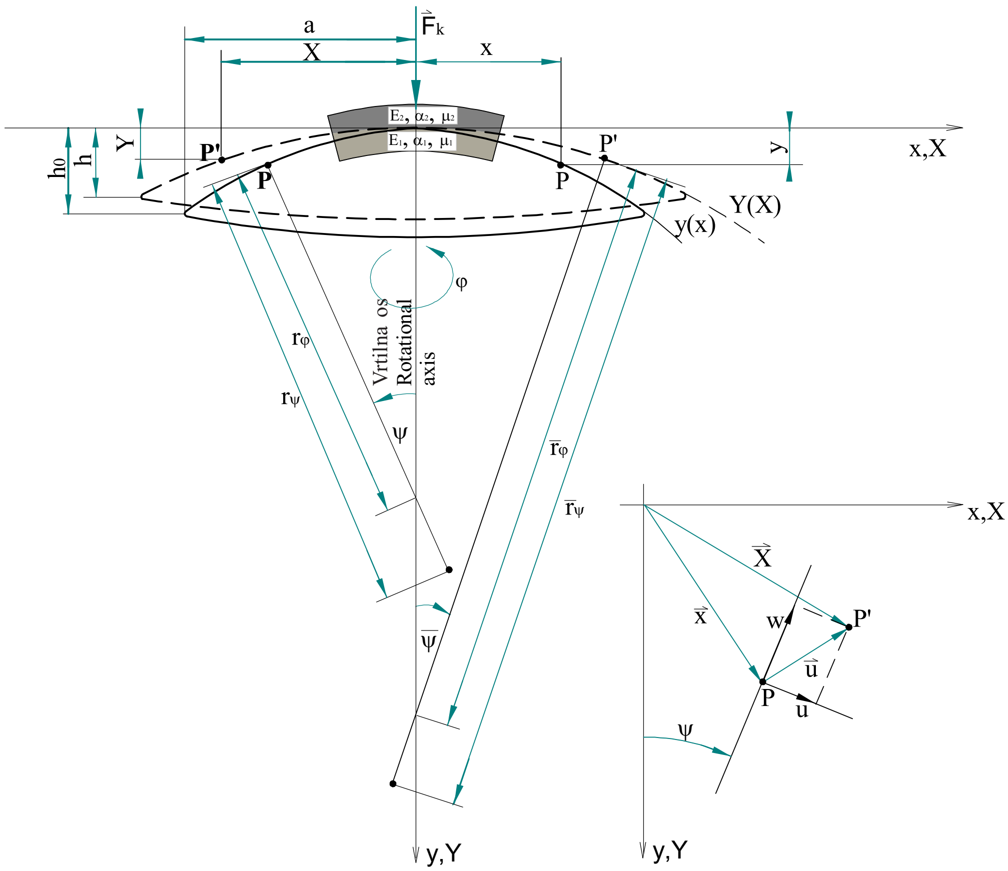

Sl. 1. *Osnosimetrična lupina v homogenem temperaturnem polju in zveza med Eulerjevim in Lagrangevim koordinatnim sistemom*

Fig. 1. *The axi-symmetric shell in the homogeneous temperature field and the connection between Euler and Lagrange coordinate system*

kjer je: / where:

$$\vec{u}(x,y)=\begin{bmatrix}\cos\psi & \sin\psi\\ \sin\psi & -\cos\psi\end{bmatrix}\begin{bmatrix}u\\ w\end{bmatrix}$$

iz česar izhaja: / following that:

$$X=x+w\sin\psi+u\cos\psi \tag{2}$$

$$Y=y-w\cos\psi+u\sin\psi \tag{3}.$$

Nadalje določimo ukrivljenost nedeformirane lupine v meridialni smeri ψ in obročni smeri φ. Infinitezimalno majhen del loka na krivulji je:
V obročni smeri:

The curvature of the undeformed shell in the meridian ψ and circular φ direction is determined. An infinitesimally small part of the arc of the curve in the circular direction is:

$$ds_{\varphi}=r_{\varphi}\cdot\sin\psi\cdot d\varphi=x\cdot d\varphi$$

v meridialni smeri : / and in the meridian direction:

$$ds_{\psi}=r_{\psi}\cdot d\psi$$

Geometrija sistema na sliki 1 določa naslednja razmerja:

The geometry of the system in Fig. 1 leads to the following relations:

$$\psi=\arctan(y') \tag{4}$$

$$k_{\psi}=\frac{1}{r_{\psi}}=\frac{y''}{\sqrt{(1+y'^2)^3}} \tag{5}$$

$$k_{\varphi}=\frac{1}{r_{\varphi}}=\frac{\sin\arctan(y')}{x}=\frac{1}{x}\frac{y'}{\sqrt{1+(y')^2}} \tag{6},$$

kjer je s k_{ψ} in k_{φ} označena ukrivljenost lupine v meridialni oziroma obročni smeri, z eno oziroma dvema črticama pa prvi oziroma drugi odvod po Lagrangevi koordinati x:

where $k\psi$ and $k\varphi$ are the curvatures of the shell in the meridian and circular directions, respectively, while the one and two apostrophes, respectively, mark the first and second derivative with respect to the independent variable x:

$$\frac{d}{dx}(\ )=(\ )',\quad \frac{d^2}{dx^2}(\ )=(\ )''$$

Zaradi deformacije lupine se kot ψ spremeni v kot $\overline{\psi}$, ukrivljenost lupine v meridialni smeri r_{ψ} oziroma obročni smeri r_{φ} smeri pa v $\overline{r}_{\psi}$ oziroma $\overline{r}_{\varphi}$. Veljajo naslednje zveze, določene z geometrijo sistema na sliki 1:

Due to the deformation of a shell the angle ψ changes into the angle $\overline{\psi}$. The curvatures of the deformed shell are $\overline{r}_{\psi}$ and $\overline{r}_{\varphi}$ in the meridian and circular directions, respectively. From the geometry of the system in Fig. 1 the following relations are determined:

$$X=\overline{r}_{\varphi}\sin\overline{\psi},\ \ \dot{Y}=\tan\overline{\psi},\ \ \overline{k}_{\psi}=\frac{1}{\overline{r}_{\psi}}=\frac{\ddot{Y}}{\sqrt{(1+\dot{Y}^2)^3}}$$

$$\overline{k}_{\varphi}=\frac{1}{\overline{r}_{\varphi}}=\frac{\sin\overline{\psi}}{X}=\frac{\sin\arctan\dot{Y}}{X}=\frac{1}{X}\frac{\dot{Y}}{\sqrt{1+(\dot{Y})^2}}$$

Z eno piko oziroma dvema pikama nad koordinato $Y(X)$ sta označena prvi oziroma drugi odvod po Eulerjevi koordinati X:

One and two points above the coordinate $Y(X)$ mark the first and the second derivatives, respectively, with respect to the variable X:

$$\dot{Y}=\frac{dY}{dX}\ \text{in/and}\ \ddot{Y}=\frac{d^2Y}{dX} \tag{7}.$$

Ker je koordinata Y zaradi enačbe (2) posredno funkcija Lagrangeve koordinate x, torej $Y = Y(X) = Y[X(x)]$ izračunamo oba odvoda v enačbah (7) z uporabo t.i. verižnega pravila. Po vstavitvi teh odvodov v enačbo za koordinato X in enačbi za ukrivljenost lupine v deformiranem stanju sledi:

Due to Equation (2) the coordinate Y is indirectly a function of the variable x , i.e., $Y = Y(X) = Y[X(x)]$. The derivatives in Equations (7) can be calculated by means of the so-called Chain Rule. After inserting into the Equation for the coordinate X and the Equations for the curvature of the shell in the undeformed state, it follows:

$$\bar{\psi} = \arctan\left(\frac{Y'}{X'}\right) \tag{8}$$

$$\bar{k}_{\psi} = \frac{1}{\bar{r}_{\psi}} = \frac{\begin{vmatrix} X' & Y' \\ X'' & Y'' \end{vmatrix}}{\sqrt{\left(X'^2 + Y'^2\right)^3}} \tag{9}$$

$$\bar{k}_{\varphi} = \frac{1}{X} \frac{Y'}{\sqrt{\left(X'\right)^2 + \left(Y'\right)^2}} \tag{10}.$$

Diferencial dol□ine $d\bar{s}_{\psi}$ v meridialni smeri deformirane lupine je:

The differential of the length $d\bar{s}_{\psi}$ in the meridian direction of the deformed shell is:

$$d\bar{s}_{\psi} = \sqrt{dX^2 + dY^2} = dx\sqrt{X'^2 + Y'^2} = \bar{r}_{\psi} d\bar{\psi} \tag{11}.$$

2 DOLOČITEV TENZORJEV DEFORMACIJ IN NAPETOSTI TER VEKTORJA PREMIKA

2 DEFINING THE STRAIN AND STRESS TENSORS AS WELL AS THE DISPLACEMENT VECTOR

Deformacijo lupine podamo z elementi vektorja premika na osrednji oziroma primerjalni ploskvi, in sicer s premikom u v meridialni ter s premikom w v prečni smeri. Osrednja ploskev se zaradi upogibnih napetosti ne deformira. Elemente deformacijskega tenzorja v krivočrtnem pravokotnem koordinatnem sistemu določimo po pravilih za spremembo tenzorjev iz enega v drugi koordinatni sistem ali pa z neposredno postavitvijo na podlagi deformiranega stanja elementarnega dela lupine, kjer upoštevamo premike na ukrivljeni ploskvi ([1] do [3]):

The shell's deformation state is shown by the displacement vector in the middle, i.e., the reference plane, and that, by the displacement of u in the meridian, and the displacement of w in the radial direction. Due to bending, the middle plane does not deform. The elements of the strain tensor in the curvilinear orthogonal coordinate system are determined by rules for tensor transformation from one into another coordinate system or by direct forming on the basis of the deformed state of the elementary part of the shell, where displacements on the curved plane are taken into account ([1] to [3]):

$$\varepsilon_r = \frac{\partial w}{\partial z} = 0 \tag{12}$$

$$\varepsilon_{\psi} = \frac{1}{r_{\psi}}\left(w + \frac{\partial u}{\partial \psi}\right) + \frac{1}{2r_{\psi}^2}\left(\frac{\partial w}{\partial \psi} - u\right)^2 = \frac{1}{r_{\psi}}\left(w + \frac{\partial u}{\partial \psi}\right) + \frac{1}{2r_{\psi}^2}\left(\frac{\partial w}{\partial \psi}\right)^2 \tag{13}$$

$$\varepsilon_{\varphi} = \frac{1}{r_{\varphi}}\left(w + \frac{\partial v}{\partial \varphi}\frac{1}{\sin\psi} + \frac{u}{\tan\psi}\right) = \frac{1}{r_{\varphi}}\left(w + \frac{u}{\tan\psi}\right) \tag{14}$$

$$\gamma_{\psi\varphi} = \frac{\partial v}{\partial \psi}\frac{1}{r_{\psi}} + \frac{\partial u}{\partial \varphi}\frac{1}{r_{\varphi}\sin\psi} - \frac{v}{r_{\psi}}\cot\psi = 0 \tag{15}$$

$$\gamma_{\psi r} = \frac{-u}{r_{\psi}} + \frac{\partial u}{\partial r} + \frac{\partial w}{\partial \psi}\frac{1}{r_{\psi}} = \frac{-u}{r_{\psi}} + \frac{\partial w}{\partial \psi}\frac{1}{r_{\psi}} \tag{16}$$

$$\gamma_{\varphi r} = \frac{-v}{r_\varphi} + \frac{\partial v}{\partial r} + \frac{\partial w}{\partial \varphi}\frac{1}{r_\varphi \cdot \sin\psi} = 0 \tag{17}$$

V enačbah od (12) do (17) smo upoštevali predpostavko, da je lupina tanka in osnosimetrična tudi v deformiranem stanju, kakor sledi:

In Equations (12) to (17) we have assumed that the shell is also thin and axially symmetric in the deformed state, as follows:

$$\frac{\partial u}{\partial z} = \frac{\partial w}{\partial z} = 0, \quad \frac{\partial}{\partial \varphi}(\ ) = 0, \quad v = 0 \tag{18}$$

V enačbi (13) smo za pravokotno specifično deformacijo ε_ψ v meridialni smeri upoštevali tudi nelinearni člen. Izkazalo se je namreč, da je upoštevanje nelinearnega člena in s tem teorije velikih premikov nujno za pravilnost rezultatov. Pri tem smo upoštevali, da je v nelinearnem členu komponenta u v primerjavi s komponento w zanemarljivo majhna.

Z uvedbo krajevne koordinate z, z izhodiščem na osrednji ploskvi lupine, so zaradi ukrivljenosti lupine elementi tenzorja specifičnih deformacij tudi funkcija koordinate z:

According to the third-order theory we also take into consideration the non-linear term in for the strain ε_ψ in the meridian direction. Furthermore, we take into account that the displacement u in the non-linear term is negligible compared with the displacement w.

By introducing the local coordinate z with the centre of origin in the middle plane of the shell, the elements of the strain tensor are, due to the shell's curvature, also a function of the coordinate z, as follows:

$$\varepsilon_\psi^z = \frac{\varepsilon_\psi}{1+\frac{z}{r_\psi}} + \frac{z}{1+\frac{z}{r_\psi}}\left(\frac{1}{\bar{r}_\psi} + \frac{\varepsilon_\psi}{\bar{r}_\psi} - \frac{1}{r_\psi}\right) = \varepsilon_\psi + z\left(\frac{1}{\bar{r}_\psi} - \frac{1}{r_\psi}\right) = \varepsilon_\psi + z\cdot\Upsilon_\psi \tag{19}$$

in / and

$$\varepsilon_\varphi^z = \frac{\varepsilon_\varphi}{1+\frac{z}{r_\varphi}} + \frac{z}{1+\frac{z}{r_\varphi}}\left(\frac{1}{\bar{r}_\varphi} + \frac{\varepsilon_\varphi}{\bar{r}_\varphi} - \frac{1}{r_\varphi}\right) = \varepsilon_\varphi + z\left(\frac{1}{\bar{r}_\varphi} - \frac{1}{r_\varphi}\right) = \varepsilon_\varphi + z\cdot\Upsilon_\varphi \tag{20}$$

kjer smo upoštevali, da je pri tankih lupinah:

where it has been taken into account that for thin shells:

$$\frac{z}{r_\psi} \cong \frac{z}{r_\varphi} \cong \frac{\varepsilon_\psi}{r_{\bar{\psi}}} \cong \frac{\varepsilon_\varphi}{r_{\bar{\varphi}}} \cong 0$$

Deformacijski in napetostni tenzor sta:

The stress and strain tensors are:

$$\varepsilon_{ij} = \begin{pmatrix} \varepsilon_\psi^z & 0 & \varepsilon_{\psi r}^z \\ 0 & \varepsilon_\varphi^z & 0 \\ \varepsilon_{\psi r}^z & 0 & 0 \end{pmatrix}, \quad \sigma_{ij} = \begin{pmatrix} \sigma_\psi^z & 0 & \tau_{\psi r}^z \\ 0 & \sigma_\varphi^z & 0 \\ \tau_{\psi r}^z & 0 & 0 \end{pmatrix} \tag{21}$$

kjer je zveza med deformacijskim in napetostnim tenzorjem [3]:

where the relationship between the stress and strain tensors [3] is:

$$\sigma_\psi^z = \frac{E}{1-\mu^2}\left(+\mu\varepsilon_\varphi^z + \varepsilon_\psi^z - (1+\mu)\alpha T\right) \tag{22}$$

$$\sigma_\varphi^z = \frac{E}{1-\mu^2}\left(+\mu\varepsilon_\psi^z + \varepsilon_\varphi^z - (1+\mu)\alpha T\right) \tag{23}$$

$$\tau_{\psi r}^z = G\cdot\gamma_{\psi r}^z \tag{24}$$

Z oznako T je v enačbah (22) in (23) označena sprememba temperature glede na primerjalno temperaturo T_0, pri kateri je napetostno stanje v lupini povsod enako nič:

where T in Equations (22) and (23) denotes the change in temperature with respect to the reference temperature T_0 at which the stress state in the shell is throughout equal to zero:

$$\sigma_\psi^z\left(T_0,\psi,z\right) = \sigma_\varphi^z\left(T_0,\psi,z\right) = \tau_{\psi r}^z\left(T_0,\psi,z\right) = 0$$

3 SILE, MOMENTI IN MEHANSKO RAVNOVESJE

Slika 2 prikazuje elementarno majhen del bimetalne lupine z napetostmi, ki se pojavijo na prereznih ploskvah lupine. Zaradi napetostnega stanja, delujejo na ploskvah elementa *ABCD* sile dN_ψ, dN_φ in d$T_{\psi r}$ ter upogibna momenta dM_ψ in dM_φ:

3 EQUILIBRIUM STATE OF THE FORCES AND MOMENTS

Fig. 2 shows an elementary small part of the bimetallic shell, with stresses that appear on the cross-section of the shell's plane. The forces dN_ψ, dN_φ, dT_ψ and the bending moments dM_ψ, dM_φ on the element *ABCD* planes are:

$$dN_\psi = \int_{-h_1}^{h_2} \sigma_\psi^z \left(\frac{\overline{r}_\varphi + z}{\overline{r}_\varphi}\right) \overline{r}_\varphi \sin\overline{\psi}\cdot dz\cdot d\varphi = n_\psi \cdot \overline{r}_\varphi \sin\overline{\psi}\cdot d\varphi = n_\psi X\cdot d\varphi \tag{25}$$

$$dN_\varphi = \int_{-h_1}^{h_2} \sigma_\varphi^z \left(\frac{\overline{r}_\psi + z}{\overline{r}_\psi}\right) \overline{r}_\psi \cdot dz\cdot d\overline{\psi} = n_\varphi \overline{r}_\psi \cdot d\overline{\psi} = n_\varphi dL \tag{26}$$

$$dT_{\psi r} = \int_{-h_1}^{h_2} \tau_{\psi r}^z \left(\frac{\overline{r}_\varphi + z}{\overline{r}_\varphi}\right) \overline{r}_\varphi \sin\overline{\psi}\cdot dz\cdot d\varphi = t_{\psi r}\overline{r}_\varphi \sin\psi\cdot d\varphi = t_{\psi r} X\cdot d\varphi \tag{27}$$

$$dM_\psi = -\int_{-h_1}^{h_2} z\sigma_\psi^z \left(\frac{\overline{r}_\varphi + z}{\overline{r}_\varphi}\right) \overline{r}_\varphi \sin\overline{\psi}\cdot dz\cdot d\varphi = m_\psi \cdot \overline{r}_\varphi \sin\overline{\psi}\cdot d\varphi = m_\psi X\cdot d\varphi \tag{28}$$

$$dM_\varphi = -\int_{-h_1}^{h_2} z\sigma_\varphi^z \left(\frac{\overline{r}_\psi + z}{\overline{r}_\psi}\right) \overline{r}_\psi \cdot dz\cdot d\overline{\psi} = m_\varphi \cdot \overline{r}_\psi \cdot d\overline{\psi} = m_\varphi dL \tag{29}$$

kjer so n_ψ, n_φ in $t_{\psi r}$ enotske sile in m_ψ, m_φ enotska momenta, ki se pri tankih lupinah poenostavijo:

where n_ψ, n_φ, t_ψ denote unit forces and m_ψ, m_φ unit moments, which are simplified in the case of thin shells:

$$n_\psi = \int_{-h_1}^{h_2} \sigma_\psi^z \cdot dz \tag{30}$$

$$n_\varphi = \int_{-h_1}^{h_2} \sigma_\varphi^z \cdot dz \tag{31}$$

$$t_{\psi r} = \int_{-h_1}^{h_2} \tau_{\psi r}^z \cdot dz \tag{32}$$

$$m_\psi = -\int_{-h_1}^{h_2} z\sigma_\psi^z \cdot dz \tag{33}$$

$$m_\varphi = -\int_{-h_1}^{h_2} z\sigma_\varphi^z \cdot dz \tag{34}.$$

Po definiciji je osrednja ali primerjalna ploskev tista ploskev na oddaljenosti h_1 od spodnjega roba lupine, ki se zaradi upogibnih napetosti ne deformira. Lego osrednje ali primerjalne ploskve dobimo iz pogoja ravnovesja notranjih osnih sil, ki se pojavijo zaradi delovanja upogibnih napetosti:

According to the definition, the middle, i.e., the reference plane is the one that lies at the distance h_1 from the lower edge of a shell. Because of the bending stresses the middle plane does not deform. The position of the middle plane is obtained from the condition that takes into account that all inner forces, as a result of the bending moment, must be in an equilibrium state:

$$\int_A \sigma_\psi^z \cdot dA = \int_{-h_1}^{\delta_1 - h_1} E_1\varepsilon_\psi^z x\,\varphi\cdot dz + \int_{\delta_1 - h_1}^{h_2} E_2\varepsilon_\psi^z x\,\varphi\cdot dz = 0 \tag{35}.$$

Specifično deformacijo ε_ψ^z računamo po enačbi (19), ki v primeru tanke lupine, ob upoštevanju, da je specifični raztezek ε_ψ osrednje ploskve enak nič, preide v obliko:

The normal strain ε_ψ^z is calculated using Equation (19), which, in the case of a thin shell and taking into account that the normal strain ε_ψ of the plane is equal to zero, takes the form:

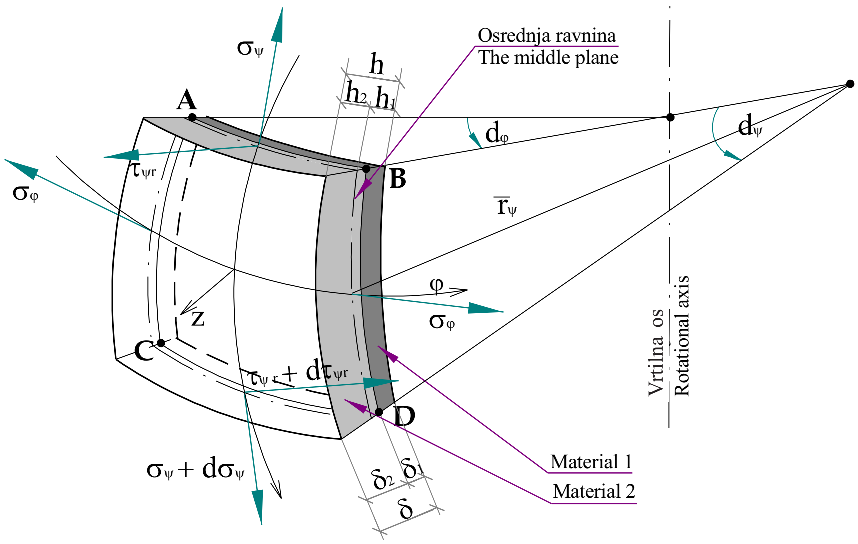

Sl. 2. *Element na deformirani lupini*
Fig. 2. *Element on deformed shell*

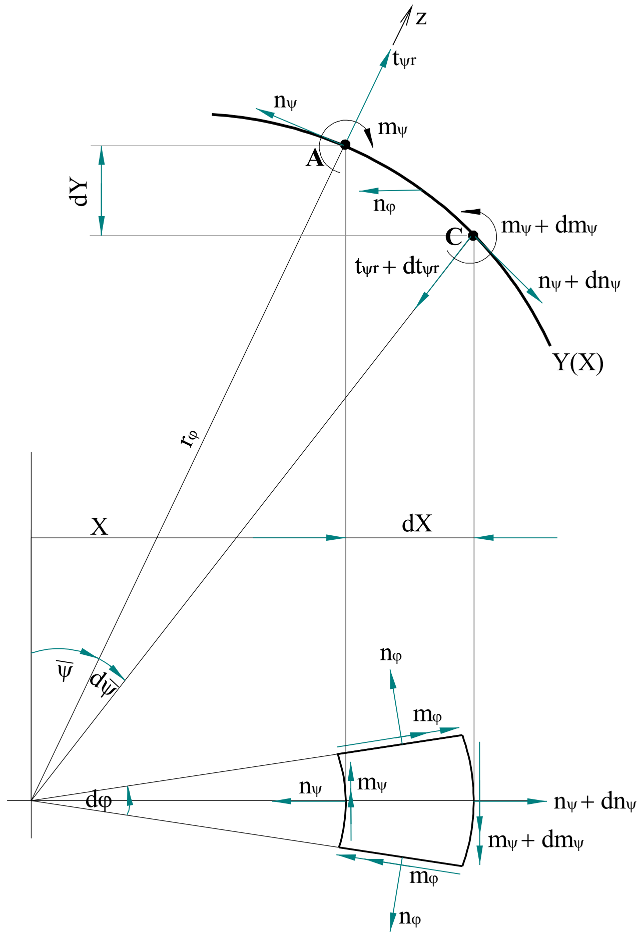

Sl. 3. *Enotske sile in momenti na elementu deformirane lupine*
Fig. 3. *Unit forces and moments in the element of deformed shell*

$$\varepsilon_{\psi}^{z} = z\left(\frac{1}{\overline{r}_{\psi}} - \frac{1}{r_{\psi}}\right) \qquad (36).$$

Po integraciji enačbe (35) z uporabo enačbe (36) je lega h_1 osrednje ploskve :

After integration of Equation (35) and by using Equation (36), the position h_1 of the middle plane is:

$$h_1 = \frac{E_1\delta_1^2 + 2E_2\delta_1\delta_2 + E_2\delta_2^2}{2\left(E_1\delta_1 + E_2\delta_2\right)} \qquad (37).$$

Iz pogoja $h_1 + h_2 = \delta$ se določi tudi vrednost h_2. Ker je element na sliki 2 v ravnovesju, lahko zapišemo enačbe ravnovesja sil in momentov (sl. 3).

Ravnovesje sil v meridialni smeri ψ:

From the condition $h_1 + h_2 = \delta$ the value for h_2 is determined. Because the element in Fig. 2 is in an equilibrium state we can write Equations of equilibrium of the forces and moments, Fig. 3.

The equilibrium Equation of the forces in the meridian direction ψ:

$$\left(dN_{\psi} + d\left(dN_{\psi}\right)\right) - dN_{\psi}\cos d\overline{\psi} - dT_{\psi}\sin d\overline{\psi} - 2dN_{\varphi}\sin\frac{d\varphi}{2}\cdot\cos\left(\overline{\psi} + \frac{d\overline{\psi}}{2}\right) = 0 \qquad (38).$$

in v prečni smeri:

and in the radial direction:

$$\left(dT_{\psi} + d(dT_{\psi r})\right) - dT_{\psi r}\cos d\psi + dN_{\psi}\sin d\overline{\psi} + 2dN_{\varphi}\sin\frac{d\varphi}{2}\cdot\sin\left(\overline{\psi} + \frac{d\overline{\psi}}{2}\right) = 0 \qquad (39).$$

Ravnovesna enačba v obročni smeri je zaradi osnosimetričnega napetostno-deformacijskega stanja enaka nič. Zapišemo še upogibno momentno ravnovesje:

Due to axially symmetric deformation, the equilibrium Equation in the circular direction is equal to zero. The equilibrium Equation for the bending moments is:

$$\begin{gathered}\left(dM_{\psi} + d\left(dM_{\psi}\right)\right) - dM_{\psi} - 2dM_{\varphi}\sin\left(\frac{d\varphi}{2}\right) - dT_{\psi r}\cos\overline{\psi}\cdot dX - \\ dT_{\psi r}\sin\overline{\psi}\cdot dY - dn_{\psi}\sin\overline{\psi}\cdot dX + dn_{\psi}\cos\overline{\psi}\cdot dY + 2dn_{\varphi}\sin\frac{d\varphi}{2}\cdot\frac{dY}{2} = 0\end{gathered} \qquad (40).$$

Upoštevajmo, da je:

Note that:

$$\sin\left(d\overline{\psi}\right) \cong d\overline{\psi}, \quad \sin\left(d\varphi\right) \cong d\varphi, \quad \cos d\overline{\psi} \cong 1$$

ter

and

$$d\left(dN_{\psi}\right) = \frac{\partial\left(dN_{\psi}\right)}{\partial\psi}d\psi = dn_{\psi}X\cdot d\varphi + n_{\psi}dX\cdot d\varphi$$

$$d\left(dT_{\psi r}\right) = \frac{\partial\left(dT_{\psi r}\right)}{\partial\psi}d\psi = dt_{\psi r}X\cdot d\varphi + t_{\psi r}dX\cdot d\varphi$$

$$d\left(dM_{\psi}\right) = \frac{\partial\left(dM_{\psi}\right)}{\partial\psi}d\psi = dm_{\psi}X\cdot d\varphi + m_{\psi}dX\cdot d\varphi$$

Tako imamo po ureditvi:

After rearranging:

$$\left(n_{\psi}X\right)' - n_{\varphi}L'\cos\overline{\psi} - t_{\psi r}X\left(\overline{\psi}\right)' = 0 \qquad (41)$$

$$\left(t_{\psi r}X\right)' + n_{\varphi}L'\sin\overline{\psi} + n_{\psi}X\cdot\left(\overline{\psi}\right)' = 0 \qquad (42)$$

$$\left(m_{\psi}X\right)' - m_{\varphi}L' + n_{\psi}X\left(Y'\cos\overline{\psi} - \sin\overline{\psi}\right) - t_{\psi r}X\left(Y'\sin\psi + \cos\overline{\psi}\right) = 0 \qquad (43).$$

4 REŠEVANJE ENAČB ZA PRIMER PLITVIH LUPIN

4 SOLUTION OF THE EQUATIONS OF A SHALLOW SHELL

Mešani sistem enačb (2), (3), (8) do (10), (13), (14), (16), (19), (20), (22) do (24), (30) do (34) in (41)

The mixed system of Equations (2), (3), (8) to (10), (13), (14), (16), (19), (20), (22) to (24), (30) to (34) do (43) z neznankami σ_ψ^z, σ_φ^z, $\tau_{\psi r}^z$, ε_ψ^z, ε_φ^z, $\gamma_{\psi r}^z$, ε_ψ, ε_φ, $\gamma_{\psi r}$, u, w, $\bar{\psi}$, $\bar{r}_\psi$, $\bar{r}_\varphi$, n_ψ, n_φ, $t_{\psi r}$, m_ψ, m_φ, X, Y rešujemo takole:

Enačbi (19) in (20) vstavimo v enačbi (22) in (23). Enačbo (22) nato vstavimo v enačbi (30) in (33), enačbo (23) pa v enačbi (31) in (34). Po integriranju imamo:

and (41) to (43) with unknowns σ_ψ^z, σ_φ^z, $\tau_{\psi r}^z$, ε_ψ^z, ε_φ^z, $\gamma_{\psi r}^z$, ε_ψ, ε_φ, $\gamma_{\psi r}$, u, w, $\bar{\psi}$, $\bar{r}_\psi$, $\bar{r}_\varphi$, n_ψ, n_φ, $t_{\psi r}$, m_ψ, m_φ, X, Y, is solved with the following steps:

Equations (19) and (20) are inserted into Equations (22) and (23). Equation (22) is then inserted into Equations (30) and (33) and Equation (23) into (31) and (34). After integration we obtain:

$$n_\psi = A\varepsilon_\psi + \bar{A}\varepsilon_\varphi - B\Upsilon_\psi - \bar{B}\Upsilon_\varphi - PT \tag{44}$$

$$n_\varphi = \bar{A}\varepsilon_\psi + A\varepsilon_\varphi - \bar{B}\Upsilon_\psi - B\Upsilon_\varphi - PT \tag{45}$$

$$m_\psi = B\varepsilon_\psi + \bar{B}\varepsilon_\varphi - C\Upsilon_\psi - \bar{C}\Upsilon_\varphi - QT \tag{46}$$

$$m_\varphi = B\varepsilon_\varphi + \bar{B}\varepsilon_\psi - C\Upsilon_\varphi - \bar{C}\Upsilon_\psi - QT \tag{47),}$$

kjer so A, $\bar{A}$, B, $\bar{B}$, C, $\bar{C}$, P in Q stalnice kakor sledi ([4] in [5]):

where A, $\bar{A}$, B, $\bar{B}$, C, $\bar{C}$, P and Q are constants as follows ([4] in [5]):

$$K1 = \frac{E_1\delta_1}{1-\mu_1^{\,2}}, \quad K_2 = \frac{E_2\delta_2}{1-\mu_2^{\,2}}, \quad A = K_1 + K_2, \quad \bar{A} = K_1\mu_1 + K_2\mu_2, \quad \mathrm{B} = \frac{1}{2}\left(2K_1h_1 - 2K_2h_2 - K_1\delta_1 + K_2\delta_2\right)$$

$$\bar{B} = \frac{1}{2}\left(2K_1h_1\mu_1 - 2K_2h_2\mu_2 - K_1\delta_1\mu_1 + K_2\delta_2\mu_2\right), \quad C = \frac{1}{3}\left(K_1\left(3h_1^2 - 3h_1\delta_1 + \delta_1^2\right) + K_2\left(3h_2^2 - 3h_2\delta_2 + \delta_2^2\right)\right)$$

$$\bar{C} = \frac{1}{3}\left(K_1\mu_1\left(3h_1^2 - 3h_1\delta_1 + \delta_1^2\right) + K_2\mu_2\left(3h_2^2 - 3h_2\delta_2 + \delta_2^2\right)\right), \quad P = K_1\left(1+\mu_1\right)\alpha_1 + K_2\left(1+\mu_2\right)\alpha_2$$

$$Q = \frac{1}{2}\left(K_1\left(1+\mu_1\right)\alpha_1\left(2h_1 - \delta_1\right) - K_2\left(1+\mu_2\right)\alpha_2\left(2h_2 - \delta_2\right)\right)$$

V prispevku obravnavamo plitve lupine. Pri takšnih lupinah je ukrivljenost $1/r_\psi$ zelo majhna, zaradi česar lahko v zgornjih enačbah poenostavimo določene izraze, saj velja:

This paper deals with shallow shells and in such shells the curvature $1/r_\psi$ is very small. For this reason, certain expressions in the above Equations can be simplified:

$$\psi \ll 1 \;\Rightarrow\; \psi \cong \sin\psi \cong \tan\psi = y', \quad \cos\psi \cong 1, \quad y'^2 \cong 0$$
$$\bar{\psi} \ll 1 \;\Rightarrow\; \bar{\psi} \cong \sin\bar{\psi} \cong \tan\bar{\psi} = \frac{Y'}{X'} \cong Y', \quad \cos\bar{\psi} \cong 1, \quad Y'^2 \cong 0$$

Eulerjevi koordinati (X,Y) v enačbi (2) sta s temi poenostavitvami sedaj:

Considering these simplifications, Euler's coordinates (X,Y) in Equation (2) are now:

$$X = x + wy' + u, \quad Y = y - w + uy' \tag{48).}$$

Iz enačb (5), (6), (9) in (10) izhaja:

From Equations (5), (6), (9) and (10) it follows that:

$$\frac{1}{r_\psi} \cong y'', \quad \frac{1}{r_\varphi} \cong \frac{y'}{x}, \quad \frac{1}{\bar{r}_\psi} \cong Y'' \cong y'' - w'', \quad \frac{1}{\bar{r}_\varphi} \cong \frac{\dot{Y}}{X} \cong \frac{y' - w'}{x}$$

ter zato:

and thus:

$$\Upsilon_\psi = \frac{1}{\bar{r}_\psi} - \frac{1}{r_\psi} \cong -w'' \tag{49}$$

$$\Upsilon_\varphi = \frac{1}{\bar{r}_\varphi} - \frac{1}{r_\varphi} \cong \frac{-w'}{x} \tag{50}$$

in iz enačb (13) in (14):

and from Equations (13) and (14):

$$\varepsilon_\psi = y''w + u' + \frac{1}{2}\left(w'\right)^2 \tag{51}$$

$$\varepsilon_{\varphi} = \frac{1}{x}\left(y'w + u\right) \quad (52).$$

V enačbah (48) upoštevamo tudi, da je premik u majhen v primerjavi s premikom w, ta pa je majhen v primerjavi z Lagrangevo koordinato x, tako da sta Eulerjevi koordinati X in Y približno:

In Equations (48) we have taken into account that the displacement u is small in comparison with the displacement w, and the latter is small in comparison with the Lagrange coordinate x, so that the Euler coordinates X and Y are approximately:

$$X \cong x \quad (53)$$

$$\mathrm{Y} \cong y - w \quad (54).$$

Ravnovesne enačbe (41) do (43) so sedaj:

Thus the equilibrium Equations (41) to (43) are:

$$\left(n_{\psi}x\right)' - n_{\varphi} - t_{\psi r}xY'' = 0 \quad (55)$$

$$\left(t_{\psi r}x\right)' + n_{\varphi}Y' + n_{\psi}xY'' = 0 \quad (56)$$

$$\left(m_{\psi}x\right)' - m_{\varphi} - t_{\psi r}x = 0 \quad (57).$$

Pomnožimo sedaj enačbo (55) z Y' ter ji prištejmo enačbo (56). Tako imamo:

Let us now multiply Equation (55) with Y' and add Equation (56). Thus, we have:

$$\left(n_{\psi}x\right)' Y' + n_{\psi}xY'' + \left(t_{\psi r}x\right)' - t_{\psi r}xY'Y'' = 0$$

Zadnji člen v enačbi zanemarimo, saj je po predpostavki:

We disregard the last term in the equation, assuming that:

$$Y'Y'' = \frac{1}{2}\left(Y'^2\right)' \cong 0$$

Tako imamo po ureditvi zvezo:

In this way we obtain the relationship:

$$\left(t_{\psi r}x\right)' = -\left(n_{\psi}xY'\right)'$$

ter po integriranju:

and after integration:

$$t_{\psi r} = -n_{\psi}Y' + \frac{c}{x} \quad (58),$$

kjer je c integracijska stalnica, ki je odvisna od zunanje sile $\vec{F}_k$ v temenu lupine. Zvezo (58) vstavimo v enačbi (56) in (57):

where c is a constant of integration, which depends on the outer force $\vec{F}_k$ in the top of the shell. The connection (58) is inserted into Equations (56) and (57):

$$\left(n_{\psi}x\right)' - n_{\varphi} = 0 \quad (59)$$

$$\left(m_{\psi}x\right)' - m_{\varphi} + n_{\psi}xY' - c = 0 \quad (60).$$

Sedaj imamo sistem enajstih enačb (44) do (47), (49) do (52), (54), (59) in (60) z enajstimi neznankami $n_{\psi}, n_{\varphi}, m_{\psi}, m_{\varphi}, u, w, \varepsilon_{\psi}, \varepsilon_{\varphi}, Y, \Upsilon_{\psi}, \Upsilon_{\varphi}$. Naprej postopamo takole. Izrazimo premik u iz enačbe (52), ga odvajamo po koordinati x ter vstavimo v enačbo (51). Nastane zveza:

Now we obtained a system of 11 Equations (44) to (47), (49) to (52), (54), (59) and (60) and with eleven variables $n_{\psi}, n_{\varphi}, m_{\psi}, m_{\varphi}, u, w, \varepsilon_{\psi}, \varepsilon_{\varphi}, Y, \Upsilon_{\psi}, \Upsilon_{\varphi}$. The next steps are as follows. The displacement u is expressed from Equation (52). The derivative of the displacement u with respect to the variable x is then obtained and inserted into Equation (51). In this way we get:

$$\left(x\varepsilon_{\varphi}\right)' + \frac{1}{2}\left(w'\right)^2 = \varepsilon_{\psi} + w'y' \quad (61).$$

Iz enačb (44) in (45) izrazimo ε_ψ in ε_φ ter ju vstavimo v enačbo (61). Υ_ψ in Υ_φ nadomestimo z enačbama (49) in (59), enotsko silo n_φ pa s prvim členom v enačbi (59). S tem dobi enačba (61) obliko:

From Equations (44) and (45) are expressed ε_ψ and ε_φ, which are inserted into Equation (61). Next, Υ_ψ and Υ_φ are substituted by Equations (49) and (59), while the unit force n_φ is substituted by the first term in Equation (59). Thus, Equation takes the form:

$$\frac{1}{x}\left(x^3 n_\psi'\right)' = \frac{A^2-\bar{A}^2}{A}\left(y'w' - \frac{1}{2}(w')^2\right) + x\left(\frac{A\bar{B}-\bar{A}B}{A}\right)\left(w'' + \frac{1}{x}w'\right)' \tag{62}$$

Sedaj v enačbo (60) vstavimo enačbi (46) in (47) ter spet izrazimo specifični deformaciji ε_ψ in ε_φ z enotskima silama n_ψ, n_φ in razlikama ukrivljenosti Υ_ψ in Υ_φ. Tako kakor prej nadomestimo Υ_ψ in Υ_φ z enačbama (49) in (50), enotsko silo n_φ pa s prvim členom v enačbi (59). Če iz enačbe (61) izrazimo še n_ψ' postane enačba (60):

Now, Equations (46) and (47) are inserted into Equation (60). The normal strains ε_ψ and ε_φ are expressed by the unit forces n_ψ, n_φ and the differences in curvature Υ_ψ and Υ_φ. Also, Υ_ψ and Υ_φ are substituted by Equations (49) and (59), and the unit force n_φ by the first term in Equation (59). If from Equation (61) n_ψ' is expressed too, Equation (60) becomes [4]:

$$xn_\psi(y-w)' = -\left(\frac{A\bar{B}-\bar{A}B}{A}\right)\left(y'w' - \frac{1}{2}(w')^2\right) - x\left(\frac{AC-B^2}{A}\right)\left(w'' + \frac{1}{x}w'\right)' - c \tag{63}$$

Prvotni sistem, ki ga je sestavljalo 21 enačb in prav toliko neznank, smo naposled prevedli v sistem dveh diferencialnih enačb (62) in (63), ki opisujeta najbolj splošen primer, ko sta $\mu_1 \neq \mu_2$ in $\delta_1 \neq \delta_2$. Enačbi (62) in (63) poenostavimo, če imata obe plasti lupine enak Poissonov količnik $\mu_1 = \mu_2$, ker je takrat: $\bar{A} = \mu A$; $\bar{B} = \mu B$; $\bar{C} = \mu C$; $A\bar{B} - \bar{A}B = 0$. Zato sta v tem primeru enačbi (62) in (63):

The initial system, originally consisting of 21 equations and as many variables, has been finally converted into a system of two differential equations, (62) and (63), which outline the commonest example where $\mu_1 \neq \mu_2$ and $\delta_1 \neq \delta_2$. Equations (62) and (63) can be simplified if both layers of a shell have an equal Poisson's coefficient $\mu_1 = \mu_2$, because then: $\bar{A} = \mu A$; $\bar{B} = \mu B$; $\bar{C} = \mu C$; $A\bar{B} - \bar{A}B = 0$. Hence, in this case Equations (62) and (63) are:

$$\frac{1}{x}\left(x^3 n_\psi'\right)' = A\left(1-\mu^2\right)\left(y'w' - \frac{1}{2}(w')^2\right) \tag{64}$$

in / and

$$xn_\psi(y-w)' = -x\left(\frac{AC-B^2}{A}\right)\left(w'' + \frac{1}{x}w'\right)' - c \tag{65}$$

Z uvedbo brezrazsežne vodoravne koordinate χ:

By introducing a dimensionless horizontal coordinate χ:

$$\chi = \left(\frac{x}{a}\right)^2 \tag{66}$$

in Wittrickovih funkcij G, F_0 in F:

and Wittrick's functions G, F_0 and F:

$$n_\psi = \frac{G(\chi)}{a^2}\left(\frac{AC-B^2}{A}\right) \tag{67}$$

$$\frac{1}{x}y' = \frac{F_0(\chi)}{a^2}\sqrt{\frac{2\left(AC-B^2\right)}{A^2-\bar{A}^2}} \tag{68}$$

$$\frac{1}{x}Y' = \frac{F(\chi)}{a^2}\sqrt{\frac{2\left(AC-B^2\right)}{A^2-\bar{A}^2}} \tag{69}$$

prevedemo problem v brezrazsežno obliko [6]. Iz enačbe (66) izhajajo namreč razmerja:

the problem is converted into the dimensionless form [6]. Because of the introduction of a dimensionless coordinate χ we can write:

$$x = a\sqrt{\chi}, \quad \frac{\partial \chi}{\partial x} = \frac{2}{a}\sqrt{\chi}, \quad \left(\frac{\partial \chi}{\partial x}\right)^2 = \frac{4}{a^2}\chi, \quad \frac{\partial^2 \chi}{\partial x^2} = \frac{2}{a^2}$$

zato so posamezni členi v enačbah (64) in (65) po spremembi:

therefore, the individual terms in Equations (64) and (65), after the transformation, are:

$$\frac{1}{x}\left(x^3 n_\psi'\right)' = 3x\frac{\partial n_\psi}{\partial x} + x^2\frac{\partial^2 n_\psi}{\partial x^2} = \frac{4\chi}{a^2}\left(\frac{AC-B^2}{A}\right)\frac{d^2}{d\chi}\left(\chi \cdot G(\chi)\right)$$

$$y'w' = y'\left(y'-Y'\right) = \frac{\chi}{a^2}\left(\frac{2\left(AC-B^2\right)}{A^2\left(1-\mu^2\right)}\right)\left(F_0(\chi)-F(\chi)\right)F_0(\chi)$$

$$x\left(w'' + \frac{1}{x}(w)'\right)' = x\left(y'-Y'\right)'' + \left(y'-Y'\right)' - \frac{1}{x}\left(y'-Y'\right) = \frac{4\chi}{a^2}\sqrt{\left(\frac{2\left(AC-B^2\right)}{A^2\left(1-\mu^2\right)}\right)}\frac{d^2}{dx^2}\left(\chi\cdot\left(F_0(\chi)-F(\chi)\right)\right)$$

$$(y-w)' = Y'$$

Diferencialni enačbi (64) in (65) v brezrazsežni obliki sta tako:

Thus, the differential equations (64) and (65) in the dimensionless form are:

$$4(\chi G)'' = F_0^2 - F^2 \tag{70}$$

$$4\left(\chi\left(F-F_0\right)\right)'' = FG - \frac{c\cdot a^2}{\chi}\frac{A^2}{AC-B^2}\sqrt{\frac{1-\mu^2}{2\left(AC-B^2\right)}} \tag{71}$$

pri čemer smo z dvema črticama označili drugi odvod po koordinati χ:

where two apostrophes mark the second derivative with respect to the coordinate χ:

$$\frac{d}{d\chi}(\ ) = (\ )', \quad \frac{d^2}{d\chi^2}(\ ) = (\ )''$$

Odvisni brezrazsežni spremenljivki, po katerih rešujemo diferencialni enačbi (70) in (71), sta torej oblikovna funkcija trenutne oblike bimetalne lupine $F(\chi)$ ter napetostna funkcija $G(\chi)$. Integracijsko stalnico c v enačbi (71) določimo z upoštevanjem ravnovesja sil na robu lupine.

Če je lupina prosto položena, je sila podpore $\vec{V}$ na robu lupine nasprotno usmerjena in po vrednosti enaka sili $\vec{F}_k$ v temenu lupine (sl. 4):

The dependable, dimensionless variables with which we are solving the differential equations (70) and (71) are thus the formative function $F(\chi)$ of the present form of the bimetallic shell and the stress function $G(\chi)$. The constant of integration c in Equation (71) is determined by taking into account the equilibrium of forces at the edge of a shell.

If the shell is simply roller supported, the force $\vec{V}$ at the edge of a shell is pointing in the opposite direction and is equal to the force $\vec{F}_k$ in the top of the shell, Fig. 4**:**

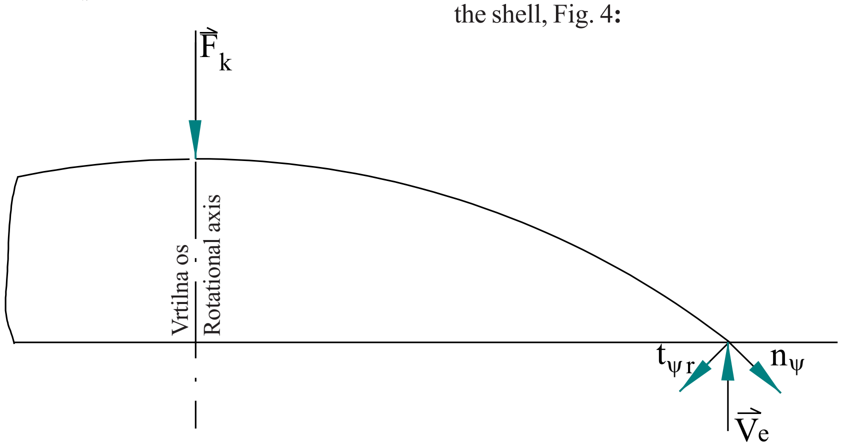

Sl. 4. *Obremenitev prosto polo□ene lupine s silo* $\vec{F}_k$

Fig. 4. *Loading of simply-roller supported shell with the force* $\vec{F}_k$

$$\vec{F}_k + \vec{V} = \vec{F}_k + (2\pi a)\vec{V}_e = 0 \tag{72}$$

kjer je z $\vec{V}_e$ označena enotska navpična sila na robu lupine. Enačba (72) je v komponentni obliki:

where $\vec{V}_e$ denotes the vertical unit force at the edge of the shell. Equation (72) in component form is:

$$F_k + \left(t_{\psi r} + n_\psi \cdot \left.\frac{dY}{dx}\right|_{x=a} \right) 2\pi a = 0, \quad -t_{\psi r} \cdot \left.\frac{dY}{dx}\right|_{x=a} + n_\psi = 0 \tag{73}$$

Rešitev sistema enačb (73) je potem, ko upoštevamo tudi plitvost:

When also taking into account the shallowness, the solution of the system of Equations (73) is:

$$n_\psi(a) = \frac{-F_k}{2\pi a} \cdot \left.\frac{dY}{dx}\right|_{x=a} \tag{74}$$

$$t_{\psi r}(a) = \frac{-F_k}{2\pi a} \tag{75}$$

Vstavimo enačbi (74) in (75) v enačbo (58) ter izrazimo stalnico c:

Equations (74) and (75) are inserted into Equation (58) and the constant c is expressed by:

$$c = \frac{-F_k}{2\pi} \tag{76}$$

Če na lupino ne deluje zunanja sila $\vec{F}_k$ je integracijska stalnica c v enačbi (76) enaka nič, diferencialni enačbi (70) in (71) pa se poenostavita v obliko, ki jo je v [6] zapisal W. H. Wittrick:

If the external force $\vec{F}_k$ does not act upon the shell, the integrating constant c in Equation (76) is equal to zero, whilst the differential Equations (70) and (71) are simplified into a form, according to W. H. Wittrick in [6]:

$$4(\chi G)'' = F_0^2 - F^2 \tag{77}$$

$$4\left(\chi\left(F - F_0\right)\right)'' = FG \tag{78}$$

5 ANALIZA RAZMER PRI KROGELNIH LUPINAH

5 ANALYSIS OF THE CIRCUMSTANCES IN SPHERICAL SHELLS

V enačbah (70) in (71) se pojavlja oblikovna funkcija začetne oblike lupine $F_0(\chi)$. Ta je odvisna od funkcije $y = y(x)$, ki opisuje osrednjo ploskev začetne, nedeformirane oblike lupine. V primeru krogelnih lupin, katerih teme je postavljeno v izhodišče koordinatnega sistema, je ta funkcija v posredni obliki: $x^2 + y^2 = 2yR$. Zaradi plitvosti lupine zanemarimo drugi člen ter dobimo po zamenjavi spremenljivke x v brezrazsežno spremenljivko χ:

In Equations (70) and (71) occurs the formative function $F_0(\chi)$ of the initial shape of the shell. It depends on the function $y = y(x)$, which describes the middle plane of the initial, undeformed shape of the shell. However, in the case of spherical shells, whose crowns are set at the beginning of the coordinate system, this function is in the implicit form $x^2 + y^2 = 2yR$. Because of the shallowness of the shell, the second term is neglected, so that after the substitution of the variable x into the dimensionless variable χ, we obtain:

$$y = \frac{x^2}{2R} = \frac{a^2\chi}{2R} = h_0\chi \tag{79}$$

Oblikovna funkcija začetne oblike lupine je po enačbi (68):

According to Equation (68) the formative function of the initial shape of the shell is:

$$F_0 = 2h_0 A\sqrt{\frac{1-\mu^2}{2\left(AC - B^2\right)}} = \text{konst} \tag{80}$$

Če upoštevamo, da je začetna oblikovna funkcija F_0 nespremenljiva, sta diferencialni enačbi

When taking into account that the initial formative function F_0 is a constant, the differential

(70) in (71):

Equations (70) and (71) are:

$$4G''\chi + 8G' = F_0^2 - F^2 \tag{81}$$

$$4F''\chi + 8F' = FG - \frac{c \cdot a^2}{\chi} \frac{A^2}{AC - B^2} \sqrt{\frac{1-\mu^2}{2\left(AC - B^2\right)}} \tag{82}$$

Diferencialni enačbi (81) in (82) najlažje rešimo za primer, ko lupina ni obremenjena z zunanjo silo $\vec{F}_k$, ker je takrat v enačbi (82) stalnica c enaka nič. Če je lupina prosto položena, so napetosti in momenti na njenem robu enaki nič, v temenu lupine pa imajo napetosti in momenti le končne vrednosti. Za napetostno funkcijo $G(\chi)$ veljata torej robna pogoja:

The easiest way to solve Equations (81) and (82) is in the case where the shell is not loaded by an external force $\vec{F}_k$ because then the constant c in Equation (82) is equal to zero. If the shell is simply roller supported, the stresses and moments at its edges are equal to zero, while the stresses and moments in the top of the shell have only limited values. For the stress function $G(\chi)$ the following boundary conditions thus hold:

$$G(1) = 0, \quad G(0) \neq \infty \tag{83}$$

Robna pogoja za oblikovno funkcijo $F(c)$ dobimo iz enačbe (46), ki jo zapišemo v brezrazsežni obliki. Iz enačbe (44) in (45) izrazimo ε_ψ in ε_φ ter vrednosti vstavimo v enačbo (46) za enotski moment m_ψ. Spremembo ukrivljenosti Υ_ψ in Υ_φ nadomestimo z enačbama (49) in (50) prvi in drugi odvod premika w pa izrazimo z odvodom enačbe (54). Če nadalje spet vzamemo enak Poissonov koeficient za obe plasti bimetalne lupine se enotski moment m_ψ izraža:

The boundary conditions for the formative function $F(\chi)$ are obtained from Equation (46), written in dimensionless form. From Equation (44) we express ε_ψ and insert the value into Equation (46) for the unit moment m_ψ. The curvature differences Υ_ψ and Υ_φ are then replaced by Equations (49) and (50), while the first and second derivatives of the displacement w are expressed by the derivative of Equation (54). In the case of an equal Poisson's ratio for both layers of the bimetallic shell, the unit moment m_ψ runs as follows:

$$m_\psi = \frac{C}{a^2}\sqrt{\frac{2C}{A(1-\mu^2)}} \cdot \Big(F_0(1+\mu) - F(\chi)(1+\mu) - 2\chi F'(\chi)\Big) - QT \tag{84}$$

kadar velja tudi:

in the special case where:

$$\delta_1 = \delta_2 = \frac{\delta}{2} \text{ in/and } E_1 = E_2 = E \tag{85}$$

Ker je na robu lupine poleg enotske sile n_ψ ničen tudi enotski moment m_ψ, izrazimo iz (84) povezavo med temperaturo lupine T in trenutno oblikovno funkcijo F:

At the edge of the shell, besides the unit force n_ψ, also the unit moment m_ψ is equal to zero. So, the relationship between the shell's temperature T and the present formative function F can be derived from Equation (84):

$$T = T_m\left(1 - \frac{1}{F_0}\left(F(1) + \frac{2}{1+\mu}F'(1)\right)\right) = T_m \cdot \tau \tag{86}$$

kjer je t brezrazsežna funkcija temperature, T_m pa nespremenljiva:

where τ is the dimensionless function of the temperature and T_m is a constant:

$$T_m = \frac{2h_0(1+\mu)\left(AC - B^2\right)}{a^2(AQ - BP)} \tag{87}$$

Za oblikovno funkcijo F sta torej robna pogoja:

Thus, the boundary conditions for the formative function F are:

$$\tau = 1 - \frac{1}{F_0}\left(F(1) + \frac{2}{1+\mu}F'(1)\right), \quad F(0) \neq \infty \tag{88}$$

Kadar je bimetalna lupina takšna, da veljajo enačbe (85), potem je iz enačbe (37): $h_1 = h_2 = \delta_1 = \delta_2 = \delta/2$. Če slednje upoštevamo pri izračunu stalnic $A, \bar{A}, B, \bar{B}, C, \bar{C}, P$ in Q, se enačbi (80) in (87) za nespremenljivi F_0 in T_m poenostavita:

Let us take into consideration the case where Equations (85) are fulfilled. Consequently, from Equation (37) it follows that $h_1 = h_2 = \delta_1 = \delta_2 = \delta/2$. If what was stated above is considered in the calculation of the constants $A, \bar{A}, B, \bar{B}, C, \bar{C}, P$ and Q, Equations (80) and (87) for the constants F_0 and T_m are simplified:

$$F_0 = \frac{2\sqrt{6}\cdot h_0}{\delta}\sqrt{1-\mu^2}, \quad T_m = \frac{2\delta}{3R(\alpha_1-\alpha_2)} = \frac{2\delta^2 F_0}{3\sqrt{6}\cdot a^2\sqrt{1-\mu^2}\cdot(\alpha_1-\alpha_2)} \qquad (89).$$

Za numerično reševanje problema pa robna pogoja $G(0)\neq\infty$ in $F(0)\neq\infty$ nista primerna, zato uvedemo novi spremenljivki $g(\chi)$ in $f(\chi)$:

For a numerical solution of the problem, however, the boundary conditions $G(0)\neq\infty$ and $F(0)\neq\infty$ are not suitable; hence new variables $g(\chi)$ and $f(\chi)$ have been introduced:

$$f = \chi\cdot F, \quad g = \chi\cdot G \qquad (90).$$

Po spremembi diferencialnih enačb (81), (82) in robnih pogojev (83) in (88) ter upoštevanju, da sta funkciji G in F v $\chi = 0$ omejeni, imamo naslednji problem robnih vrednosti:

After transforming the differential equations (81) and (82), the boundary conditions (83) and (88), and taking into consideration that functions G and F in $\chi = 0$ are limited, we obtain the following boundary-value problem:

$$\begin{aligned} &4g'' = F_0^2 - \frac{f^2}{\chi^2}, \quad 4f'' = \frac{f\cdot g}{\chi^2} \\ &g(0) = g(1) = f(0) = 0, \ \tau = 1 - \frac{1}{F_0(1+\mu)}\big(2f'(1) - f(1)\cdot(1-\mu)\big) \end{aligned} \qquad (91).$$

Prevedemo ga v sistem navadnih diferencialnih enačb prvega reda:

It is then converted into a system of ordinary differential equations of the first order:

$$\begin{aligned} &y_1' = y_2, \ y_2' = \frac{1}{4}\left(F_0^2 - \frac{y_3^2}{\chi^2}\right), \ y_3' = y_4, \ y_4' = \frac{1}{4}\frac{y_1 y_3}{\chi^2} \\ &y_1(0) = y_1(1) = y_3(0) = 0, \ \ \tau = 1 - \frac{1}{F_0(1+\mu)}\big(2y_4(1) - y_3(1)\cdot(1-\mu)\big) \end{aligned} \qquad (92),$$

če uvedemo zamenjavo:

when the substitution is introduced:

$$g = y_1, \ g' = \frac{dg}{d\chi} = y_2, \ f = y_3, \ f' = \frac{df}{d\chi} = y_4$$

Sistem enačb (92) s temperaturo τ v območju $0\leq\tau\leq 2$ smo rešili z uporabo nelinearne strelske metode. Izbrali smo približni vrednosti $y_2(1)$ in $y_4(1)$ ter izračunali približne vrednosti funkcij g in f po običajni enokoračni metodi Runge Kutta 4. reda. Določanje natančnejših vrednosti $y_2(1)$ in $y_4(1)$ je potekalo po Newtonovi metodi reševanja nelinearnih enačb. Ker je sistem enačb (92) v točki $\chi = 0$ singularen, smo odstopanje približnih vrednosti g in f od danih robnih pogojev v $\chi = 0$ računali v točki $\chi = \chi_0 = 10^{-10}$. Deformacijo lupine smo zapisali z razmerjem ξ med trenutno višino deformirane lupine in začetno višino nedeformirane lupine:

The system of Equations (92) with a temperature τ in the interval $0\leq\tau\leq 2$ was solved using the non-linear shooting method. We took approximate values for $y_2(1)$ and $y_4(1)$ and calculated rough values for the functions g and f using the classical one-step Runge Kutta method of the fourth order. For defining more exact values of $y_2(1)$ and $y_4(1)$, the Newton method of solving non-linear equations was used. And since the system of Equations (92) at the point $\chi = 0$ is singular, the digressions from the approximate values g and f from the given boundary conditions in $\chi = 0$ were calculated at the point $\chi = \chi_0 = 10^{-10}$. The shell's deformation was recorded with the ratio ξ between the present height of the deformed shell and the initial height of the undeformed shell:

$$\xi = \frac{h}{h_0} = \frac{Y(1)}{y(1)} = \frac{1}{F_0}\int_{\chi_0}^{1}\frac{1}{\chi}f(\chi)\cdot d\chi \qquad (93).$$

Integral v (93) smo računali numerično. Zaradi singularnosti v $\chi = 0$ je integracija potekala od $\chi = 1$ do $\chi = \chi_0$. Tako smo izračunali razmerje višin ξ pri različnih temperaturah τ. Problem robnih vrednosti (91) lahko rešimo tudi po metodi, ki jo je v [6] predlagal W. H. Wittrick. Ker sta funkciji g in f v točki $\chi = 0$ singularni, ju v okolici te točke zapišemo v obliki potenčne vrste, tako da zadostimo robnim pogojem v $\chi = 0$:

The integral (93) was solved numerically. Due to the singularity in $\chi = 0$ the integration occurred from $\chi = 1$ to $\chi = \chi_0$. Consequently, we have calculated the values of ratio ξ at various temperatures τ. The boundary value problem (91) could be solved too using the method proposed by W. H. Wittrick in [6]. Because the functions g and f at the point $\chi = 0$ are singular, they have been written in the form of power series about the point $\chi = 0$ in such a way as to meet the boundary conditions in $\chi = 0$:

$$g = \sum_{n=0}^{\infty} g_n \chi^{n+1}, \quad f = \sum_{n=0}^{\infty} f_n \chi^{n+1} \tag{94}$$

Po vstavitvi potenčnih vrst (94) v diferencialni enačbi robnega problema (91) ter primerjavi koeficientov pri enakih potencah spremenljivke χ na obeh straneh enačb, dobimo razmerja med koeficienti:

After inserting the power series (94) into the boundary-value problem (91) and comparing the coefficients in equal exponents of the variable χ on both sides of the equations, we obtain the relations between the coefficients:

$$\begin{aligned} g_1 &= \frac{F_0^2 - f_0^2}{8}, \quad f_1 = \frac{f_0 g_0}{8} \\ g_2 &= \frac{-2 f_0 f_1}{24}, \quad f_2 = \frac{f_0 g_1 + f_1 g_0}{24} \\ g_3 &= \frac{-2 f_0 f_2 - f_1^2}{48}, \quad f_3 = \frac{f_0 g_2 + f_1 g_1 + f_2 g_0}{48} \\ g_4 &= \frac{-2 f_0 f_3 - 2 f_1 f_2}{80}, \quad f_4 = \frac{f_0 g_3 + f_1 g_2 + f_2 g_1 + f_3 g_0}{80} \quad \text{itn./etc.} \end{aligned} \tag{95}$$

Sistem enačb (95) je rekurziven. Pri izbranem g_0 in f_0 so določeni vsi nadaljnji koeficienti g_n in f_n funkcije g in f. Koeficienta g_0 in f_0 seveda izberemo tako, da funkciji g in f na robu lupine v $\chi = 1$ zadoščata robnima pogojema v enačbi (91). Za izbrani koeficient g_0 smo izbrali neko začetno vrednost koeficienta f_0 ter v območju $0 \leq \chi \leq 0{,}05$ določili člene potenčne vrste funkcij g in f. S potenčnima vrstama smo izračunali funkcijske vrednosti $g(0{,}05)$, $g'(0{,}05)$, $f(0{,}05)$ in $f'(0{,}05)$ ter s temi začetnimi vrednostmi numerično izračunali vrednosti funkcij g in f v območju $0{,}05 < \chi \leq 1$. Ker je izbrana začetna vrednost koeficienta f_0 le približek, funkcija g v točki $\chi = 1$ odstopa od robnega pogoja v enačbi (91). Po Newtonovi metodi smo zato določili novo, natančnejšo vrednost koeficienta f_0, ter postopek ponovili tolikokrat, da je postala absolutna vrednost funkcije $g(1)$ natančna do vnaprej predpisane vrednosti. Prednost tega numeričnega postopka pred prej opisanim je v tem, da z Newtonovo metodo ali bisekcijo računamo vrednost samo ene neznanke, in sicer vrednost koeficienta f_0 oziroma $y_3(0{,}05)$, medtem ko je treba pri strelski metodi izračunati vrednosti dveh

The system of Equations (95) is recursive. By selecting g_0 and f_0 all further coefficients g_n and f_n of the function g and f have been determined. Clearly, the coefficients g_0 and f_0 are selected in such a way that the functions g and f at the edge of a shell in $\chi = 1$ meet the boundary conditions in Equation (91). For the selected coefficient g_0 we have taken an initial value for the coefficient f_0 and in the interval $0 \leq \chi \leq 0{,}05$ determined the elements of the power series' for functions g and f. Then we have calculated, using power series, the functional values $g(0{,}05)$, $g'(0{,}05)$, $f(0{,}05)$ and $f'(0{,}05)$. These initial values were used to compute the numerical values of the functions g and f in the interval $0{,}05 < \chi \leq 1$. Because the selected initial value for the coefficient f_0 is only an approximation, the function g at the point $\chi = 1$ deviates from the boundary condition in Equation (91). Using Newton's method we have then determined a new, more exact value for the coefficient f_0 and kept repeating the procedure until the absolute value of the function $g(1)$ was as precise as set up initially. The advantage of this numerical procedure over the one described before is that by using Newton's method or bisection we calculate the value of only one variable $y_3(0{,}05)$, while with the shooting method it is necessary to calculate the values of two variables, $y_2(1)$

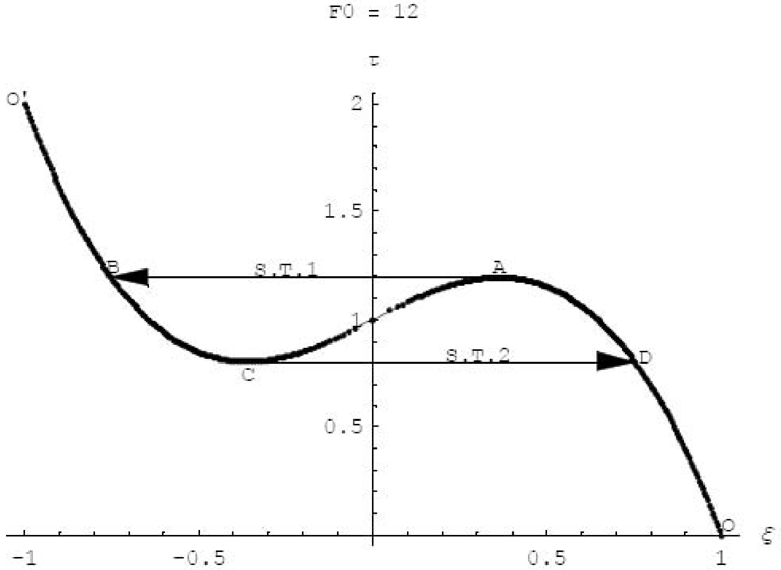

Sl. 5. *Funkcija $\tau = \tau(\xi)$ za primer osnosimetrične lupine s $F_0 = 12$ in $\mu = 1/3$, ki izkazuje pojav preskoka sistema med točkama AB ob segrevanju in točkama CD ob ohlajanju*

Fig. 5. *The function $\tau = \tau(\xi)$ as an example of axi-symmetric shell for $F_0 = 12$ and $\mu = 1/3$ expressing the phenomenon of a snap-through system between points AB in the process of heating up and the points CD in the process of cooling*

spremenljivk $y_2(1)$ in $y_4(1)$. Po obeh numeričnih postopkih smo dobili enake rezultate.

Slika 5 prikazuje razmere v lupini s Poissonovim koeficientom $\mu = 1/3$ in začetno oblikovno funkcijo $F_0 = 12$. Graf funkcije brezrazsežne temperature t v odvisnosti od razmerja višin ξ predstavlja stabilnostne razmere ob temperaturnem obremenjevanju bimetalne lupine .

V začetnem, temperaturno neobremenjenem stanju $\tau = 0$, v točki $O(1,0)$ je razmerje višin ξ enako ena. S povečevanjem brezrazsežne temperature t se to razmerje zmanjšuje. Kakor je razvidno s slike 5, je območje na krivulji med točko O in točko $A(\xi_{p1}, \tau_{p1}) = A(0,360;1,195)$, kjer ima funkcija $\tau(\xi)$ lokalni vrh, območje stabilnega ravnovesja. Do preskoka lupine bo torej prišlo v točki A pri temperaturi τ_{p1} = 1,195, ker je korak med točko A in točko $C(\xi_{p2}, \tau_{p2}) = C(-0,360;0,805)$, kjer ima funkcija lokalni dol, območje nestabilnega ravnovesja. Po preskoku bo lupina zavzela novo ravnovesno lego v točki $B(-0,752;1,195)$ pri temperaturi τ = 1,195. Pri nadaljnjem segrevanju lupine razmerje ξ še naprej zmanjšuje.

Pri ohlajanju lupine imamo nasproten pojav in v točki C pri temperaturi τ_{p2} = 0,805, ponoven preskok. Tokrat lupina preskoči v ravnovesno lego v točki $D(0,752;0,805)$ pri temperaturi τ = 0,805. S

and $y_4(1)$. Nevertheless, with both of these numerical methods we obtained the same results.

Fig. 5 shows the condition for the shell with Poisson's ratio $\mu = 1/3$ and the initial formative function $F_0 = 12$. The graph of the function of dimensionless temperature τ depending on the ratio of heights ξ represents the stability circumstances during the shell's temperature load.

In the initial state with temperature $\tau = 0$, at point $O(1,0)$ the ratio of heights ξ is equal to one. By increasing the dimensionless temperature τ this ratio is decreasing. As shown in Fig. 5, the portion of the curvature between point O and point $A(\xi_{p1}, \tau_{p1}) = A(0.360,1.195)$ where the function $\tau(\xi)$ has the local maximum is the range of stable equilibrium. Hence, the snap-through of the shell will happen at point A at temperature τ_{p1} = 1.195 because the interval between point A and point $C(\xi_{p2}, \tau_{p2}) = C(-0.360,0.805)$ where the function has the local minimum is the range of unstable equilibrium. After the snap-through, the shell will take a new equilibrium state at point $B(-0.752,1.195)$ at temperature τ = 1.195. In the course of the shell's further heating up, the ratio of heights ξ continues to decrease.

However, in the cooling down of the shell the reverse situation occurs and at point C at temperature τ_{p2} = 0.805, another snap-through happens. This time the shell snaps into the equilibrium state at point

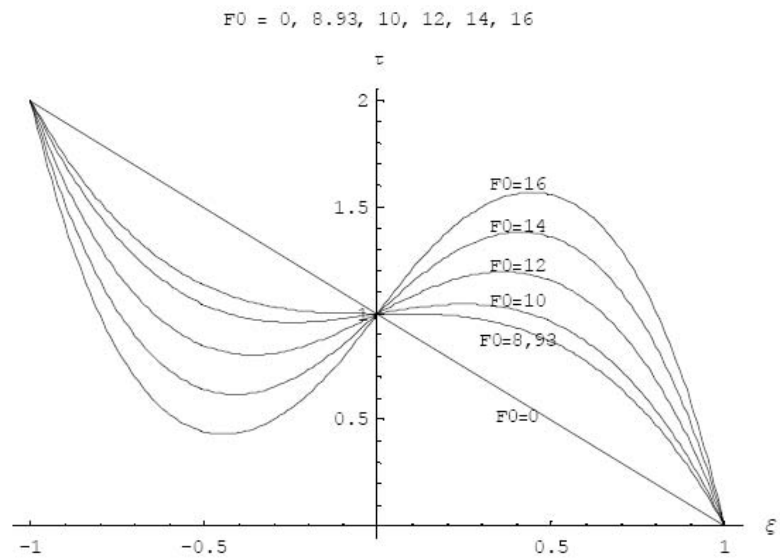

Sl. 6. *Stabilnostne razmere pri lupinah z različnimi vrednostmi funkcije F_0 in μ = 1/3*
Fig. 6. *Snap-through behaviour for shells with various values of function F_0 and μ = 1/3*

Preglednica 1. *Temperatura in lega preskoka lupine za različne vrednosti funkcije F_0 in μ = 1/3*
Table 1. *Temperature and position of the shell's snap-through for different values of function F_0 and μ = 1/3*

F_0	$8,93$	10	12	14	16
$S.T.1$	$\tau_{p1}=1$ $\xi_{p1}=0$	$\tau_{p1}=1,043$ $\xi_{p1}=0,248$	$\tau_{p1}=1,195$ $\xi_{p1}=0,361$	$\tau_{p1}=1,381$ $\xi_{p1}=0,411$	$\tau_{p1}=1,567$ $\xi_{p1}=0,445$
$S.T.2$	$\tau_{p2}=1$ $\xi_{p2}=0$	$\tau_{p2}=0.957$ $\xi_{p2}=-0,248$	$\tau_{p2}=0,805$ $\xi_{p2}=-0,361$	$\tau_{p2}=0,619$ $\xi_{p2}=-0,411$	$\tau_{p2}=0,433$ $\xi_{p2}=-0,445$

ponovnim segrevanjem lupine do temperature prvega preskoka τ_{p1} = 1,195 lahko celoten krog preskokov lupine ponovimo.

Stabilnostne razmere pri lupinah z drugačnimi vrednostmi začetne oblikovne funkcije F_0 so prikazane na sliki 6, pregledniče vrednosti za temperaturo preskoka τ_p in razmerje višin ξ_p v trenutku preskoka lupine pa so zapisane v preglednici 1.

Kritična vrednost začetne oblikovne funkcije F_0 izpod katere preskok lupine ni mogoč, znaša za lupine s Poissonovim količnikom μ = 1/3, $F_0 = F_{kr}$ = 8,93. Krivulja s F_0 = 0 ponazarja razmere pri okrogli bimetalni plošči. Potek krivulje za brezrazsežno temperaturo τ v odvisnosti od razmerja višin ξ je asimetrična glede na premico F_0 = 0.

D(0.752,0.805) at the temperature τ = 0.805. By heating the shell up to the temperature of the first snap-through τ_{p1} = 1.195, the whole cycle of the shell's snaps is repeated.

The snap-through behaviour of the shells with different values of the initial formative function F_0 is shown in Fig. 6, while the tabulated values of the snap-through temperature τ_p and the ratio of height ξ_p at the moment of the shell's snap-through are presented in Table 1.

The critical value of the initial formative function F_0 under which the shell's snap-through is not possible amounts to $F_0 = F_{kr}$ = 8.93 for the shells with Poisson's ratio μ = 1/3. The curve with F_0 = 0 shows the conditions for the round bimetallic plate. The curve's line for dimensionless temperature τ relative to ratio ξ, is asymmetrical with respect to the straight line F_0 = 0.

Na sliki 7 sta prikazani krivulji za temperaturo prvega preskoka τ_{p1} in razmerje višin ξ_{p1} v odvisnosti od začetne oblikovne funkcije F_0.

Posledica temperaturne obremenitve prosto položene lupine je tudi vodoravni premik, določen z razliko med Eulerjevo in Lagrangevo koordinato *X-x*.

Enačba (48) za Eulerjevo koordinato *X* je, potem ko izrazimo komponento *u* vektorja premika $\vec{u}$ iz enačbe (52), specifično deformacijo ε_φ pa iz enačb (44) in (45):

Fig. 7 shows the curvatures for the temperature of the first snap-through τ_{p1} and the ratio of heights ξ_{p1} depending on the initial formative function F_0.

The consequence of the temperature loading of the simply roller-supported shell is also a horizontal displacement, determined by the difference between the Euler and Lagrange coordinates *X-x*.

After expressing the component *u* of the displacement vector $\vec{u}$ from Equation (52) and the normal strain ε_φ from Equations (44) and (45), Equation (48) for the Euler coordinate *X* is:

$$X = a\sqrt{\chi}\left(1 + \frac{n_\varphi - \mu n_\psi}{A\left(1-\mu^2\right)} + \frac{PT}{A\left(1+\mu\right)}\right) \qquad (96).$$

Enotsko silo n_ψ izrazimo iz enačbe (67), enotsko silo n_φ pa z zvezo med obema enotskima silama iz enačbe (59). Vodoravni premik $X(\chi,\tau)$ je torej pri danih parametrih lupine odvisen od napetostne funkcije $G(\chi,\tau)$:

The unit force n_ψ is expressed by Equation (67) and the unit force n_φ by the connection between both unit forces by means of Equation (59). Hence, the horizontal displacement $X(\chi,\tau)$, for the given parameters of the shell, depends on the stress function $G(\chi,\tau)$:

$$X\left(\chi,\tau\right) = a\sqrt{\chi}\left(1 + \frac{C\left(2G'\chi + G\left(1-\mu\right)\right)}{a^2 A\left(1-\mu^2\right)} + \frac{P\cdot\tau\cdot T_M}{A\left(1+\mu\right)}\right) \qquad (97).$$

Za primer smo izračunali brezrazsežni vodoravni premik $(X(a) - a)/a$ v odvisnosti od temperature *t* za lupino s parametri :

As an example, we have calculated the dimensionless horizontal displacement $(X(a) - a)/a$ depending on the temperature τ for the shell with the parameters:

$$F_0 = 12,\quad \mathrm{h}_0 = 0{,}78mm,\quad \mathrm{a{=}15mm},\quad \delta\mathrm{{=}0{,}3mm},\quad \alpha_1 = 3{,}41\cdot 10^{-5}\,/\,K,\quad \alpha_2 = 1{,}41\cdot 10^{-5}\,/\,K$$

Kakor je razvidno s slike 8, se vodoravni premik bimetalne lupine s temperaturo veča. Največji vodoravni premik je v trenutku preskoka v

As shown in Fig. 8, the horizontal displacement of the bimetallic shell increases with temperature. The biggest horizontal displacement is at the beginning of

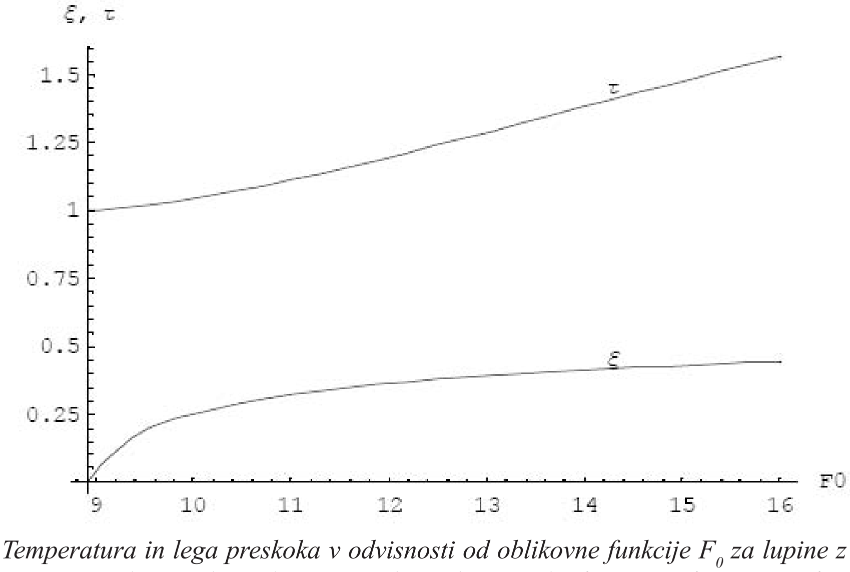

Sl. 7. *Temperatura in lega preskoka v odvisnosti od oblikovne funkcije F_0 za lupine z μ = 1/3*

Fig. 7. *Temperature and snap-through position depending on the formative function F_0 for the shells with μ = 1/3*

$F_0 = 12,\ \ h_0 = 0,78mm,\ \ a=15\text{mm},\ \ \delta=0,3\text{mm},\ \ \alpha_1 = 3,41\cdot10^{-5}\,/\,K,\ \ \alpha_2 = 1,41\cdot10^{-5}\,/\,K$

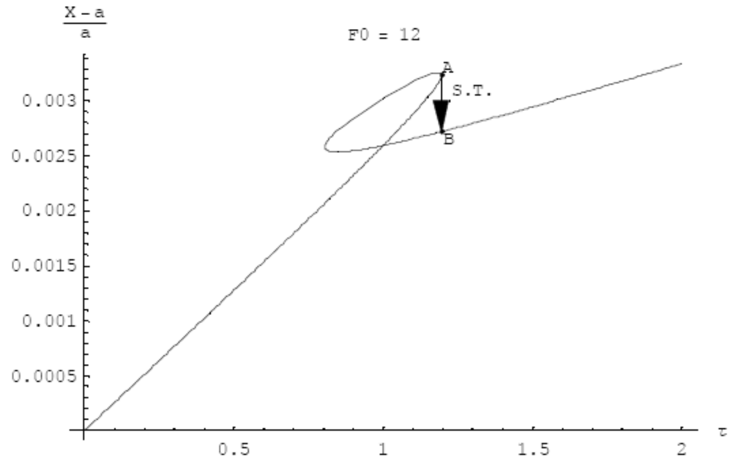

Sl. 8. *Vodoravni premik na robu lupine v odvisnosti od temperature t za prosto položeno lupino*
Fig. 8. *Horizontal displacement at the edge of the simply-roller supported shell relative to temperature* τ

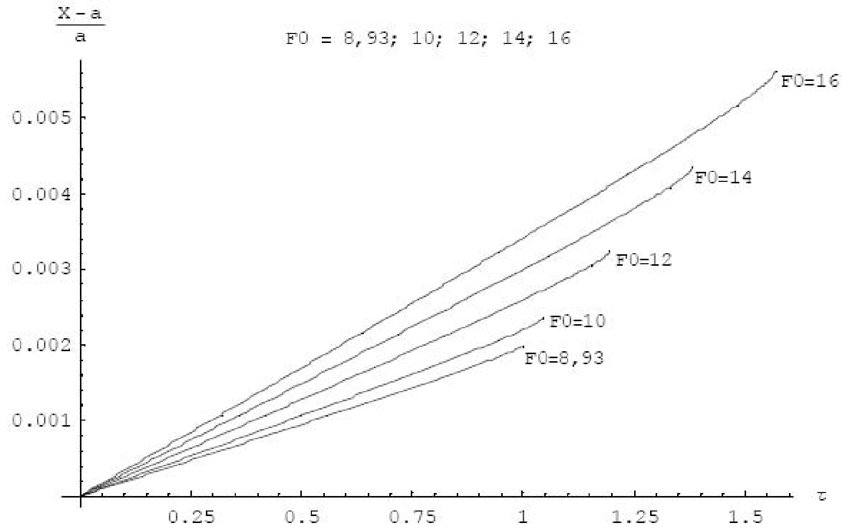

Sl. 9. *Vodoravni premik na robu lupine za prosto položene lupine različnih vrednosti začetne oblikovne funkcije* F_0
Fig. 9. *Horizontal displacement at the edge of the simply-roller supported shell of various values of the initial formative function* F_0

točki *A*. Po preskoku zavzame lupina novo ravnovesno lego, vodoravni premik pa preide v točko *B*.

Na sliki 9 je prikazan vodoravni premik na robu lupine za lupine z debelino δ = 0,3 mm, tlorisnim polmerom a = 15 mm, razteznostnima koeficientoma $\alpha_1 = 3{,}41\cdot10^{-5}$ /K in $\alpha_2 = 1{,}41\cdot10^{-5}$ /K ter začetno oblikovno funkcijo F_0, kar izhaja s slike. S povečevanjem začetne višine h_0 in s tem

the snap-through process, at the point *A*. After the snap-through, the shell assumes a new equilibrium position, while the horizontal displacement passes to the point *B*.

Fig. 9 shows the horizontal displacement at the edge of the shell with thickness δ= 0.3 mm and horizontal radius a = 15 mm, coefficients of linear temperature expansion $\alpha_1 = 3.41\cdot10^{-5}$ /K and $\alpha_2 = 1.41\cdot10^{-5}$ /K and initial formative function F_0, as follows from the graphical presentation. By increasing the initial height h_0 and funkcije F_0 poleg temperature preskoka se zvečuje tudi vodoravni premik na robu lupine v $x = a$.

Obravnavali bomo tudi preskok sistema lupine z vrtljivim vodoravno nepomično vpetim robom. Takšen je primer, če lupino vstavimo v valj ter tako preprečimo širjenje lupine v smeri osi X. V tem primeru vpetja je premer lupine a med temperaturnim obremenjevanjem stalen: $a(T) = a =$ konst. Veljata robna pogoja: $\varepsilon_\varphi(1) = 0$; $m_\psi(1) = 0$.

Specifična deformacija ε_φ ima v primeru, ko sta debelini slojev enaki $\delta_1 = \delta_2 = \delta/2$ naslednjo obliko:

subsequently the function F_0, as well as an increase in the snap-through temperature the horizontal displacement at the edge of the shell at $x = a$ is increased too.

The next example we will discuss is the snap-through of the simply bearing-supported shell. This is the case when the shell is inserted into a cylinder, preventing in this way the expansion of the shell in the direction of the X axis. In this type of support, the radius of the shell a remains constant: $a(T) = a =$ const. during the temperature loading. The boundary conditions are: $\varepsilon_\varphi(1) = 0$; $m_\psi(1) = 0$.

The normal strain ε_φ has, in the case where the thicknesses of layers are equal, the following form:

$$\varepsilon_\varphi = \frac{\left(n_\varphi - \mu n_\psi\right) + PT\left(1-\mu\right)}{A\left(1-\mu^2\right)} \qquad (98).$$

Ker se n_ψ in n_φ v (98) izražata z enačbama (67) in (59), zapišemo problem robnih vrednosti za vrtljivo vodoravno nepomično vpeto lupino:

Because n_ψ and n_φ in (98) are expressed by Equations (67) and (59) we can write the boundary-value problem for simply bearing-supported shells:

$$\begin{gathered} 4g'' = F_0^2 - \frac{f^2}{\chi^2}, \quad 4f'' = \frac{f \cdot g}{\chi^2} \\ g(0) = f(0) = 0, \quad g'(1) - g(1)\left(\frac{1+\mu}{2}\right) = \frac{-\sqrt{2/3} \cdot F_0\left(\alpha_1 + \alpha_2\right)\sqrt{1-\mu^2}}{\alpha_1 - \alpha_2} \cdot \tau \\ \tau = 1 - \frac{1}{F_0\left(1+\mu\right)}\left(2f'(1) - f(1)\cdot(1-\mu)\right) \end{gathered} \qquad (99).$$

Sistem enačb (99) smo rešili numerično s predhodno opisano nelinearno strelsko metodo.

The system of Equations (99) was solved numerically using the above-described non-linear

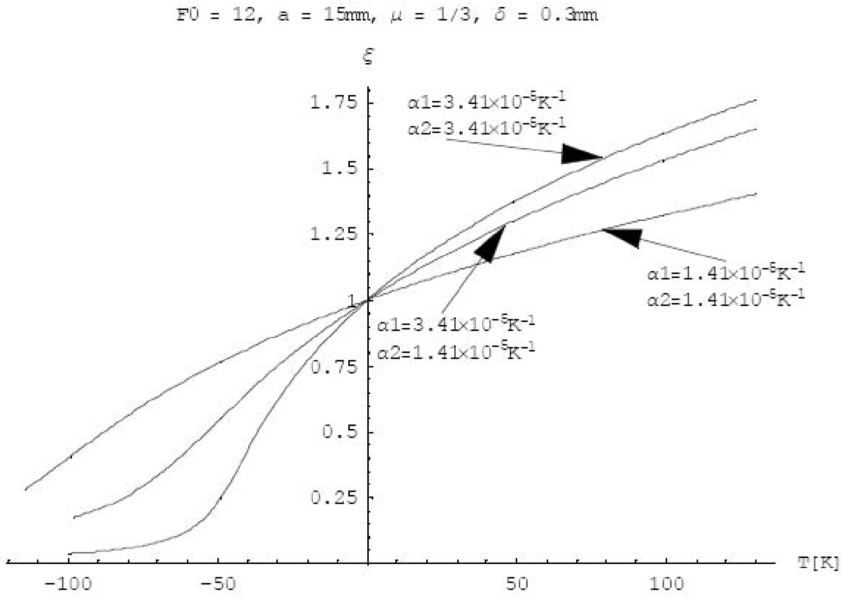

Sl. 10. *Razmerje višin ξ v odvisnosti od temperature T za vrtljivo vodoravno nepomično vpeto lupino*
Fig. 10. *Ratio of heights ξ relative to the temperature T for simply bearing-supported shell*

Izbrali smo približni začetni vrednosti za funkciji g in f v točki $\chi = 1$ ter problem začetnih vrednosti rešili po metodi Runge Kutta 4. reda. Bolj natančne funkcijske vrednosti $g(1)$ in $f(1)$ smo spet računali z Newtonovo metodo za reševanje nelinearnih enačb.

Na sliki 10 so predstavljene razmere pri temperaturnem obremenjevanju vrtljivo vodoravno nepomično vpete lupine za številčni primer $F_0 = 12$; $a = 15$ mm; $\mu = 1/3$; $\delta = 0{,}3$ mm.

Pri takšnem vpetju bimetalne lupine se razmerje višin ξ s povečevanjem temperature povečuje. Zaradi segrevanja se lupina razteza. Ker je raztezanje lupine v vodoravni smeri onemogočeno, se lupina razteza v smeri navpičnice. S temperaturo T se povečuje trenutna višina lupine Y in s tem razmerje ξ. Ker funkcija $\xi(T)$ nima lokalnega ekstrema sklepamo, da vrtljivo vpeta lupina za ta primer nima preskoka. Podobne razmere opažamo tudi pri enoslojnih lupinah oziroma lupinah z nespremenljivim koeficientom linearnega temperaturnega raztezka $\alpha_1 = \alpha_2$. Kakor je razvidno s slike 10, je deformacija bimetalne lupine s temperaturnim raztezkom slojev $\alpha_1 > \alpha_2$ nekje med deformacijama enoslojnih lupin z nespremenljivim temperaturnim raztezkom α_1 in α_2. Deformacijske krivulje, ki prikazujejo obliko lupine glede na temperaturno obremenitev, so razvidne s slike 11.

shooting method. The approximate initial values for the functions g and f at the point $\chi = 1$ were selected and the problem of the initial values solved by the Runge Kutta method of the fourth order. More precise functional values $g(1)$ and $f(1)$ were again calculated by means of Newton's method for solving non-linear equations.

Fig. 10 shows the conditions in the temperature loading of simply bearing-supported shells for the numerical sample $F_0 = 12$; $a = 15$ mm; $\mu = 1/3$; $\delta = 0.3$ mm.

In this example of the bimetallic shell, the ratio ξ increases with increasing temperature. Because of the heating, the shell is expanding. And since the expansion of a shell in the horizontal direction is not possible, the shell is expanding in the vertical direction. Along with the temperature T the height of the shell Y is also expanding, and with this the ratio ξ. Since the function $\xi(T)$ does not have a local extreme we can conclude that shells with a simple bearing-support do not have a snap-through. Similar results were also observed in the single-layer shells with a constant coefficient of linear temperature expansion $\alpha_1 = \alpha_2$. As seen from Fig. 10, the deformation of the bimetallic shell with a temperature expansion of layers $\alpha_1 > \alpha_2$ is somewhere between the deformations of single layer shells with constant temperature expansion α_1 and α_2. The deformation states of the shell relative to the temperature are shown in Fig. 11.

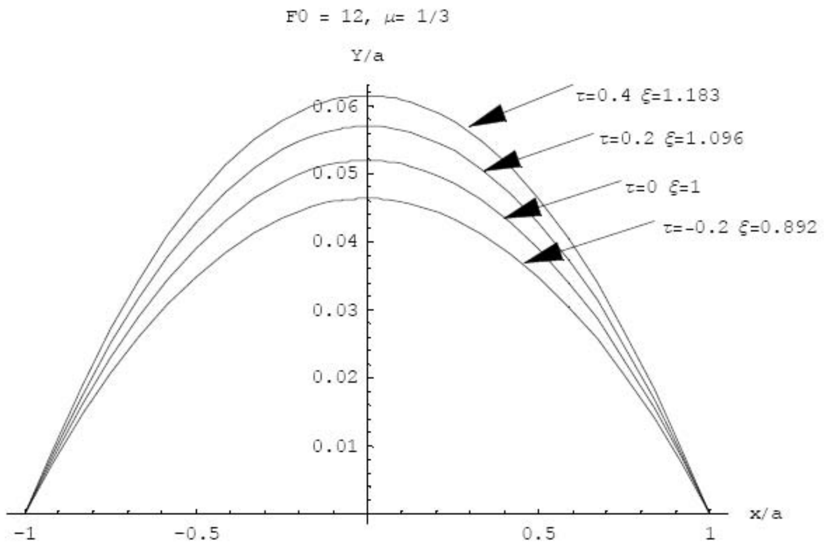

Sl. 11. *Deformacijske krivulje za vrtljivo vodoravno nepomično vpeto lupino s $F_0 = 12$ in $\mu = 1/3$*
Fig. 11. *Displacement states for simply bearing-supported shell with $F_0 = 12$ and $\mu = 1/3$*

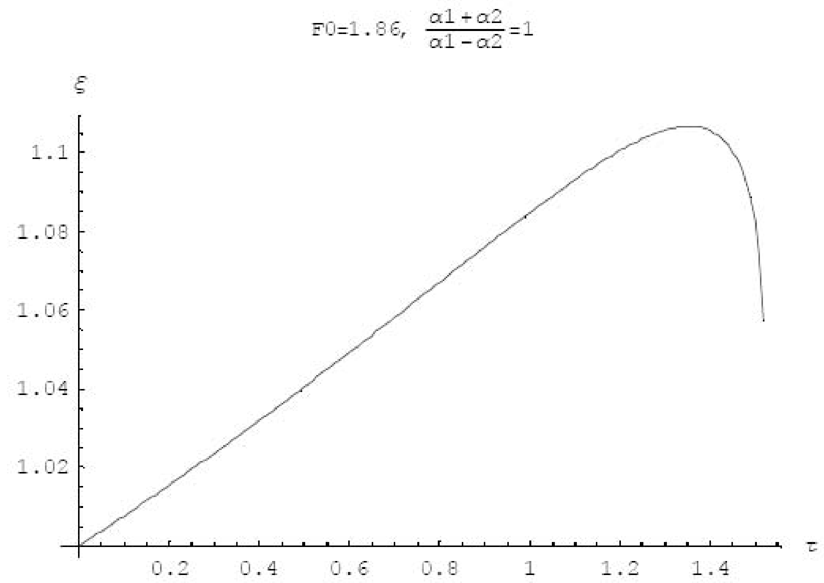

Sl. 12. *Razmerje višin ξ v odvisnosti od temperature T za vrtljivo vodoravno nepomično vpeto lupino z μ = 1/3, $(\alpha_1 + \alpha_2)/(\alpha_1 - \alpha_2) = 1$ in F_0 = 1,86*

Fig. 12. *Ratio of heights ξ relative to temperature T for simply bearing-supported shell with μ = 1/3, $(\alpha_1 + \alpha_2)/(\alpha_1 - \alpha_2) = 1$ and F_0 = 1.86*

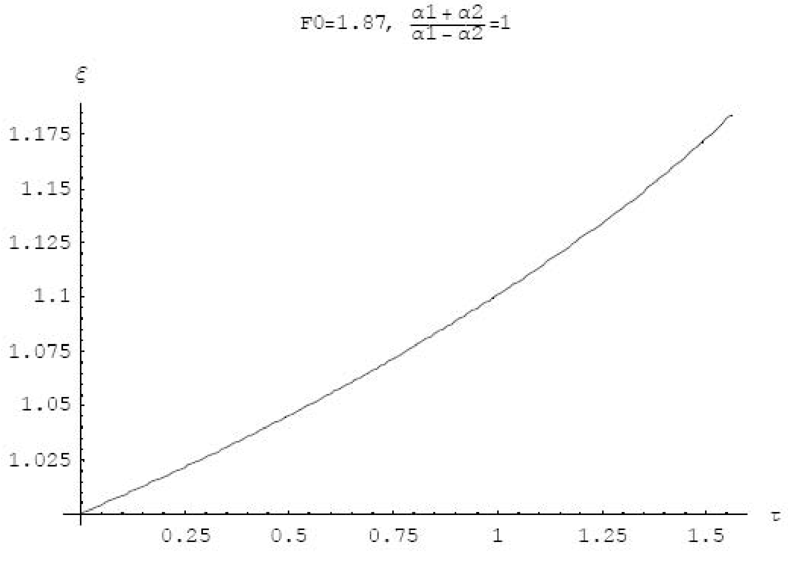

Sl. 13. *Razmerje višin ξ v odvisnosti od temperature T za vrtljivo vodoravno nepomično vpeto lupino z μ = 1/3, $(\alpha_1 + \alpha_2)/(\alpha_1 - \alpha_2) = 1$ in F_0 = 1,87*

Fig. 13. *Ratio of heights ξ relative to the temperature T for simply bearing-supported shell with μ = 1/3, $(\alpha_1 + \alpha_2)/(\alpha_1 - \alpha_2) = 1$ in F_0 = 1.87*

Analizirali smo tudi razmere pri zelo plitvih lupinah z majhno začetno višino h_0. Izkazalo se je, da se pri takšnih lupinah razmerje višin $\xi(T)$ z višanjem temperature T zmanjšuje, če je le začetna oblikovna funkcija F_0 dovolj majhna glede na

We have also analyzed the conditions in very shallow shells with a small initial height h_0. It turned out that in such shells the ratio $\xi(T)$ decreased with increasing temperature T only if the initial formative function F_0 was small enough compared to the ratio razmerje $(\alpha_1 + \alpha_2)/(\alpha_1 - \alpha_2)$ v sistemu enačb (99). Največja vrednost za začetno oblikovno funkcijo, pri kateri se razmerje višin $\xi(T)$ z višanjem temperature T še vedno zmanjšuje, znaša $F_0 = 1{,}86$ (sl. 12). Takrat ima razmerje med vsoto in razliko razteznostnih koeficientov najmanjšo mogočo vrednost $(\alpha_1 + \alpha_2)/(\alpha_1 - \alpha_2) = 1$.

Če vrednost začetne oblikovne funkcije F_0 le malenkostno povečamo, se bo razmerje višin $\xi(T)$ z višanjem temperature T zvečalo, kar je razvidno s slike 13.

V primeru konzolno vpete lupine sta robna pogoja: $\varepsilon_\varphi(1) = 0$; $Y'(1) = y'(1) =$ konst. Funkciji Y' in y' izrazimo iz enačb (69) in (68). Po krajšanju enakih členov je robni pogoj: $F(1) = F_0$. Problem robnih vrednosti za konzolno vpeto lupino je s tem:

$(\alpha_1 + \alpha_2)/(\alpha_1 - \alpha_2)$ in the system of equations (99). The highest value for the initial formative function, in which the ratio of heights $\xi(T)$ with increasing temperature T is still decreasing, is $F_0 = 1.86$, Fig. 12. In this case the relation between the sum and the difference of the expansion factor has the smallest possible value $(\alpha_1 + \alpha_2)/(\alpha_1 - \alpha_2) = 1$.

If we only slightly increase the value of initial formative function F_0, the ratio $\xi(T)$ will increase with the increase of the temperature T, as is clear from Fig. 13.

In the case of the clamped shell, the boundary conditions are: $\varepsilon_\varphi(1) = 0$; $Y'(1) = y'(1) =$ const. The functions Y' and y' are expressed from Equations (69) and (68). After reducing the same terms, the boundary condition is: $F(1) = F_0$. Then, the boundary-value problem for the clamped shell is:

$$4g'' = F_0^2 - \frac{f^2}{\chi^2}, \quad 4f'' = \frac{f \cdot g}{\chi^2}$$
$$g(0) = f(0) = 0, \quad f(1) = F_0, \quad g'(1) - g(1)\left(\frac{1+\mu}{2}\right) = \frac{-\sqrt{2/3} \cdot F_0 \left(\alpha_1 + \alpha_2\right)\sqrt{1-\mu^2}}{\alpha_1 - \alpha_2} \cdot \tau \qquad (100).$$

Tokrat smo izbrali približni vrednosti za $g(1)$ in $f'(1)$. Ob vsakem koraku smo preverili, kolikšno je odstopanje od robnih pogojev v točki $\chi = 0$ ter z Newtonovo metodo izračunali boljša približka za $g(1)$ in $f'(1)$. Rezultati so razvidni s slik 14 in 15 in so podobni razmeram pri vrtljivo vodoravno nepomično vpeti lupini.

Razlika v stopnji deformacije različno vpetih lupin z enakimi snovno geometrijskimi značilkami je razvidna s slik 16 in 17. S C_0 smo označili obliko obeh lupin v nedeformiranem stanju, s C_1 obliko za vrtljivo vodoravno nepomično vpeto lupino in s C_2 obliko za konzolno vpeto lupino. Pri tem pomenita zgornji deformacijski krivulji obliko lupin pri temperaturi $\tau = 1$, spodnji krivulji pa obliko pri temperaturi $\tau = -1$. Kakor je razvidno s slike 16 je razlika v deformaciji različno vpetih lupin očitnejša šele pri večji temperaturni obremenitvi. Pri konzolno vpeti lupini se razmerje višin $\xi(T)$ z višanjem temperature T povečuje ne glede na vrednost začetne oblikovne funkcije F_0.

Oglejmo si še razmere pri analizi preskoka sistema pri prosto položeni lupini, ki je v temenu obremenjena z zunanjo silo $\vec{F}_k$. Ta obremenitveni primer opisujeta diferencialni enačbi (81) in (82). Iz primerjave enačb (74) in (75) izhaja, da je normalna enotska sila n_φ v primerjavi s strižno enotsko silo $\tau_{\psi r}$ majhna, zato jo zanemarimo: $n_\psi(1) \cong 0$.

We chose approximate values for $g(1)$ and $f'(1)$. In each step we checked how far the digression from the boundary conditions can go at point $\chi = 0$ and by means of Newton's method, better proximities for $g(1)$ and $f'(1)$ are computed The results can be seen in Figures 14 and 15; they are similar to the conditions found in the simple bearing-supported shell.

Displacement states for different kinds of boundary conditions of the shells of the same material and geometrical characteristics can be seen in Figures 16 and 17. C_0 denotes the shape of both shells in the undeformed state, C_1 denotes the simple bearing-supported shell and C_2 the clamped shell. In such case the upper displacement curves represent the shell's shape at temperature $\tau = 1$ and the lower ones the shape at the temperature $\tau = -1$. As is clear from Figures 16 and 17, the difference in the displacement of the various boundary conditions of the shells is clearly expressed only in the case of higher temperature loads. In the clamped shells, the ratio of heights $\xi(T)$ is increasing with increasing temperature T, regardless of the value of the initial formative function F_0.

The object of discussion is also the snap-through phenomenon in the simple roller-supported shell, which is additionally loaded with an external force $\vec{F}_k$ in its top. This loading example is outlined by the differential equations (81) and (82). When comparing Equations (74) and (75) it follows that the normal unit force n_φ compared to the tangential force τ_ψ is small, hence it can be neglected: $n_\psi(1) \cong 0$.

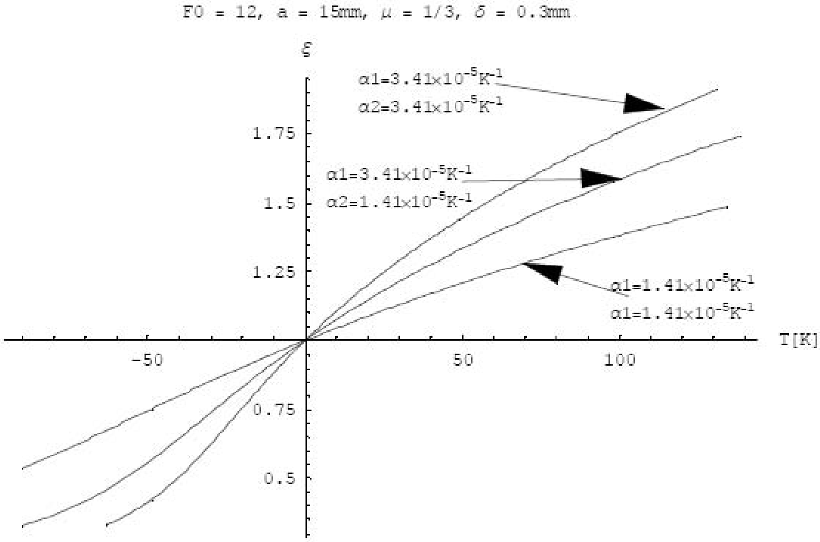

Sl. 14. *Razmerje višin ξ v odvisnosti od temperature T za konzolno vpeto lupino*
Fig. 14. *Ratio of heights ξ relative to the temperature T for clamped shell*

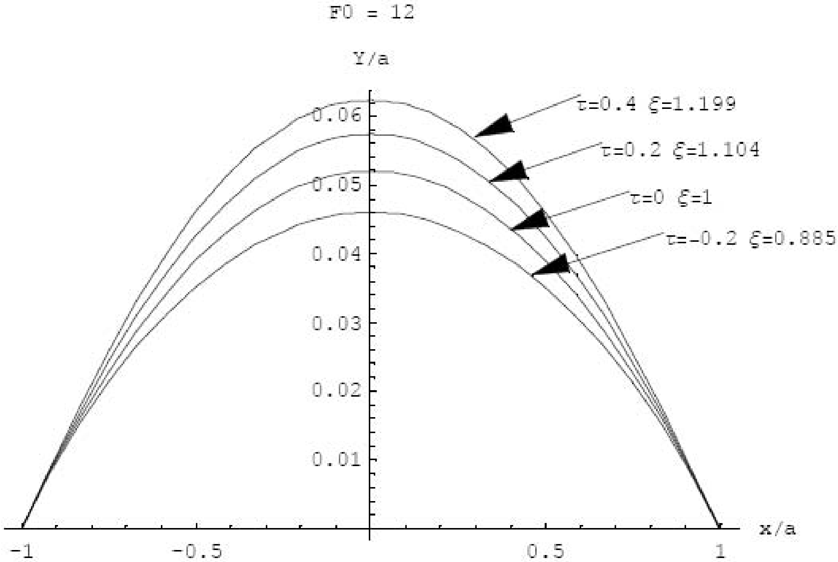

Sl. 15. *Deformacijske krivulje za konzolno vpeto lupino s F_0 = 12 in μ = 1/3*
Fig. 15. *Displacement states for clamped shell with F_0 = 12 and μ = 1/3*

Če ponovno upoštevamo, da sta funkciji G in F v točki $\chi = 0$ omejeni, zapišemo problem robnih vrednosti:

Considering that functions G and F at point $\chi = 0$ are limited, the boundary-value problem can be expressed as:

$$4g'' = F_0^2 - \frac{f^2}{\chi^2},\quad 4f'' = \frac{f \cdot g}{\chi^2} + \frac{f_k}{\chi}$$
$$g(0) = g(1) = f(0) = 0,\quad \tau = 1 - \frac{1}{F_0(1+\mu)}\left(2f'(1) - f(1)\cdot(1-\mu)\right) \tag{101}$$

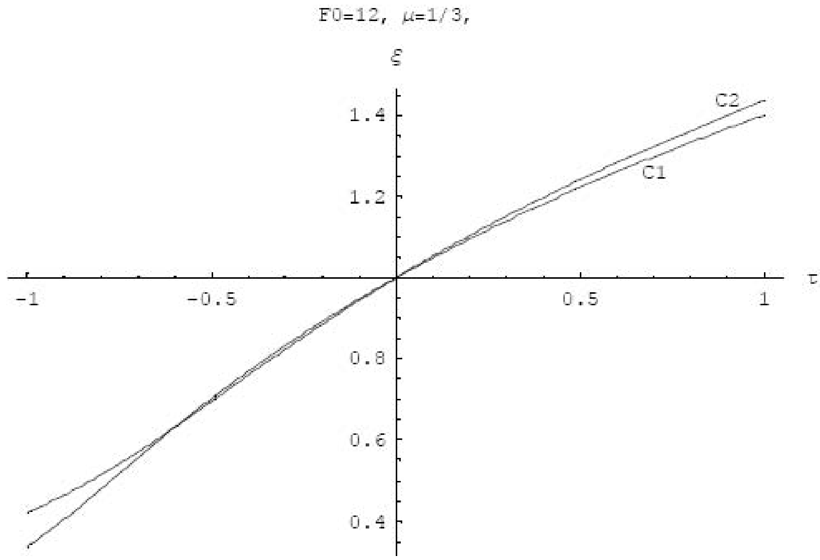

Sl. 16. *Razmerje višin ξ pri vrtljivo vodoravno nepomično vpeti lupini (C_1) in konzolno vpeti lupini (C_2) v odvisnosti od temperaturnega obremenjevanja za lupine s $F_0 = 12$ in $\mu = 1/3$*

Fig. 16. *Ratio of heights ξ in simply bearing-supported shell (C_1) and clamped shell (C_2) depending on temperature loading for shells with $F_0 = 12$ and $\mu = 1/3$*

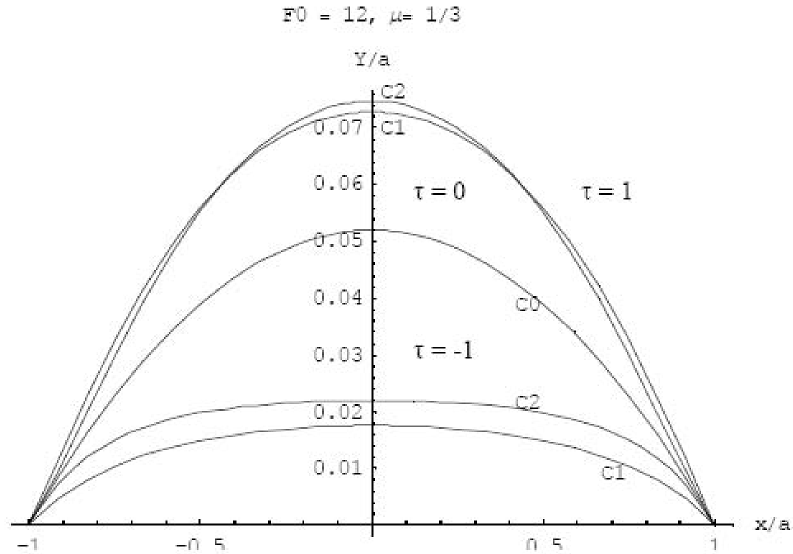

Sl. 17. *Deformacijske krivulje pri vrtljivo vodoravno nepomično vpeti lupini (C_1) in konzolno vpeti lupini (C_2) za temperaturne vrednosti $\tau = 0$, $\tau = -1$, $\tau = 1$*

Fig. 17. *Displacement states in simply bearing-supported shell (C_1) and clamped supported shell (C_2) for . temperature values $\tau = 0$, $\tau = -1$, $\tau = 1$*

kjer je f_k, po analogiji z brezrazsežnotemperaturo τ, brezrazsežna sila, F_M pa nespremenljiva:

where f_k is a dimensionless force, and F_M is a constant:

$$F_k = f_k \cdot F_M; \quad F_M = \frac{2\pi}{a^2}\sqrt{\frac{2C^3}{A\left(1-\mu^2\right)}} = \frac{E\,\pi\,\delta^4}{a^2 6\sqrt{6\left(1-\mu^2\right)^3}}$$

Reševanje sistema enačb (101) je potekalo po prej opisani numerični metodi. Zaradi nazornosti

To solve the system of Equations we use the above-described numerical method. For the sake of

Preglednica 2. *Temperatura in lega preskoka lupine za različne vrednosti sile F_k*
Table 2. *Temperature and shell's snap-through position for different force values F_k*

$F_k\,[N]$	$0N$	$10N$	$20N$	$30N$	$F_{kr}=34,44N$	$40N$
$S.T.1$	$\tau_{p1}=1,195$ $\xi_1=0,361$	$\tau_{p1}=0.879$ $\xi_{p1}=0.366$	$\tau_{p1}=0.535$ $\xi_{p1}=0,360$	$\tau_{p1}=0.166$ $\xi_{p1}=0,335$	$\tau_{p1}=0$ $\xi_{p1}=0,312$	$\tau_{p1}=-0,214$ $\xi_{p1}=0,269$
$S.T.2$	$\tau_{p2}=0,805$ $\xi_{p2}=-0,361$	$\tau_{p2}=0.510$ $\xi_{p2}=-0.348$	$\tau_{p2}=0.231$ $\xi_{p2}=-0,327$	$\tau_{p2}=-0,040$ $\xi_{p2}=-0,293$	$\tau_{p2}=-0.159$ $\xi_{p2}=-0,274$	$\tau_{p2}=-0,308$ $\xi_{p2}=-0,240$

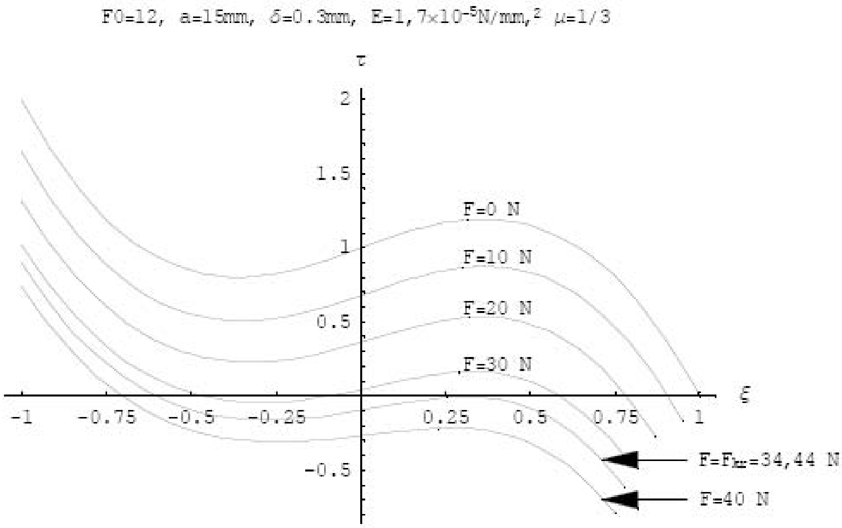

Sl. 18. *Stabilnostne razmere pri različnih vrednostih sile F_k*
Fig. 18. *Snap-through behaviour for different force values F_k*

predstavljamo grafične in pregledniče rezultate za lupino z naslednjimi podatki:

$$F_0=12,\quad h_0=0,78mm,\quad a=15mm,\quad \delta=0.3mm,\quad E=1,7\cdot 10^5\,MPa \tag{102}$$

S slike 18 je razvidno, da se temperatura preskoka lupine τ_p znižuje z večanjem sile F_k. Pri sili F_k = 0 smo za temperaturo τ_p in lego ξ_p preskoka lupine dobili enake rezultate, kakor smo jih predhodno izračunali za samo temperaturno obremenjeno lupino. Temperaturo preskoka τ_{p1} za vmesne vrednosti sile F_k v območju [0,40] smo določili z interpolacijskim polinomom 4. stopnje (sl. 19):

clarity, the graphical and tabular results for the shell are shown below, with the following data:

From Fig.18 it follows that the snap-through temperature τ_p is decreasing with increasing force F_k. For the force F_k = 0 we get the same results for the temperature τ_p and position ξ_p of shell's snap-through as those previously calculated for the shell that was loaded only by temperature. The snap-through temperature τ_{p1} for the intermediate values of the force F_k in the interval [0,40] was determined by the interpolating polynomial of the fourth degree, Fig. 19:

$$\tau_{p1}\left(F_k\right)=1,195-3,03\cdot 10^{-2}F_k-1,045\cdot 10^{-4}F_k^2-2,25\cdot 10^{-6}F_k^3+4,583\cdot 10^{-8}F_k^4 \tag{103}$$

S polinomom (103) smo določili kritično silo F_{kr}, pri kateri lupina preskoči pri temperaturi $\tau=0$:

Using the polynomial (103) the critical force F_{kr}, at which the shell snaps-through at temperature $\tau=0$, is determined:

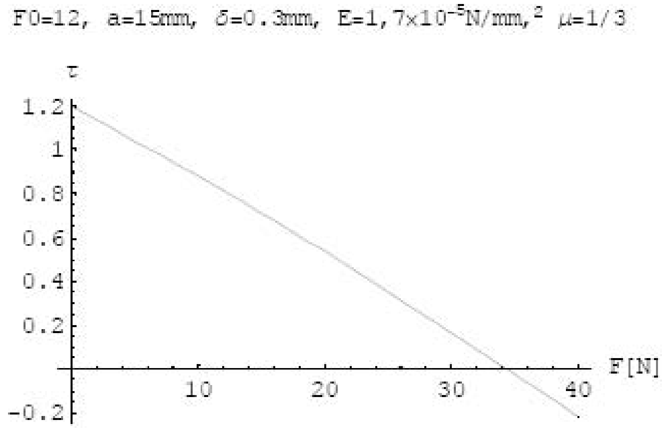

Sl. 19. *Temperatura preskoka* τ_{p1} *v odvisnosti od zunanje sile* $\vec{F}_k$

Fig. 19. *Snap-through temperature* τ_{p1} *depending on the external force* $\vec{F}_k$

Pri kritični sili F_{kr} = 34,44 N lupina preskoči, ne da bi jo bilo potrebno segrevati. Če se po preskoku lupine sila zmanjša, se zmanjša tudi razmerje višin ξ. Kadar je lupina dovolj plitva, se po prenehanju sile vrne v izhodiščno lego. Obravnavana lupina je že takšna, saj je pri mehansko neobremenjeni lupini F_k = 0 možno samo eno ravnovesno stanje pri temperaturi τ = 0 in sicer pri razmerju višin ξ = 1. Da bi lupina po prenehanju kritične sile F_{kr} ne preskočila v izhodiščno lego, mora krivulja za temperaturo τ v odvisnosti od razmerja višin ξ sekati negativni del abscisne osi ali se je vsaj dotakne. Samo v tem primeru sta mogoči dve stabilni ravnovesni stanji in razmerje višin $\xi \neq 1$ pri temperaturi τ = 0. Približno najmanjšo vrednost začetne oblikovne funkcije $F_{0\min}$ izračunamo z interpolacijskim polinomom. Interpoliramo preglednico 1, in sicer temperaturo τ_{p2} drugega preskoka (S.T.2) z začetno oblikovno funkcijo F_0 v območju $[8,93 \le F_0 \le 16]$:

At the critical force F_{kr} = 34.44 N the shell snaps-through without being heated up. If after the shell's snap-through the force decreases, the ratio ξ is decreased too. When the shell is shallow enough, on removal of the force it returns to the initial position. The shell we are discussing is of this type, because only one equilibrium state is possible at temperature τ = 0 at ξ = 1 if there is no external force in the top of the shell. To prevent the shell snapping-through into the initial position on removal of the critical force F_{kr} the curve for the temperature τ depending on the ratio ξ should be crossing the negative part of the abscissa axis or at least touch it. Only in this way are two stable equilibrium conditions and a ratio of heights $\xi \neq 1$ possible at the temperature τ = 0. As an approximation, the lowest value of the initial formative function $F_{0\min}$ is calculated using the interpolating polynomial. In Table 2 we interpolate the temperature τ_{p2} of the second snap-through (S.T.2) with the initial formative function F_0 in the interval $[8,93 \le F_0 \le 16]$:

$$\tau_{p2}\left(F_0\right) = -2,85 + 1,23F_0 - 1,36 \cdot 10^{-1} F_0^2 + 6,26 \cdot 10^{-3} F_0^3 - 1,07 \cdot 10^{-4} F_0^4$$

Postavimo:

Thus:

$$\tau_{p2}\left(F_{0\min}\right) = 0 \Rightarrow F_{0\min} \cong 19,96$$

Ekstrapolirana vrednost za $F_{0\min}$ je seveda približna, ker leži zunaj interpolacijskega območja [8,93;16]. Vseeno je dober približek za numerični izračun temperature preskoka τ_{p2}. V drugi iteraciji že dobimo praktično dovolj natančno vrednost, $F_{0\min}$ = 21,66 s temperaturo 2. preskoka τ_{p2} = -0,0001 in razmerjem ξ_{p2} = -0,530.

The extrapolated value $F_{0\min}$ is an approximate value, since it lies outside the interpolation interval [8.93,16]. Nevertheless, it is a good approximation for the numerical calculation of the temperature τ_{p2} snap-through. In the second iteration we already obtain a sufficiently accurate value, $F_{0\min}$ = 21.66 with the temperature of the second snap-through τ_{p2} = -0.0001 and the ratio ξ_{p2} = -0.530.

6 SKLEP

Prosto položene tankostenske plitve bimetalne lupine imajo lastnost, da pri določeni temperaturi preskočijo v novo ravnovesno lego. Temperatura preskoka T_p je odvisna od snovno geometrijskih lastnosti lupin. Kot poseben primer smo analizirali razmere pri sferičnih lupinah, ki imajo oba sloja enako debela $\delta_1 = \delta_2 = \delta/2$, sloja pa imata tudi enak Poissonov koeficient $\mu_1 = \mu_2 = \mu$. Iz enačbe (89) izhaja, da je lega preskoka ξ_p, pri lupinah z enako debelino δ in Poissonovim številom μ, odvisna samo od začetne višine lupine h_0. Ukrivljenost lupine $1/R$ in razlika temperaturnih koeficientov linearnega raztezka α_1 - α_2 vplivata samo na temperaturo preskoka T_p, ne pa tudi na lego preskoka ξ_p. Pri plitvih enoslojnih lupinah z nespremenljivim koeficientom linearnega temperaturnega raztezka $\alpha(z) = \alpha$ = konst ostaja razmerje višin $\xi(T)$ stalno ne glede na temperaturno obremenitev. Z višanjem temperature T se veča vodoravni premer lupine a, medtem ko ostaja navpična komponenta deformacije Y na robu lupine ves čas enaka:

6 CONCLUSION

In thin-walled, shallow bimetallic shells a snap-through into a new equilibrium state occurs when a certain temperature is reached. The snap-through temperature T_p depends on the material and the geometrical properties of the shell. As a special case, the stability conditions for spherical shells whose two layers have equal thickness $\delta_1 = \delta_2 = \delta/2$ and the same Poisson's ratio $\mu_1 = \mu_2 = \mu$ were analyzed. From Equation (89) it follows that the position of a snap-through ξ_p, in shells with equal thickness δ and Poisson's number μ, depends only on the initial value of the shell's height h_0. The curvature of the shell $1/R$ and the difference in the coefficients of the linear expansion α_1 - α_2 affect only the snap-through temperature T_p and have no influence on the snap-through ξ_p position. In shallow, single-layer shells with a constant coefficient of the linear temperature expansion $\alpha(z) = \alpha$ = const. the ratio of heights $\xi(T)$ remains constant, regardless of the temperature loading. With increasing temperature T the shell's horizontal radius a increases while the vertical component of the deformation Y at the edge of the shell always remains the same:

$$Y(a) = y(a) = \text{konst} \qquad (104).$$

Iz enačbe (104) izhaja, da enoslojne lupine nimajo preskoka. Prav tako nimajo preskoka plitve bimetalne lupine, ki imajo vrednost začetne oblikovne funkcije $F_0 < 8{,}93$, če znaša Poissonov koeficient $\mu = 1/3$. Da se pojavi pri bimetalnih lupinah preskok, je treba poleg dovolj visoke temperature zagotoviti, da se rob lupine lahko v vodoravni smeri prosto razteza. Največji vodoravni premik nastane na robu lupine v trenutku preskoka lupine. Bimetalne lupine z večjo začetno višino h_0 imajo ob enakih snovno geometrijskih značilkah večji vodoravni premik.

Vpete bimetalne lupine se v vodoravni smeri ne morejo raztezati. Ker je raztezanje takšne lupine v vodoravni smeri onemogočeno, se lupina razteza v smeri navpičnice, zaradi česar se razmerje višin $\xi(T)$ s povečevanjem temperature povečuje, $\xi(T) > 1$ za $T < 0$, razen pri vrtljivo vodoravno nepomično vpeti lupini z majhno začetno oblikovno funkcijo F_0.

Če na lupino poleg spremembe temperature T deluje tudi sila F_k v temenu lupine, se pojavi preskok lupine pri nižji temperaturi τ_p. Pri dovolj veliki sili F_{kr} lupina preskoči, ne da bi jo bilo treba dodatno segrevati. Velikost kritične sile F_{kr} je odvisna od snovno geometrijskih lastnosti lupine v enačbah

From Equation (104) it follows that single-layer shells have no snap-through. Also, very thin bimetallic shells with the initial formative function $F_0 < 8.93$ and Poisson's ratio $\mu = 1/3$ have no snap-through. In order that snap-through can occur in bimetallic shells, it is necessary, besides a high enough temperature, to ensure that the edge of the shell can freely expand in the horizontal direction. The greatest horizontal displacement occurs at the edge of a shell at the moment of the shell's snap-through. Bimetallic shells with a greater initial height h_0 have, for the same material and geometrical characteristics, a greater horizontal displacement.

Clamped bimetallic shells cannot expand in the horizontal direction. Because the expansion in the horizontal direction of such shell is prevented, the shell is expanding vertically. Consequently, the ratio of heights $\xi(T)$ increases along with the temperature increase $\xi(T) > 1$ for $T < 0$, except in simple bearing-supported shells with a small initial formative function F_0.

When in addition to the temperature T, also a force F_k is acting on the shell's top, the snap-through occurs at a lower temperature τ_p. When the force F_{kr} is high enough, the shell snaps-through without the need to be additionally loaded with temperature. The value of the critical force F_{kr} depends on the material and the geometrical

(102). Po prenehanju kritične sile se lupina vrne v začetno ravnovesno lego, razen pri manj plitvih lupinah, pri katerih je vrednost začetne oblikovne funkcije $F_{0\min} \geq 21,66$ za lupine z značilkami v enačbah (102).

properties of the shell in Equations (102). When the force is removed, the shell returns to its initial equilibrium state, except in the case of shallower shells, whose value of initial formative function is $F_{0\min} \geq 21,66$ for shells with the characteristics in Equations (102).

7 OZNAKE
7 SYMBOLS

tlorisni polmer nedeformirane lupine	a	horizontal radius of undeformed shell
Youngov elastièni modul materiala 1 in 2	E_1, E_2	Young's elastic modulus of materials 1 and 2
zaèetna oblikovna nedeformirana funkcija	$F_0(\chi)$	initial formative function
trenutna oblikovna deformirana funkcija	$F(\chi)$	present formative function
sila v temenu lupine	F_k	force acting at the top of a shell
kritièna sila v temenu lupine	F_{kr}	critical force acting at the top of a shell
èleni potenène vrste trenutne oblikovne funkcije	f_i	elements of power series of the present formative function
napetostna funkcija	$G(\chi)$	stress function
èleni potenène vrste trenutne napetostne funkcije	g_i	elements of power series of the stress function
zaèetna višina nedeformirane lupine	h_0	initial height of the undeformed shell
razdalji osrednje ploskve od spodnje (h_1) oziroma zgornje (h_2) ploskve bimetalne lupine	h_1, h_2	middle plane distance from the lower (h_1) and upper (h_2) plane of the bimetallic shell
ukrivljenosti nedeformirane lupine	k_ψ, k_φ	the curvatures of the undeformed shell
ukrivljenosti deformirane lupine	$\overline{k}_\psi, \overline{k}_\varphi$	the curvatures of the deformed shell
notranja momenta v lupini	M_ψ, M_φ	internal moments in the shell
notranja enotska momenta v lupini	m_ψ, m_φ	internal unit moments in the shell
notranji sili v smeri normale v lupini	N_ψ, N_φ	internal forces in the direction normal to the shell
notranji enotski sili v smeri normale na lupino	n_ψ, n_φ	internal unit forces in the direction normal to the shell
polmer nedeformirane krogelne lupine	R	radius of the undeformed spherical shell
polmera ukrivljenosti nedeformirane lupine	r_ψ, r_φ	radii of the undeformed shell
polmera ukrivljenosti deformirane lupine	$\overline{r}_\psi, \overline{r}_\varphi$	radii of the deformed shell
dol□ina na nedeformirani lupini	s	the length on the undeformed shell
dol□ina na deformirani lupini	$\overline{s}$	the length on the deformed shell
primerjalna temperatura	T_0	reference temperature
temperatura, temperatura preskoka	T, T_p	temperature, snap-through temperature
notranja stri□na sila na lupini	$T_{\psi r}$	internal tangential force in the shell
notranja enotska stri□na sila v lupini	$t_{\psi r}$	internal unit tangential force in the shell
vektor premika	$\vec{u}$	displacement vector
èleni vektorja premika	u, v, w	elements of the displacement vector
sila podpore, enotska sila podpore	V, V_e	reaction force, unit reaction force
Lagrangev koordinatni sistem	(x, y, z)	Lagrange coordinates
Eulerjev koordinatni sistem	(X, Y, Z)	Euler coordinates
temperaturna koeficienta dol□inskega raztezka materiala 1 in 2	α_1, α_2	linear temperature expansion coefficients of material 1 and material 2

debelina lupine	δ	shell's thickness
debelini slojev iz materiala 1 in 2	δ_1, δ_2	thickness of layers made of material 1 and 2
deformacijski tenzor	ε_{ij}	strain tensor
Poissonovi števili za material 1 in 2	μ_1, μ_2	Poisson's ratios of materials 1 and 2
napetostni tenzor	σ_{ij}	stress tensor
brezrazse□na temperatura, temperatura preskoka	τ, τ_p	dimensionless temperature, snap-through temperature
brezrazse□na neodvisna spremenljivka	χ	dimensionless independent variable
razliki ukrivljenosti	$\Upsilon_\psi, \Upsilon_\varphi$	curvature differences
kota na nedeformirani lupini	ψ, φ	angles of the undeformed shell
kot na deformirani lupini	$\bar{\psi}$	angles of the deformed shell

8 LITERATURA
8 REFERENCES

[1] Timoshenko S. (1959) Theory of plates and shells. *McGraw-Hill Book*, New York.
[2] Alfutov N. A. (2000) Stability of elastic structures. *Springer-Verlag*.
[3] Reddy J. N. (1999) Theory and analysis of elastic plates. *Taylor & Francis*.
[4] Drole R., Kosel F. (1993) Stability analysis of shallow axi-symmetric bimetallic shells in a homogeneous temperature field. *The 14th Canadian Congress of Applied Mechanics*, Kingston, Ontario, June 1993.
[5] Drole R., Kosel F. (1994) Analysis of stress-strain state in shallow spherical bimetallic shells by non-linear theory, *Z. angew. Math. Mech*.
[6] Wittrick. W. H. (1953) Stability of bimetallic disk, *The Quarterly Journal of Mechanics and Applied Mathematics*.

Naslovi avtorjev: dr. Marko Jakomin
Univerza na Primorskem
Primorski inštitut za naravoslovne in tehnične vede,
Pristaniška cesta 14
6000 Koper
marko.jakomin@pint.upr.si

prof. dr. Franc Kosel
doc. dr. Tadej Kosel
Univerza v Ljubljani
Fakulteta za strojništvo
Aškerčeva 6
1000 Ljubljana
franc.kosel@fs.uni-lj
tadej.kosel@fs.uni-lj

prof. dr. Milan Batista
Univerza v Ljubljani
Fakulteta za pomorstvo in promet
Pot pomorščakov 4
6320 Portorož
milan.batista@fpp.edu

Authors' Addresses: Dr. Marko Jakomin
University of Primorska
Primorska Institute for Natural Sciences and Technology
Pristaniška cesta 14
6000 Koper , Slovenia
marko.jakomin@pint.upr.si

Prof. Dr. Franc Kosel
Doc. Dr. Tadej Kosel
University of Ljubljana
Faculty of Mechanical Eng.
Aškerčeva 6
1000 Ljubljana, Slovenia
franc.kosel@fs.uni-lj
tadej.kosel@fs.uni-lj

Prof. Dr. Milan Batista
University of Ljubljana
Faculty of Maritime studies and Transport
Pot pomorščakov 4
6320 Portorož, Slovenia
milan.batista@fpp.edu

Prejeto:
Received: 12.5.2005

Sprejeto:
Accepted: 22.6.2006

Odprto za diskusijo: 1 leto
Open for discussion: 1 year

Strojniški vestnik - Journal of Mechanical Engineering 52(2006)12, 817-834
UDK - UDC 628.1:53.08
Izvirni znanstveni članek - Original scientific paper (1.01)

Izbira merilnih mest v vodovodnih sistemih z genetskimi algoritmi

Sampling Design for Water Distribution System Models by Genetic Algorithms

Primož Banovec - Daniel Kozelj - Sašo Šantl - Franci Steinman
(Fakulteta za gradbeništvo in geodezijo, Ljubljana)

Obravnavana je izbira merilnih mest za umerjanje hidravličnih modelov vodovodnih sistemov. Izbira merilnih mest za umerjanje hidravličnih modelov je podana kot optimizacijski problem, ki je sestavljen iz dveh normaliziranih ciljnih funkcij. S prvo ciljno funkcijo se povečuje natančnost umerjanja parametrov hidravličnega modela, z drugo pa zmanjšuje število potrebnih merilnih mest. Predstavljeno je reševanje optimizacijskega problema z uporabo genetskih algoritmov. Overitev in uporaba razvitega optimizacijskega modela (imenovan IMMe) je bila opravljena na hidravličnem modelu teoretičnega vodovodnega sistema "Anytown", ki je namenjen kot primerjalni model za testiranje različnih raziskav pri hidravličnem modeliranju. Overjeni model IMMe je bil uporabljen na stvarnem vodovodnem sistemu mesta Sežane. Uporaba genetskih algoritmov se je v obeh primerih izkazala za zelo učinkovito optimizacijsko orodje pri izjemno kombinatornih optimizacijskih problemih. Razvita modela umerjanja in izbire merilnih mest omogočata vzpostavitev kar se da natančnih hidravličnih modelov vodovodnih sistemov, ki bodo v prihodnosti ključnega pomena za zagotavljanje gospodarnosti in učinkovitosti oskrbe s pitno vodo.

(Ključne besede: hidravlika, vodovodi, modeliranje, optimiranje, merilna mesta, algoritmi genetski)

In this paper we discuss sampling design for the calibration of water distribution system hydraulic models. The sampling design for the calibration of water distribution-system models is formulated as an optimisation problem consisting of two normalised objective functions. The first objective function is used to increase the calibration accuracy of the model parameters, and the second one is used to reduce the number of necessary measurement locations. The optimisation problem was solved by using genetic algorithms. The verification and application of the developed optimisation model (called IMMe) were carried out on the artificial water distribution system of Anytown, which serves as a reference model for testing various researches in hydraulic modelling. The verified IMMe model was applied to a real water-distribution system in the town of Sežana. For both water distribution models, the use of genetic algorithms proved very efficient with extremely combinatorial optimisation problems. The developed calibration and sampling design allow very accurate hydraulic modelling of the water distribution systems, which is of key importance for ensuring the economy and efficiency of drinking-water supplies in the future.

(Keywords: hydraulic, water distribution systems, modelling, optimisation, measurement locations, genetic algorithms)

0 UVOD

Hidravlično modeliranje vodovodnih sistemov (v nadaljevanju VS) je znanstveno zelo dobro razvita panoga, ki rabi kot učinkovito orodje za podporo pri odločanju, upravljanju, načrtovanju in obnovi VS. Podpora informacijske tehnologije pri vodenju katastra komunalnih naprav in zbiranju podatkov ter meritev omogoča učinkovito

0 INTRODUCTION

The hydraulic modelling of water distribution systems (hereinafter referred to as WDS) is a scientifically well-developed discipline serving as an efficient decision-support tool for the management, development and rehabilitation of WDS. The information technology supports the asset management of the WDS and the data acquisition allows the effivzpostavitev hidravličnih modelov in njihovo vključitev v analize, vsakdanje obratovanje in načrtovanje ter v končni fazi tudi izvajanje potrebnih ukrepov. Informacijski sistem se uporablja kot vir razpoložljivih podatkov o fizičnih značilkah VS, ki izhajajo iz dejansko znanih podatkov oziroma meritev in pa iz ocen posameznih hidravličnih parametrov, če količine niso natančno znane. S temi podatki je mogoče postaviti "surov" hidravlični model, katerega obsežnost je treba prilagoditi upravljavsko obvladljivim razmeram. Hidravlični modeli istega VS se lahko med seboj razlikujejo glede na namen analize, ki bo izvedena s tem modelom. Namen modela je bistvenega pomena, saj določa stopnjo natančnosti modela in njegove poenostavitve. Poenostavitev hidravličnega modela se imenuje ogrodenje (skeletiranje), cilj katerega je, iz modela izključiti elemente, ki niso bistveni za njegovo hidravlično enakost z dejanskim dogajanjem v VS. Po postavitvi takega modela se najprej izvede postopek grobega umerjanja oziroma makrokalibracije (sl. 1), cilj katerega je prilagajanje parametrov hidravličnega modela, dokler delovanje hidravličnega modela VS ne izkazuje ujemanja s sedanjimi meritvami z odstopanjem največ 30 odstotkov [1]. Makrokalibracija je usmerjena v odpravljanje posameznih virov odstopanj, to so napačni podatki o topologiji omrežja, nastavitev tlačnih con, parametrov elementov VS, napak merilnih naprav in odčitavanja meritev kakor tudi odpravljanje človeških napak.

Običajno z makrokalibracijo hidravlični model postane grob približek stvarnega VS z določeno stopnjo natančnosti. Hidravlični model je namenjen podpori pri odločanju na tehničnem, ekonomskem in pravnem področju, kar terja, da je hidravlični model natančneje umerjen. Kot uvod v postopek natančnejšega umerjanja oziroma mikrokalibracije (v

cient building of hydraulic models and their integration into analysis, daily operation and planning, and finally also the carrying out of the necessary measures. The information system serves as a source of available data on the physical characteristics of WDS deriving from actually known data or measurements as well as from the evaluations of individual hydraulic parameters if the exact quantities are not known. These data allow us to build a rough hydraulic model, the size of which has to be adapted to a manageable extent. Hydraulic models of the same WDS can vary substantially in their configuration with regard to the purpose of the model and the analysis to be performed with it. The model's purpose is essential since it determines the accuracy level to be applied. The model's adaptation involves a procedure of skeletonization, i.e., simplification of the model, the aim of which is to exclude those elements that are not essential to represent the model's hydraulic behaviour according to the real WDS. With such a model, the procedure of macro-calibration is first carried out (Fig. 1), with the adjustment of certain model parameters to achieve correspondence with the hydraulic behaviour of WDS, i.e., the system variables should not exceed 30 percent, based on the existing measurements [1]. Macro-calibration strives to eliminate the sources of differences, such as incorrect data on network topology, pressure-zone settings, the parameters of network elements, the errors of the measurement equipment and readings, as well as human error.

Normally, macro-calibration turns the hydraulic model into a rough approximation of the real WDS, with a certain level of accuracy. Decision making should tackled with technical, economic and legal issues, so the hydraulic model has to be calibrated more precisely. As an introduction to the so-called micro-calibration (hereinafter referred to as

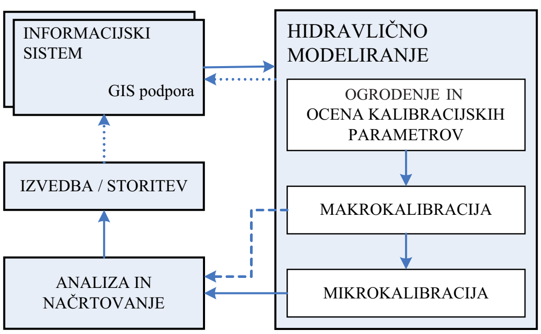

Sl. 1. *Upravljanje vodovodnih sistemov s poudarkom na modeliranju*

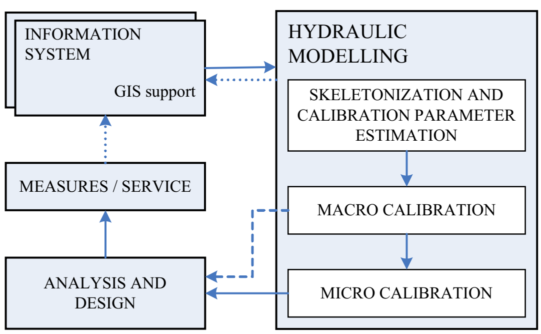

Fig. 1. *Water distribution system management with the emphasis on modelling*

nadaljevanju umerjanje) se uporablja postopek izbire merilnih mest, ki zagotavlja zbiranje pomembnih vzorcev meritev. Izbira merilnih mest za potrebe umerjanja je osredotočena na zbiranje meritev za razpoznavanje značilk in parametrov hidravličnega modela VS, odkrivanje virov težav pri vsakodnevnem obratovanju VS in za določene raziskovalne potrebe. Namen pričujočega prispevka je določitev merilnih mest in zbiranje meritev za natančno razpoznavanje, tj. umerjanje, fizičnih parametrov hidravličnih modelov VS.

1 UMERJANJE HIDRAVLIČNIH MODELOV VS

Postopek umerjanja se izvaja zaradi vzpostavitve zaupanja v napovedi hidravličnega modela. Poleg zanesljivosti napovedovanja daje umerjanje tudi natančen vpogled v delovanje VS, kar omogoča tudi vrednotenje občutljivosti modela na spremembe posameznih fizikalnih in/ali nefizikalnih parametrov. Umerjanje je torej postopek določitve posameznih neznanih parametrov hidravličnega modela, s katerim se zmanjšajo razlike med meritvami opravljenimi na stvarnem VS, in napovedmi oz. rezultati hidravličnega modela. Nastavljen problem umerjanja se lahko rešuje z zapisom ciljne funkcije v naslednji obliki:

$$\min E = \sum_{i=1}^{N_V} \alpha_i \sqrt{\frac{\sum_{j=1}^{N_M}\sum_{k=1}^{N_L}(y^*_{ijk} - y_{ijk})^2}{N_M * N_L}} \quad (1),$$

kjer so: E - vrednost ciljne funkcije umerjanja; y^*_{ijk} – meritve hidravličnih veličin na VS; y_{ijk} - napovedi modela za (i=1,…N_L; j=1,…N_M; k=1,…N_V); N_L – število obtežnih primerov; N_M - število merilnih mest; N_V – tip hidravlične veličine (tj. tlaki, pretoki …); a_i – utežni koeficient

Na področju umerjanja VS je bilo razvitih več postopkov in metod, ki jih v splošnem delimo na metodo poskus - napaka ter izrecne in posredne metode. Razvite posredne metode umerjanja so metode, ki so formulirane in se rešujejo kot optimizacijski problemi in so se izkazale za zelo učinkovite ([2] in [3]). Njihova ciljna funkcija je običajno izražena v obliki, ki omogoča zmanjšanje razlik med meritvami in napovedmi oziroma rezultati modela (en. 1). Razvoj optimizacijskih modelov za umerjanje je v veliki meri pripomogel k povečani natančnosti hidravličnih modelov VS. Merila natančnosti napovedovanja hidravličnih veličin so podana v različnih smernicah, ki določajo meje

"calibration") level, a sampling design programme would provide representative samples of measurements for the calibration. Sampling design is focused on collecting measurements for the determination of WDS model properties, on the detection of problems in the daily operation of WDS, as well as covering certain research needs. The aim of the presented paper is to determine the measurement locations in which the measurements allow accurate identification, i.e., the calibration of the physical parameters of WDS hydraulic models.

1 CALIBRATING HYDRAULIC MODELS OF WDS

The calibration process is conducted to provide confidence in the predictions of the WDS model. Besides the reliability of the predictions, calibration offers a deep insight into the WDS operation, which enables an assessment of the model's sensitivity to changes in individual physical and/or non-physical parameters. The calibration of hydraulic models is thus a procedure of determining individual unknown model parameters, which minimises the differences of predicted and measured system variables. The calibration problem is formulated to minimise the differences of predicted and measured system variables, and its general objective function is expressed as:

where E is the value of the objective function; y^*_{ijk} are measurements of the system variables; y_{ijk} are model predictions of the system variables for (i=1,…N_L; j=1,…N_M; k=1,…N_V); N_L is the number of loading conditions; NM is the number of measurement locations; N_V is the type of system variables (e.g. pressure, flow); and a_i are a weighting coefficients.

In the area of WDS model calibration, several approaches and methods were developed, which, in general, comprise the trial-and-error method and the explicit and implicit methods. The developed implicit methods of calibration, formulated and solved as optimisation problems, have proven their effectiveness ([2] and [3]). Their objective function is expressed in a form that allows minimisation of the differences between the measurements and predictions of the model (Eq. 1). The developments of optimisation models for calibration have to a great extent contributed to the increased accuracy of WDS models. The levels of accuracy according to the purpose of the WDS model odstopanj med meritvami in rezultati modela, vezane na namene analiz hidravličnih modelov [4].

Za uspešno umerjanje je treba najprej zbrati niz meritev, ki se pridobijo z načrtnim zbiranjem podatkov hidravličnih veličin pri obratovanju na pomembnih mestih na VS. Kakovost informacij, pridobljenih iz meritev, ima velik vpliv na natančnost umerjanja hidravličnega modela, večje število informacij pa daje v končni fazi tudi večjo stopnjo zaupanja v model.

2 IZBIRA MERILNIH MEST ZA UMERJANJE HIDRAVLIČNIH MODELOV VS

Izbira merilnih mest se v praksi pogosto izvaja po načelu "ad hoc", pri katerem se izdelovalec hidravličnega modela s pomočjo svojih strokovnih ocen odloči in predlaga kraje merilnih mest. Glavni poudarek pri zagotovitvi kakovosti in uporabnosti rezultatov izbire merilnih mest obsega določevanje [5]: (a) katere hidravlične veličine opazovati, (b) kje opazovati, (c) kdaj opazovati in (d) v kakšnih okoliščinah oz. obtežnih primerih opazovati. Odgovore na vprašanja pod točko (a), (c) in (d) mora predhodno podati inženir s svojim strokovnim znanjem. Glavni poudarek optimizacije izbire merilnih mest je osredotočen na vprašanje (b), ki je najzahtevnejše in obsega določevanje najboljših krajev merilnih mest.

Izkazalo se je, da je občutljivost merilnih mest bistvenega pomena za določevanje najboljših merilnih mest. Za določevanje občutljivosti hidravličnih veličin merilnih mest glede na spremembe parametrov hidravličnega modela se uporablja t.i. Jacobijeva matrika. Koeficienti Jacobijeve matrike (*i,j*) so parcialni odvodi izrazov hidravličnih veličin glede na parametre modela in jih je mogoče določiti z numerično aproksimacijo, metodo končnih razlik [3]:

are expressed as the differences between the measurements and the model's predictions [4].

For a successful calibration, a set of measurements has to be gathered, first by means of systematic sampling of the hydraulic quantities on a WDS. Since the relationship between the quality and quantity of a measurement is not predefined and self-evident, much attention needs to be paid to evaluating the informational content and its impact on the calibration accuracy.

2 SAMPLING DESIGN FOR THE CALIBRATION OF WDS MODELS

Sampling design is often carried out according to the ad-hoc principle, where a designer of a WDS model determines and proposes the measurement location on the basis of his or her expertise. To ensure the quality and relevance of the measurements, the main emphasis in sampling design involves determining [5]: (a) which model parameters to observe, (b) where to observe them, (c) when to observe them and (d) in what circumstances or loading conditions to observe them. While the answers to questions under points (a), (c) and (d) have to be provided in advance by an engineer using his or her expert knowledge, the main emphasis of sampling design is focused on question (b), which in turn is the most demanding and involves a determination of the optimal measurement locations.

It has been proven that model parameter sensitivities are essential for the determination of optimal measurement locations. To determine the optimal measurement locations with regard to model sensitivities, the so-called Jacobian matrix is used. The coefficients (*i,j*) of the Jacobian matrix are partial derivatives of the model predictions with regard to the model parameters and can be determined by applying numerical approximations, e.g., the finite-difference method [3]:

$$\left|\frac{\partial y_i}{\partial a_j}\right| = \left|\frac{y_i(a_j^*) - y_i(a_j)}{a_j^* - a_j}\right| \text{ za vsak/for each } (i=1,\ldots,N_O; j=1,\ldots,N_a) \qquad (2),$$

kjer so: ∂y - sprememba hidravlične veličine *i*; ∂a - sprememba parametra umerjanja hidravličnega modela *j*; $y_i(a^*_j)$ - vrednost hidravlične veličine pri izhodiščni vrednosti parametra umerjanja; $y_i(a_j)$ - vrednost hidravlične veličine pri spremembi vrednosti parametra umerjanja; a^*_j - vrednost izhodiščnega parametra umerjanja; a_j - vrednost spremenjenega parametra umerjanja; N_O - število meritev in N_a - število parametrov umerjanja. Za

where ∂y is the change of the hydraulic quantity *i*; ∂a is the change of the hydraulic parameter of the model *j*; $y_i(a^*_j)$ is the value of the hydraulic quantity at the initial calibration parameter value; $y_i(a_j)$ is the value of the hydraulic quantity at the change of the calibration parameter value; a^*_j is the value of the initial calibration parameter value; a_j is the value of the hydraulic quantity at the changed calibration parameter value; N_O is the number of observations and N_a is the number of rešitev izraza (2) uporabimo metodo končnih razlik, za katero je potrebno N_a+1 hidravličnih simulacij, pri čemer je dodatna simulacija pridobljena s predhodno oceno vrednosti parametrov modela.

Bolje umerjeni parametri hidravličnega modela dajejo natančnejše vrednosti koeficientov Jacobijeve matrike. Iz tega izhaja, da je smiselno izvajati iterativni postopek umerjanja in izbire merilnih mest (sl. 1) in to do sprejemljive natančnosti glede na namen hidravličnega modela [6]. Optimizacijski problem izbire merilnih mest je obravnavan z vidika izpolnjevanja dveh ciljnih funkcij, ki bosta podrobneje obravnavani v nadaljevanju.

calibration parameters. Eq. (2) is solved using the finite-difference method with N_a+1 hydraulic simulations, where the additional simulation is obtained for the initial values, i.e., by a preliminary parameter-value assessment.

Better calibrated model parameters give more precise values of the Jacobian matrix coefficients. Consequently, it is reasonable to carry out an iterative procedure of calibration and sampling design (Fig. 1) to reach an acceptable accuracy level with regard to the hydraulic model's purpose [6]. The optimisation problem of the sampling design has two objectives and will be further discussed in the next sections.

2.1 Ciljna funkcija natančnosti umerjanja

Z večanjem števila merilnih mest se povečuje tudi natančnost umerjanja parametrov hidravličnega modela. Metoda, ki je uporabljena za vrednotenje prve ciljne funkcije natančnosti umerjanja hidravličnega modela, je povzeta s področja teorije regresijske analize in je bila uspešno uporabljena pri razvoju modelov za umerjanje in izbiro merilnih mest modelov podtalnice [7]. Kasneje se je ta metoda uspešno uporabila tudi na področju izbire merilnih mest za izvedbo umerjanja hidravličnih modelov VS.

S prvo ciljno funkcijo se vrednoti prostornina območja zaupanja parametrov. V nasprotju z določevanjem intervalov zaupanja se prostornina območja zaupanja parametrov ukvarja z verjetnostjo, da so iskane vrednosti N_a parametrov hkrati v določenem N_a - razsežnem območju. Prostornina območja zaupanja je sorazmerna kvadratnemu korenu determinante kovariančne matrike parametrov hidravličnega modela in se ga matematično lahko izrazi takole [6]:

2.1 The Objective Function of Calibration Accuracy

An increase in the number of measurement locations will consequently increase the confidence level or the accuracy of the obtained parameter assessments. The method used to evaluate the first objective function of the calibration accuracy derives from the regression analysis theory and was successfully used in the development of models for the calibration and sampling design of groundwater models [7]. Later on it was also successfully used in the area of WDS hydraulic models.

The first objective function is to evaluate the parameter's confidence region volume. In contrast to the determination of confidence intervals, the volume of a parameter's confidence region deals with the probability that the sought values of N_a parameters can at the same time be found in a certain N_a dimensional area. The confidence region volume is proportional to the square root of the determinant of the covariance matrix of hydraulic model parameters and can be mathematically expressed as follows [6]:

$$\left(\det Cov_a\right)^{\frac{1}{2}} \tag{3}$$

kjer sta: Cov_a - kovariančna matrika parametrov hidravličnega modela; det() – determinanta matrike. Kovariančna matrika iz enačbe (3) je podana z izrazom:

where Cov_a is the covariance matrix of the hydraulic model parameters; and det() is the matrix determinant. The covariance matrix from Eq. (3) is expressed as follows:

$$Cov_a = s^2 \cdot (J^T W J)^{-1} \tag{4}$$

kjer so: s^2 - varianca regresijske napake; J - Jacobijeva matrika z elementi matrike $\partial y_i / \partial a_j$ (i=1,…,N_o; j=1,…,N_a); W - simetrična, pozitivno definirana matrika utežnih koeficientov; J^T - transponirana Jacobijeva matrika.

where s^2 is the regression error variance; J is the Jacobian matrix with the matrix elements $\partial y_i / \partial a_j$ (i=1,…,N_o; j=1,…,N_a); W is the symmetrical, positively defined matrix of weight coefficients; and J^T is the transposed Jacobian matrix.

Pri oblikovanju prve ciljne funkcije se lahko brez večje izgube splošnosti izrazov v enačbi (4) predpostavi, da veljajo tipične domneve regresijske analize: natančnost meritev je neodvisna od kraja na VS; vsa merilna oprema, ki bo uporabljena pri zbiranju meritev, ima podobno natančnost; in samo tlaki so predmet obravnave pri optimizaciji izbire merilnih mest. Posledično se lahko matriko utežnih koeficientov W približno izrazi kot diagonalno matriko, katere diagonalni elementi zavzemajo vrednosti $1/\sigma^2_H$, kjer je σ_H nespremenljiva standardna napaka vseh tlačnih meritev. Z upoštevanjem teh predpostavk se lahko enačba (3) oblikuje na način, da se prostornina N_a razsežnega območja zaupanja parametrov idealizira kot kubični prostor [6]. Tako se namesto enačbe (3) uporabi izraz:

When formulating the first objective function, it can be assumed - without any major loss in the generality of the expressions in Eq. (4) - that the typical assumptions of the regression analysis hold true: the measurement accuracy is independent of the location on a WDS; all the measuring equipment that will be used in gathering the measurements have similar accuracies; and the only pressures are the subject of the discussion in the sampling design optimisation. Consequently, the weighting matrix, W, can be approximated by a diagonal matrix with all non-zero elements equal to $1/\sigma^2_H$, where σ_H is the constant standard error of all the pressure measurements. The first objective function from Eq. (3) can be formulated so as to idealise the volume of N_a dimensional parameter's confidence region as a three-dimensional space [6]. Therefore, instead of Eq. (3), the following expression is used:

$$\left(\det Cov_a\right)^{\frac{1}{2N_a}} \qquad (5),$$

Enačba (5) se uporabi v optimizacijskem postopku prve ciljne funkcije, kjer se zmanjšuje negotovost v ocene parametrov umerjanja hidravličnih modelov. Ker je zmanjševanje determinante kovariančne matrike parametrov računsko in algoritmično zahtevno, se uvede preoblikovanje ciljne funkcije, ki zvečuje determinanto inverzne kovariančne matrike:

Eq. (5) is used in optimising the first objective function, where the uncertainty in the model parameters is minimised. Since minimising the determinant of the covariance matrix of parameters is computationally and algorithmically very demanding, a transformation of the objective function is introduced, which maximises the determinant of the inverse covariance matrix:

$$F_1 = \min\left(\det Cov_a\right)^{\frac{1}{2N_a}} = \max\left(\det Cov_a^{-1}\right)^{\frac{1}{2N_a}} \qquad (6),$$

kjer je izraz za inverzno kovariančno matriko Cov_a^{-1} podan z enačbo [6]:

where the inverse covariance matrix Cov_a^{-1} is obtained using Equation [6]:

$$Cov_a^{-1} = \frac{1}{\sigma_H^2} J^T J \qquad (7).$$

Predstavljena ciljna funkcija F_1, s katero se zvečuje determinanto inverzne kovariančne matrike, se imenuje kriterij D-optimalnosti. Knopman in Voss [7] sta omenjeni kriterij D-optimalnosti primerjala tudi z drugimi metodami za ocenjevanje stopnje zaupanja v parametre hidravličnega modela in povzela, da D-optimalnost izkazuje enake rezultate v smislu izbire merilnih mest ob večji računski učinkovitosti v računalniških uporabah.

Ker se bo prva ciljna funkcija združila še z drugo ciljno funkcijo, je primerno, da se vrednotena shema izbire merilnih mest iz enačbe (6) normalizira z vrednostjo determinante celotne inverzne kovariančne matrike, tako da bo prva ciljna funkcija zavzemala vrednosti od 0 do 1. Z uvedbo normalizacije enačbe (6) je končna oblika prve ciljne funkcije enaka:

The presented objective function F_1, used to maximise the determinant of the inverse covariance matrix, is called the D-Optimality criterion. Knopman and Voss [7] analysed the D-Optimality criterion by other methods for assessing the level of confidence in hydraulic parameters and summarised that D-Optimality yields the same results in terms of sampling design at a higher computational efficiency in computer applications.

Since the first objective function will be joined with the second objective function, it is appropriate to normalise the evaluated sampling design scheme from Eq. (6) with the value of the determinant of the full inverse covariance matrix, so the first objective function will assume the values from 0 to 1. Normalisation of Eq. (6) gives the final form of the first objective function:

$$\max F_1 = \left[\frac{\det Cov_a^{-1}}{\det Cov_{a\ F}^{-1}} \right]^{\frac{1}{2N_a}} \qquad (8),$$

kjer je $Cov_{a\ F}^{-1}$ – cela inverzna kovariančna matrika z upoštevanjem vseh možnih merilnih mest [5]. Determinanto inverzne kovariančne matrike se izračuna z numerično metodo oblikovanja spodnje in zgornje trikotne matrike (LU razstavitev) [8]. Determinanta je po razstavljanju matrik zmnožek diagonalnih elementov zgornje trikotne matrike.

where $Cov_{a\ F}^{-1}$ is the full inverse covariance matrix taking into account all the potential measurement locations [5]. The determinant of the inverse covariance matrix is calculated by means of a numerical method for defining the lower and upper triangular matrix (LU Decomposition) [8]. After the decomposition of the matrices, the determinant is a product of the diagonal elements of the upper triangular matrix.

2.2 Ciljna funkcija stroškov izvajanja meritev

Druga ciljna funkcija optimira skupne stroške izvajanja meritev na VS. Upoštevani so stroški: (a) stalni oz. investicijski stroški in (b) spremenljivi oz. operativni stroški.

Splošne enačbe za vrednotenje stroškov izvajanja meritev je težko določiti, zato se postopek poenostavi s predpostavko, da je glavni strošek vsakokratnega zbiranja meritev vezan le na spremenljivi oziroma operativni del skupnih stroškov. Ciljno funkcijo se zato izrazi v odvisnosti od števila merilnih mest, njen namen pa je zmanjšanje stroškov izvajanja meritev in s tem posredno tudi števila merilnih mest. Zaželena je uporaba druge ciljne funkcije v normalizirani obliki [5]:

2.2 The Objective Function of Measurement Costs

The second objective function is optimising the costs related to measurements performed on a system. Considered here are the following: (a) capital or investment costs and (b) variable or operational costs.

It is difficult to determine general equations to estimate the measurement costs; therefore, the procedure is simplified by the assumption that the main measurement costs for each measurement performed are related only to the operational part of the total costs. The objective function can thus be expressed with regard to the number of measurement locations. Its purpose is to minimize the measurement costs and indirectly also the number of measurement locations. It is desirable to use the second objective function in a normalised form [5]:

$$\min F_2 = N \quad \Rightarrow \quad \max F_2 = 1 - \frac{N}{N_F} \qquad (9),$$

kjer sta: N - število merilnih mest na sistemu; N_F - število vseh možnih merilnih mest v sistemu. Iz izraza (9) je razvidno, da tako oblikovana druga ciljna funkcija teži k čim manjšemu številu merilnih mest.

where N is the number of measurement locations in the system; N_F is the number of all potential measurement locations in the system. Eq. (9) shows that the thus formulated second objective function tends towards the lowest possible number of measurement locations.

2.3 Vzpostavitev optimizacijskega problema

Ker sta si zgoraj navedeni ciljni funkciji protislovni, je treba najti rešitev, ki bo v največji meri zadovoljevala tako prvo kakor drugo ciljno funkcijo. Prva ciljna funkcija bo najboljša, če bodo meritve zbrane na vseh možnih merilnih mestih, medtem ko bo druga najboljša, če bo število merilnih mest čim manjše, saj bodo s tem povezani tudi najnižji stroški. Optimizacijski problem je sestavljen iz naslednjih delov: (a) ciljne funkcije, (b) optimizacijskih spremenljivk oziroma neznank in (c) robnih pogojev. Formulacija optimizacijskega problema za izbiro merilnih mest je sestavljena iz dveh ciljnih funkcij, opredeljenih v zgornjih

2.3 Definition of the Optimisation Problem

Since the above-mentioned objective functions are mutually contradictory, a solution has to be found that will, to the largest extent, satisfy both the objective functions. The first objective function will be optimal if measurements are collected at all possible measurement locations, while the second will be optimal if the number of measurement locations is zero, since this will incur the lowest costs. The optimisation problem involves the following parts: (a) the objective function; (b) the optimisation variables or unknowns; and (c) the constraints. The optimisation problem formulation for the sampling odstavkih. Normalizirana izraza (8) in (9), ki sta oblikovana na način, da se njuni vrednosti zveča, sta združena v en izraz:

design consists of two objective functions defined in the previous paragraphs. The normalised Eq. (8) and Eq. (9), formulated so as to maximise their values, are joined into a single expression:

$$\max E = \left(\sum_{i=1}^{2} w_i \cdot F_i^p \right)^{1/p} - Pe \qquad (10),$$

kjer so: E - skupna ciljna funkcija; w_i - utežni koeficient za določevanje pomembnosti posamezne ciljne funkcije; p - potenca; F_i - i-ta ciljna funkcija; Pe - kazenska funkcija. Utežna koeficienta w_1 in w_2 sta izbrana na način, da je njuna vsota enaka 1. Vrednosti, ki jih zavzema skupna funkcija E, so v območju (0, 1), če niso kršeni robni pogoji. Kazenska funkcija se uporablja za vključevanje izrecnih robnih pogojev v optimizacijskem problemu in pomeni največje in najmanjše število merilnih mest:

where E is the common objective function; w_i are the weight coefficients to determine the importance of an individual objective function; p is the norm order; F_i is the i-th objective function; and Pe is the penalty function. The weight coefficients w_1 and w_2 are selected so that their sum is equal to 1. The values assumed by the joint objective function E are within the interval (0, 1), if this does not exceed the constraints. The penalty function is used to introduce explicit constraints into an optimisation problem and will represent the maximum and minimum values of the number of measurement locations:

$$Pe = \begin{cases} pc_1 \cdot (N_{\min} - N), & N < N_{\min} \\ pc_2 \cdot (N - N_{\max}), & N > N_{\max} \\ 0 \quad , & N_{\min} \le N \le N_{\max} \end{cases} \qquad (11),$$

kjer so: N - dejansko število merilnih mest v sistemu; N_{min} - najmanjše potrebno število merilnih mest na sistemu ($N_{min} > 0$); N_{max} - največje število merilnih mest v sistemu ($N_{max} < N_F$); N_F - število vseh možnih merilnih mest v sistemu; pc_1 in pc_2 - stroškovna koeficienta kazenske funkcije.

Optimizacijska orodja se uporabljajo za reševanje zahtevnih in obsežnih optimizacijskih problemov. Genetski algoritmi (v nadaljevanju GA) so razred nelinearnih, prilagodljivih in hevrističnih metod za iskanje in optimizacijske probleme in spadajo v skupino razvojnih algoritmov. GA posnemajo naravno načelo reprodukcije, mutacije in naravne izbire za zagotovitev preživetja najbolj sposobnega oziroma najboljšega osebka, tj. rešitve. Načelo GA in njegova uporaba pri optimizaciji VS je podano v [9] do [11].

GA so optimizacijska metoda, ki se posebej dobro izkaže pri reševanju velikih in zapletenih problemov z mnogimi lokalnimi ekstremi in s katero se skoraj vedno najdejo rešitve blizu najboljše [12]. Ta lastnost izvira iz dejstva, da GA raziskujejo prostor rešitev s skupnostjo (populacijo) kromosomov, tj. možnimi rešitvami, ki so naključno razpršene po celotnem prostoru rešitev. Ena od prednosti GA je tudi ta, da zahtevajo le vrednotenje ciljne funkcije za optimizacijski postopek brez zahtevnih numeričnih opravil ter možnost uporabe tako

where N is the actual number of measurement locations in the system; N_{min} is the minimum required number of measurement locations in the system ($N_{min} > 0$); N_{max} is the maximum number of measurement locations on the system ($N_{max} < N_F$); N_F is the number of all the potential measurement locations in the system; and pc_1 and pc_2 are the cost coefficients of the penalty function.

Optimisation tools are used for solving demanding and comprehensive optimisation problems. Genetic algorithms (hereinafter referred to as GAs) are a class of nonlinear, adaptive and heuristic methods for search and optimisation problems and belong to the group of evolutionary algorithms. GAs mimic nature's principles of reproduction, mutation and natural selection to ensure the survival of the fittest and therefore the best individual, i.e., the best solution. The principle of GAs and their application to WDS optimisation are given by [9] to [11].

GAs are an optimisation method especially useful in solving large and complex problems with many local minimums and maximums that almost always provides a solution close to the optimum one [12]. This feature arises from the fact that GAs explore the solution space with a population of chromosomes, i.e., possible solutions randomly distributed across the entire solution space. One of the advantages of GAs is that they require only the evaluation of the objective function for the optimisation procedure, without demanding numerical operations, as well as diskretnih kakor tudi zveznih spremenljivk v postopku optimizacije [13].

3 OVERITEV MODELA ZA IZBOR MERILNIH MEST NA VS ANYTOWN

Za uporabo in overitev prikazane metode je bil izdelan optimizacijski model za najboljšo izbiro merilnih mest z uporabo GA, ki je poimenovan IMMe. Samo preizkušanje pa je bilo izvedeno na hidravličnem modelu "Anytown", ki ga je prvi definiral Thomas M. Walski [14]. Omenjeni model je bil izbran zaradi njegove razširjenosti na področju preizkušanja različnih orodij za analizo VS in zasnove, ki vključuje tudi določene značilnosti dejanskih VS. Optimizacijski model izbire merilnih mest je namenjen določevanju merilnih mest, ki bodo sporočali najboljše informacije v fazi umerjanja izbranih parametrov hidravličnega modela. Koeficienti hrapavosti cevi po Hazen-Williamsu so bili izbrani kot parametri umerjanja. Čeprav je v hidravličnem modelu "Anytown" število parametrov enako številu cevi (tj. 34 cevi), se lahko število parametrov znatno zmanjša prek združevanja koeficientov hrapavosti, s čimer se je določilo pet skupin ($N_a = 5$).

Umerjanje parametrov hidravličnih modelov, tj. koeficientov hrapavosti cevi, zahteva kakovostne meritve hidravličnih veličin, ki bodo v največji meri podajale zadostno količino informacij za učinkovito umerjanje [15]. Optimizacijski problem je bil oblikovan na način, da določa najboljša merilna mesta za pet neodvisnih ustaljenih hidravličnih simulacij, tj. štirje neodvisni požarni odvzemi vode in ob normalni porabi. Ker je skupno število vozlišč $N_{max} = 16$, je največje število meritev $N_O = 80$ vrstic (16 vozlišč krat 5 obtežnih primerov). Izhajajoč iz teoretičnega ozadja izbire merilnih mest, se tlačna občutljivost vseh možnih merilnih mest zapiše v Jacobijevi matriki, ki ima $N_O = 80$ vrstic in $N_a = 5$ stolpcev.

Optimizacija ciljne funkcije (enačba (10)) z GA se je posebno dobro izkazala v izjemno kombinatornih problemih, kamor spadata tako umerjanje kakor tudi izbira merilnih mest [12]. Uporabljeni so bili Simple GA v povezavi z binarnim kodiranjem kromosomov, sestavljenih iz 16 genov (16 možnih merilnih mest). Populacija 100 kromosomov je bila začeta in iz nje so se izbirali starševski kromosomi z uporabo t.i. "ruletnega kolesa" ter verjetnostjo križanja 0,75 in verjetnostjo pojava mutacije 0,07. Vzpostavitev nove generacije

the possibility of using both discrete and continuous variables in the optimisation procedure [13].

3 SAMPLING DESIGN MODEL VERIFICATION FOR AN ARTIFICIAL WDS IN ANYTOWN

For the application and verification of the presented method, an optimisation model (called IMMe) for the optimal selection of measurement locations using GAs was developed. The verification process was carried out on the Anytown hydraulic model, which was first defined by Thomas M. Walski [14]. His model is seen as a benchmarking model for testing various tools of WDS analysis and implies realistic concepts of real WDS characteristics. The sampling design optimisation model was applied to determine the measurement locations that will provide the most information for the model's parameter calibration. Pipe-roughness coefficients according to Hazen-Williams were selected as the calibration parameters. Although the Anytown model consists of only 34 individual pipe-roughness coefficients, their number was seriously reduced by introducing pipe grouping criteria, which resulted in five groups ($N_a = 5$).

Calibrating the model parameters, i.e., the pipe roughness coefficients, requires high-quality measurements of system variables, which will, to the largest extent possible, provide sufficient information for an efficient calibration [15]. The sampling design optimisation problem was formulated to determine optimal measurement locations for five independent steady-state loading conditions, i.e., four independent fire flow tests and a normal operation loading condition. Since the total number of nodes is $N_{max} = 16$, the maximum number of observations is $N_O = 80$ rows (16 nodes × 5 loading conditions). Following the theoretical background of the sampling design, the pressure sensitivity of the possible measurement locations is expressed by the Jacobian matrix consisting of $N_O = 80$ rows and $N_a = 5$ columns.

The optimisation of the objective function (Eq. (10)) by the GA thus proved to be successful in extremely combinatorial problems, like sampling design and calibration [12]. Simple GAs were applied and solutions were presented in binary coding for the chromosome composed of 16 genes (16 possible measurement locations). A population of 100 chromosomes was initialised to perform an evolution chromosome based on a roulette-wheel parent selection with a probability of 0.75 and a mutation probability of 0.07. Full generation replacement with elitism was potomcev iz starševskih kromosomov je potekala s popolno zamenjavo populacije skupaj s funkcijo odličnosti [13]. Poleg opisanega primera Simple GA so bili za potrebe overitve modela in njegove uporabe na primeru VS Sežana uporabljeni tudi ustaljeni GA s celoštevilčnim kodiranjem kromosomov. Ostali parametri GA so ostali enaki kakor v zgornjem primeru. Pri reševanju optimizacijskega problema izbire merilnih mest so bili uporabljeni tako Simple kakor ustaljeni GA.

Rezultati optimizacijskega postopka so prikazani na sliki 2, na kateri je prikazana prva ciljna funkcija F_1, tj. natančnosti umerjanja, v odvisnosti od števila merilnih mest. Na splošno se lahko podata dve ugotovitvi, tj. vključevanje dodatnih merilnih mest povečuje natančnost umerjanja in krivulja ciljne funkcije F_1 spremeni nagib. V pričujočem primeru se nagib spremeni med 4. in 5. merilnim mestom, kar pomeni, da je uvajanje nadaljnjih merilnih mest manj učinkovito. Rezultati na sliki 2 so prikazani skupaj s primerjavo z rezultati modela Kapelan idr. [5], ki so povzeti iz literature in so namenjeni postopku verifikacije.

Opravljena overitev modela za izbiro merilnih mest v obeh primerih uporabe posameznih tipov GA izkazuje enake rezultate. Ker je obsežnost optimizacijskega problema na dejanskem VS Sežane prevelika za uporabo Simple GA z binarnim kodiranjem, bodo uporabljeni le ustaljeni GA v kombinaciji s celoštevilčnim kodiranjem kromosomov.

applied to create a new generation of offspring chromosomes [13]. Besides the described example of the Simple GA, also a Steady-state GA with integer coding were used for model verification for its later use on the Sežana WDS example. The other GA parameter settings remained the same as those above. The optimisation problem of sampling design was solved by using both Simple and Steady-state GAs.

The results of the optimisation process are presented in Fig. 2, where the first objective function F_1, i.e., the objective function of the calibration accuracy, is presented in relation to the number of measurement locations. In general, two characteristics can be perceived, i.e., the inclusion of additional measurement locations results in a higher calibration accuracy, and the curve of the objective function F_1 has a change of slope. In the presented case the slope changes between the 4th and 5th measurement locations, which indicates that the introduction of further measurement locations would be far less efficient. The results in Fig. 2 are also compared to the sampling design model of Kapelan et al. [5] by literature review for model verification purposes.

The performed verification of the sampling design model shows the same results in both cases of the use of individual types of GA. Since the application of the optimisation problem to the real Sežana WDS is considered to be too large for solving the problem by the use of the Simple GA with a binary coding, only the steady-state GA in combination with integer coding will be applied to the aforementioned case study.

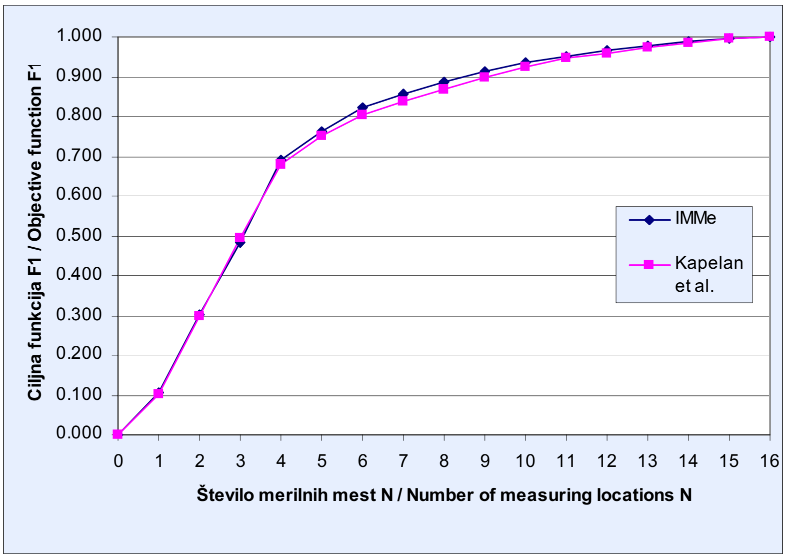

Sl. 2. *Rezultati modela izbire merilnih mest IMMe in primerjava s Kapelan idr. [5]*
Fig. 2. *Results of "IMMe" model and a comparison to Kapelan et al. "CAO1" model [5]*

4 PRIMER VS SEŽANA

Overjena metoda izbire merilnih mest je bila uporabljena na dejanskem VS mesta Sežana, da bi vzpostavili niza merilnih mest na VS za zbiranje kakovostnih meritev za razpoznavo parametrov umerjanja. Uporaba optimizacijskega modela z uporabo genetskih algoritmov je bila izvedena za določevanje merilnih mest tlakov za umerjanje koeficientov hrapavosti cevovodov pod neodvisnimi požarnimi odvzemi vode, tj. odpiranje hidrantov.

VS mesta Sežana je na Primorskem in oskrbuje približno 5.500 prebivalcev, povprečna poraba pa je ocenjena na 16,55 l/s. Popoln hidravlični model VS je bil vzpostavljen z uporabo ustreznih podatkov geografskega informacijskega sistema (GIS) in računalniško podprtega načrtovanja upravljalca Kraški vodovod Sežana. Postavljeni model sestavljajo 1 vodni vir, 6 vodnih zbiralnikov, 4 črpalke, 696 vozlišč, 738 cevi in 1 zniževalni ventil tlakov. Osrednji oz. mestni del VS je oskrbovan prek dveh vodnih zbiralnikov, ta dva sta v bližini prenosnega cevovoda, ki dovaja vodo naprej na obalno področje. Popoln hidravlični model je bil poenostavljen, tako da je ogrodni model sestavljalo le še 132 vozlišč in 173 cevi. Oba hidravlična modela sta bila grobo umerjena z meritvami pretoka v cevovodih in ravni vode v vodohranih.

4.1 Oblikovanje problema izbire merilnih mest

Koeficienti hrapavosti cevovodov ogrodnega hidravličnega modela so bili razvrščeni po “ameriškem” kriteriju združevanja [2]. Končno število skupin koeficientov hrapavosti je bilo 48, kar pa bi posledično privedlo do izjemno velikega števila merilnih mest, potrebnega za rešitev inverznega problema določevanja parametrov, tj. umerjanja [15]. Nanašajoč se na ciljno funkcijo stroškov izvajanja meritev, lahko ugotovimo, da je množično zbiranje meritev zelo drag postopek. Zato je bilo število skupin koeficientov hrapavosti zmanjšamo z uporabo ohlapnejših kriterijev, vezanih samo na podatke materiala in starosti cevovodov, ki so bili najbolj nezanesljivi. Tako je bilo določenih 16 skupin hrapavosti ($N_a = 16$), kar naj bi omogočalo vzpostavitev dobro določenega problema umerjanja. Za potrebe določitve občutljivostnih koeficientov za postavitev Jacobijeve matrike so bile določene predhodne ocene koeficientov hrapavosti za vsako skupino na podlagi strokovnih ocen in ustreznih preglednic.

4 CASE STUDY OF SEŽANA

The verified IMMe sampling design model was applied to the real-life WDS of the town of Sežana, to find an optimal set of measurement locations on the WDS to collect quality measurements for the identification of model parameters. To identify the pressure measurement locations for the calibration of the pipe roughness values, the multiple independent fire flow loading conditions, i.e., hydrant flushing, were assessed and GAs were applied to perform the optimisation task.

The WDS of Sežana is located in the coastal region of Slovenia, supplying a population of around 5,500 residents, while the average residential and industrial demand is estimated to be 16.55 l/s. A full-pipe WDS model was established using the relevant GIS and CAD data, resulting in a WDS model consisting of 1 reservoir, 6 tanks, 4 pumps, 696 junctions, 738 pipes and 1 pressure reducing valve. The inner part of the WDS is supplied through two tanks, which are located near the transmission main, delivering water to the coastal region. For the purposes of the sampling design analysis the full pipe model was skeletonized to a model of 132 junctions and 173 pipes. Both, full pipe and skeletonized WDS models were macro-calibrated for demands using flow and tank level measurements.

4.1 Formulation of the Sampling-Design Problem

Using the sampling design approach on the skeletonized WDS model, pipe roughness values were grouped using the "American" grouping criterion [2]. The resulting number of pipe roughness groups is 48, which would consequently lead to a high number of measurement locations for the inverse problem of parameter identification, i.e., the calibration [15]. According to the second objective function, measurement collection is a costly process. Therefore, the number of pipe roughness groups was reduced according to loosened criteria of the pipe material and age, which were unreliable and sparse. A total of 16 pipe roughness groups ($N_a = 16$) were created, which should ennsure a well-posed calibration problem. The pipe roughness values for each group were previously estimated using expert judgment and relevant pipe roughness tables for the purpose of sensitivity analysis and Jacobian matrix determination.

Poleg krajev tlačnih meritev je bilo treba določiti tudi kraje odpiranja hidrantov, število mogočih lokacij je 95 ($N_{Load,max}$ = 95) od skupaj 132 vozlišč. Izvedena je bila občutljivostna analiza krajev odpiranja hidrantov, kjer so vozlišča najbolj občutljiva na povečanje hitrosti v ceveh [16]. Skupaj je bilo določenih 14 krajev odpiranja hidrantov (N_{Load} = 14), pri katerih se je reševal problem izbire merilnih mest za umerjanje koeficientov hrapavosti.

Optimizacijski problem izbire merilnih mest je bil oblikovan skladno s ciljem določitve najboljših krajev merilnih mest za umerjanje 16 skupin hrapavosti cevovodov (N_a = 16). Kraji zbiranja tlačnih meritev na sistemu so bile omejene na 95 (N_{max} = 95) mogočih krajev merilnih mest, kjer bodo zbrane meritve pri 14 (N_{Load} = 14) neodvisnih ustaljenih obtežnih primerih. Izvedena je bila analiza občutljivosti tlakov v vozliščih za vse mogoče kraje merilnih mest in vse obtežne primere za določitev tlačnih občutljivosti za 16 skupin hrapavosti cevovodov. Postavljena je bila ti. “cela” Jacobijeva matrika za vsa mogoča merilna mesta z N_O = 1330 vrsticami (95 vozlišč × 14 obtežnih primerov) in N_a = 16 stolpcev (16 skupin koeficientov hrapavosti cevovodov). Ker je Jacobijeva matrika edinstvena matrika za definiran problem izbire merilnih mest VS, jo je treba le enkrat izračunati pred optimizacijskim postopkom [5], medtem ko so vse rešitve optimizacijskega postopka izpeljane iz polne Jacobijeve matrike.

Rešitve postopka izbire merilnih mest so bile pridobljene z ustaljenim GA skupaj s celoštevilčnim kodiranjem kromosomov, ki predstavljajo indekse krajev merilnih mest. Kodiranje s celimi števili je dobilo prednost pred binarnim kodiranjem, ker je primernejše za reševanje izbire merilnih mest na velikih realnih VS [5]. Možnost ponavljanja ista merilna mesta v eni in isti rešitvi je bila odpravljena z izbrisom vsakega dodatnega kraja merilnega mesta iz te rešitve, če bi se le-ta ponavljala. V optimizacijskem postopku GA je bila uporabljena skupnost 200 kromosomov z možnostjo križanja v dveh točkah kromosoma z verjetnostjo 0,85 in verjetnostjo mutacije v genu 0,07. Za določevanje funkcije sposobnosti so bile uporabljene naslednje vrednosti utežnih koeficientov ciljnih funkcij w_1 = 1 in w_2 = 0 ter potenca p = 1. Večkratni zagoni GA so bili uporabljeni v optimizacijskem postopku izbire merilnih mest.

Besides the determination of pressure measurement locations, hydrant flushing locations needed to be identified. A total number of 95 ($N_{Load,max}$ = 95) out of 132 junctions were identified. A sensitivity analysis was performed to identify the hydrant flushing locations, i.e., junctions at which pipes were most sensitive to increased velocities [16]. A total of 14 locations (N_{Load} = 14) were determined, at which the sampling design problem for the calibration of the pipe roughness values was solved.

The sampling design problem was formulated in order to obtain the optimal measurement locations for identifying a total number of 16 pipe roughness groups (N_a = 16). The pressure data collection locations were reduced to 95 (N_{max} = 95) possible measurement locations, where data could be obtained from 14 (N_{Load} = 14) independent steady-state loading conditions. A pressure sensitivity analysis was performed for all the possible measurement locations and all the loading conditions to obtain the pressure sensitivities of the 16 pipe roughness groups. A full Jacobian matrix was written with N_O = 1330 rows (95 nodes × 14 loading conditions) and N_a = 16 columns (16 pipe roughness groups). Since the Jacobian matrix is a unique matrix for a defined sampling design problem of a WDS it has to be calculated only once prior to the optimisation process [5], while the estimations on sampling design solutions are derived from the full Jacobian matrix.

The sampling design solutions were obtained using a Steady-State GA together with integer coding of the chromosomes, which in turn represent the IDs of the measurement locations. Integer coding was preferred to binary coding since integer coding is more suitable for large, real-life sampling design problems [5]. The possibility of repeated measurement locations in one sampling design solution was handled with the exclusion of all the additional measurement devices at one and the same measurement location. In the GA search process a population of 200 chromosomes was used with a two-point crossover probability of 0.85 and a gene mutation probability of 0.07. The weighting coefficients w_1 = 1 and w_2 = 0, and an exponent of p = 1 were used to evaluate the fitness function. Trivial solutions (with N = 0 and N = 95) were excluded and multiple GA runs were performed to identify non-trivial sampling design solutions.

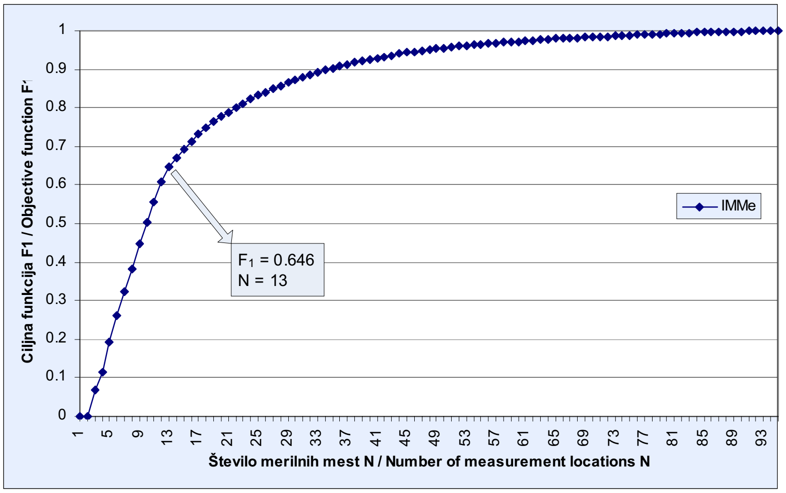

Sl. 3. *Rezultati izbora merilnih mest modela IMMe v VS Sežana*
Fig. 3. *Results of IMMe sampling design model on WDS of Sežana*

4.2 Rezultati izbire merilnih mest VS Sežana

Pri izbiri merilnih mest se določa razmerje med prvo in ciljno funkcijo z uporabo utežnih koeficientov w_1 in w_2. Ker je razmerje utežnih koeficientov težko natančno določiti, se lahko v postopku uporabi stalno število iskanih merilnih mest. Zato je bil izbran utežni koeficient $w_2 = 0$. Z uporabo celoštevilčnega kodiranja vseh mogočih merilnih mest (indeksacija) in z določitvijo dolžine kromosoma z želenim številom merilnih mest je možno točno določiti najboljša merilna mesta. Rezultat takšnega postopka je diagram na sliki 3, ki pomeni natančnost umerjanja parametrov (prva ciljna funkcija) v odvisnosti od določenega števila merilnih mest (druga ciljna funkcija).

Na sliki 3, ki prikazuje natančnost umerjanja parametrov, tj. prvo ciljno funkcijo, je razvidno strmo naraščanje funkcije F_1 do 13 merilnih mest. Zatem se z dodajanjem števila merilnih mest rast funkcije F_1 upočasni, kar pomeni, da vsako dodano merilno mesto prispeva manj "informacije" k natančnosti umerjanja parametrov. Optimizacijski model podaja potrebno pomoč pri določevanju razporeditve merilnih mest po VS. Rezultati s slike 3 so lahko pomoč v dveh primerih odločanja: (a) če je vnaprej izbrana natančnost umerjanja parametrov, ki jo želimo doseči v samem postopku umerjanja, lahko ugotovimo koliko merilnih mest je potrebnih; (b) ocenimo kakšno natančnost umerjanja lahko pričakujemo pri izbranem številu

4.2 Results of the Sampling Design Case Study - WDS of Sežana

The sampling design problem deals with the trade-off between the first and the second objective functions using the weighting coefficients w_1 and w_2. Since such a trade-off and the corresponding weights are hard to correctly identify, it is preferable to apply the search process for a fixed number of measurement locations; therefore, $w_2 = 0$. Using integer coding of all the measurement locations and a chromosome length equal to the number of desired measurement locations, it is possible to correctly identify a sampling design solution within those constraints. The result of such a search process is a diagram of the calibration parameter accuracy (the first objective function) against the number of measurement locations (the second objective function), and is shown Fig. 3.

Fig. 3 shows that the calibration parameter accuracy, i.e., the objective function 1, rapidly increases until it reaches a total of 13 measurement locations. Later, the slope rises more slowly, indicating that every additional measurement location adds less "information" to the calibration parameter accuracy. The optimisation model provides the necessary support in determining how the selected number of measurement locations is to be distributed across the WDS. There are two ways to interpret the results from Fig. 3: (1) one can determine in advance what level of calibration parameter accuracy is desirable for the calibration process, and through that the number of measurement locations can be identified; (2) the level of calibration parameter accuracy can be estimated from a certain

Preglednica 1. *Rezultati izbire merilnih mest za primer VS Sežane*
Table 1. *Results of sampling design for WDS of Sežana*

Ciljna funkcija *Objective function*		ID vozlišč / *Node ID*																					
F_1	N	13	41	42	45	49	50	52	55	67	68	70	83	90	97	98	99	112	114	117	118	119	132
0.502	10				1			1	1	1					1	1			1		1	1	1
0.556	11			1				1	1	1			1		1	1			1		1	1	1
0.608	12				1			1	1	1			1		1	1		1	1		1	1	1
0.646	13			1	1			1	1	1		1	1			1	1		1		1	1	1
0.671	14		1	1	1			1	1	1		1	1			1	1		1		1	1	1
0.693	15		1	1	1			1	1	1		1	1		1	1	1		1		1	1	1
0.712	16		1	1	1			1	1	1	1	1	1		1	1	1		1		1	1	1
0.731	17	1	1	1	1			1	1	1	1	1	1		1	1	1		1		1	1	1
0.748	18	1	1	1	1			1	1	1	1	1	1		1	1	1	1	1		1	1	1
0.764	19	1	1	1	1		1	1	1	1	1	1	1		1	1	1	1	1		1	1	1
0.777	20	1	1	1	1	1	1	1	1	1	1	1	1		1	1	1	1	1		1	1	1
0.789	21	1	1	1	1	1	1	1	1	1	1	1	1	1	1	1	1	1	1		1	1	1
0.800	22	1	1	1	1	1	1	1	1	1	1	1	1	1	1	1	1	1	1	1	1	1	1

merilnih mest oziroma razpoložljivi merilni opremi. Končni rezultat je določitev najboljših merilnih mest z uporabo GA. Optimizacijski rezultati s slike 3 so ločeno podani v preglednici 1, kjer so prikazana najboljša vozlišča za izbrano število merilnih mest. V preglednici 1 je podan le delež celotnih rešitev optimizacije in predstavlja rešitve za 10 do 22 merilnih mest, tj. določitev vozlišč, kjer bo nameščena merilna oprema.

Metodologija izbire merilnih mest modela IMMe sloni na vrednotenju tlačnih občutljivosti na spremembe parametrov umerjanja, zato je primerno postaviti vprašanje tlačnih občutljivosti in merilnih mest [8]. Vsota tlačnih občutljivosti posameznih merilnih mest, ki je podana na sliki 4, prikazuje, da večja ko je tlačna občutljivost vozlišča, bolj je vozlišče primerno, da postane merilno mesto. Kot primer bo obravnavano vozlišče 99, ki ima veliko tlačno občutljivost pri spremembi parametrov umerjanja in je blizu odvzema požarne vode, kar povzroča povečane pretoke in s tem tudi hidravlične izgube, poleg tega pa je tudi oddaljeno od vodnih virov. Izsledki, ki izhajajo iz predhodnih ugotovitev, so v skladu z ugotovitvami drugih raziskovalcev ([5] in [6]), ki trdijo, da naj se tlačne meritve zbirajo blizu vozlišč z veliko porabo (odjemom) in naj bodo na obrobju VS, daleč proč od vodnih virov.

Določevanje najboljših *N* merilnih mest z uporabo kriterija občutljivosti posameznih merilnih mest ni vedno tudi najboljše za določevanje skupine *N*-1 merilnih mest [6]. Upoštevanje načela nalaganja v tem primeru lahko vodi v napačne razlage, če upoštevamo povezavo med parametri umerjanja ob izračunu prve ciljne funkcije.

number of available measurement locations, e.g., the measurement equipment that can be installed. The final result is an optimal set of measurement locations obtained within the GA search process. The optimisation results in Fig. 3 are directly related to Table 1, where optimal sets of measurement location IDs are given. Table 1 is just a segment of the entire sampling design results and presents solutions from 10 to 22 measurement locations, i.e., the table determines the node IDs where the measurement devices are to be placed.

The sampling design methodology of the IMMe model is based on quantifying the pressure sensitivities to the calibration parameter changes; therefore, the pressure sensitivities and measurement location selection should be addressed [8]. Fig. 4 shows briefly the sums of the pressure sensitivities at individual measurement locations, just to indicate that the higher the node sensitivity the better the node is suited to being selected as a measurement location. The case of node 99, with the high pressure sensitivity for all the calibration parameters changes, situated near the fire flow discharges, which causes high flows and thus large hydraulic losses, is also quite remote from the water sources. This behaviour is also in agreement with the general findings by different researchers ([5] and [6]) stating that pressure measurements should be collected near the high consumption nodes and on the margin of the WDS far away from the water sources.

Determination of an optimal set of *N* measurement locations by using the sensitivity criterion for a certain measurement location is not always optimal for determining the set of *N*-1 measurement locations [6]. Using the superposition principle could be misleading if the correlation between the calibration parameters becomes significant when calculating the first objective function.

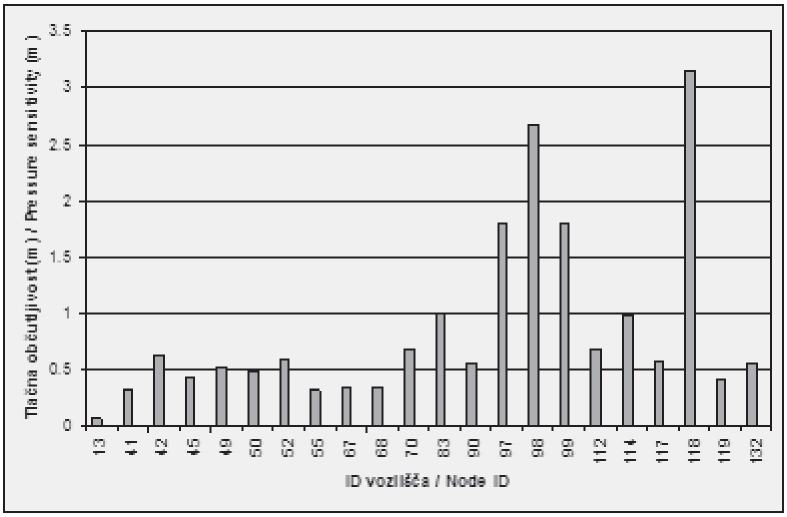

Sl. 4. *Vsota tlačnih občutljivosti vozlišč*
Fig. 4. *Sum of pressure sensitivities*

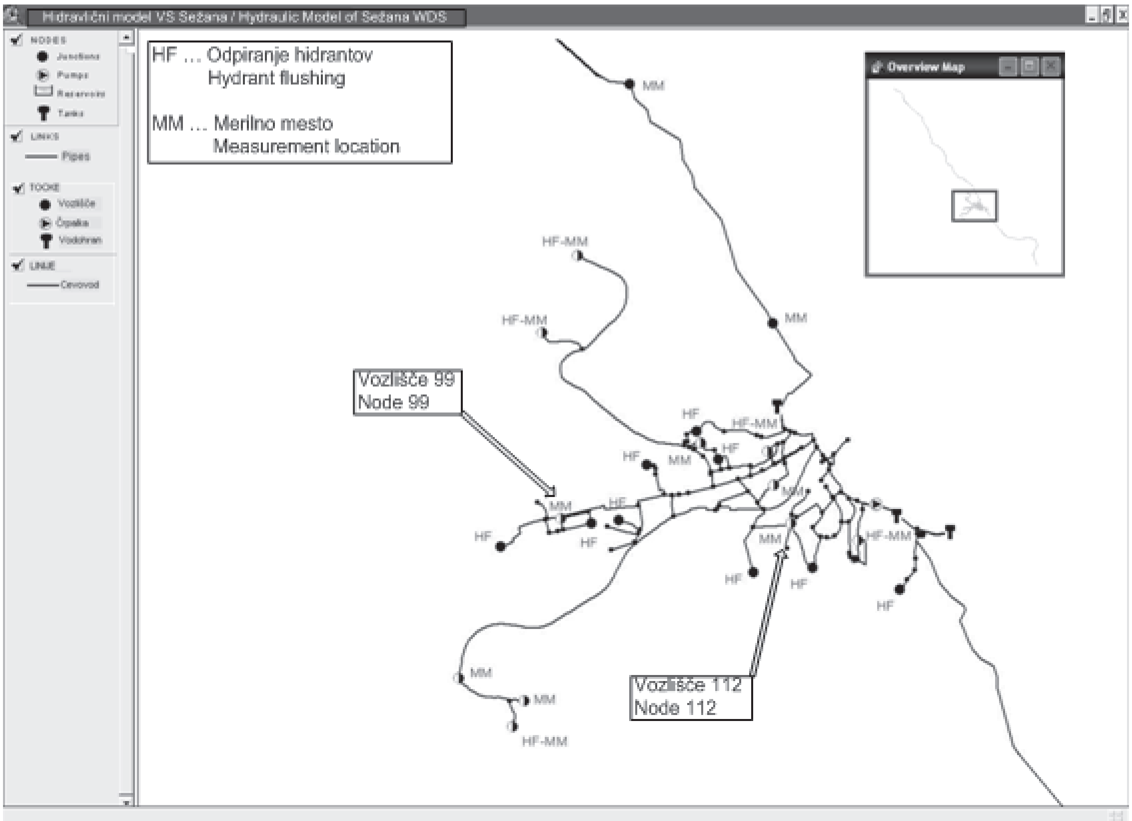

Sl. 5. *Najboljše lokacije merilnih mest za primer 13 merilnih mest*
Fig. 5. *Optimal locations for 13 measurement locations*

Izjavo lahko podkrepimo kar z rezultati izbire najboljših merilnih mest iz preglednice 1 in tlačnih občutljivosti s slike 4. Zanimiva primerjava z vidika tlačnih občutljivosti je med vozliščema 99 in 112. S

This case can be underlined by examining the sampling design results from Table 1 and the pressure sensitivities from Fig. 4. From the point of view of the pressure sensitivity of the measurement slike 4 je razvidno, da izkazuje vozlišče 99 precej večjo tlačno občutljivost kakor vozlišče 112, medtem ko je mogoče iz preglednice 1 razbrati, da je vozlišče 112 najboljše merilno mesto v primeru N= 12, medtem ko se vozlišče 99 ne uvršča v najboljši niz merilnih mest. Načelo nalaganja merilnih mest se izkaže za napačno, saj se vozlišče 112 ne pojavlja v nobenem od naslednjih petih naborov najboljših merilnih mest. Obstaja več razlogov za omenjene razlike, ki pa imajo odločilen vpliv na izbiro merilnih mest: (a) razvrščanje parametrov umerjanja, (b) hidravlične razmere, ki jih povzročijo požarni preizkusi in povečane hidravlične izgube, (c) bližina vozlišča 112 vozlišču s povečano porabo in (d) vpliv topologije omrežja. Pri razlagi primera N= 12 merilnih mest prispevajo vozlišča 112 in preostala izmed najboljših merilnih mest večjo natančnost umerjanja parametrov, kakor to izkazujejo njihove posamične tlačne občutljivosti. Opazovana lastnost izhaja iz povezave med koeficienti Jacobijeve matrike, ki določa strukturo najboljših merilnih mest glede na največjo natančnost umerjanja parametrov hidravličnega modela.

Prostorska porazdelitev najboljših 13 merilnih mest, podanega z vozlišč ID, je prikazana na sliki 5. Od 14 leg povečanega odvzema je bilo za namestitev merilne opreme izbranih samo pet vozlišč, medtem ko je preostalih 8 razporejenih drugod po VS Sežane. Z upoštevanjem dejstva, da največ "informacije" podajo prav vozlišča s povečano porabo, obravnavani primer dokazuje, da to le delno drži. Glede na dejstvo, da so se koeficienti hrapavosti cevi razvrstiti glede na podane kriterije, so najboljša merilna mesta določena na krajih, kjer bodo meritve zagotavljale največ "informacij" za čim večjo natančnost umerjanja koeficientov hrapavosti cevi.

5 SKLEPI

Razvoj, overitev in uporaba računalniškega optimizacijskega modela IMMe za najboljšo izbiro merilnih mest z uporabo GA so bili uspešni. Metodologija izbire merilnih mest upošteva lastnosti občutljivostne matrike, ki je določena s strukturo parametrov umerjanja, hidravličnimi razmerami ob zbiranju meritev, hidravličnimi veličinami, ki se merijo, in kraji zbiranja meritev. Optimizacijski problem izbire merilnih mest je določen z dvema kriterijema, in sicer največje natančnosti umerjanja in najmanjšega števila merilnih mest. Uporaba GA v postopku izbora

locations, a comparison of the nodes 112 and 99 is interesting. As can be seen from Fig. 4., node 99 has a much higher pressure sensitivity than node 112, while Table 1 in turn shows that node 112 presents the optimal measurement location in the case of N = 12, when node 99 is not selected. Differences to the superposition principle arise because node 112 does not occur in any of the following five sets of optimal measurement locations. There could be several reasons for the mentioned differences, all having a decisive impact on the sampling design: (a) calibration parameter grouping, (b) hydraulic conditions caused by the fire flow tests and its increased head losses, (c) proximity of node 112 to a node with increased consumption, (d) influence of network topology. When considering N = 12 measurement locations, node 112 and others from the optimal set contribute to a higher calibration parameter accuracy due to the first objective function, regardless of the individual pressure sensitivities. This property can be observed because of the correlation of the coefficients of the sensitivity matrix, which indicates that the optimal measurement locations are those which contribute the most to the identification of the calibration parameters.

The resulting node IDs for the 13 most informative measurement locations from Table 1 are presented in Fig. 5. Out of 14 hydrant flushings only 5 measurement locations correspond to the same location, while the remaining 8 are located elsewhere throughout the WDS. When referring to the fact that measurement data provides the most "information" at locations of high discharge, the presented case study shows this is only partly true. Optimal measurement locations were placed at positions where measurements provide most "information" for calibrating those parameters, i.e., the calibration grouped pipe roughness coefficients.

5 CONCLUSIONS

The development, verification and application of the optimisation model called IMMe for optimal sampling design by using GAs were successful. The sampling design methodology takes into account the properties of a sensitivity matrix determined by the structure of the calibration parameters, the hydraulic conditions during measurement collection, the hydraulic quantities measured, and the measurement locations. The optimisation problem of the sampling design is determined by two criteria, i.e., on the maximisation of the calibration accuracy and on the najboljših merilnih mest hidravličnega modela Anytown se je izkazala za zelo učinkovito. Po opravljeni overitvi je bil model IMMe uporabljen na dejanskem VS Sežana, kjer so bila določena najboljša merilna mesta za umerjanje koeficientov hrapavosti cevovodov. Nadaljnje raziskovalno delo naj bi bilo usmerjeno v določitev ustreznejšega zapisa druge ciljne funkcije, ki bi bila izražena oziroma odvisna neposredno od stroškov izvajanja meritev, hkrati pa tudi v vrednotenje uporabe metodologij na dejanskih VS.

minimisation of the number of measurement locations. The use of GAs in the sampling design procedure on the artificial hydraulic model of Anytown proved very efficient. After verification, the IMMe model was applied to a real WDS of Sežana, where optimal measurement locations were obtained for the pipe roughness calibration. Further research work is focused on a more appropriate expression for the second objective function, which would be directly dependent on the measurement costs and, in parallel research, on other assessments of the sampling on the WDS.

Zahvala

Rezultati raziskave so delno financirani v okviru raziskovalnega programa P2-180 in raziskovalnega projekta L2-6468, za katerega je sredstva zagotovila Agencija za raziskovalno dejavnost Republike Slovenije, s tesnim sodelovanjem University of Exeter, VB.

Acknowledgments

The obtained results are partially supported by the research programme P2-180 and research project L2-6468-0792 by the Slovenian Research Agency, with the close collaboration of the University of Exeter, UK.

6 LITERATURA
6 REFERENCES

[1] Ormsbee, L.E., Lingireddy, S. (1997) Calibrating hydraulic network models, *Journal AWWA*, Volume 89, Number 2, 1997, p. 42-50.

[2] Walters, G.A., Savic, D.A., Morley, M., de Schaetzen, W. (1998) Calibration of water distribution network models using genetic algorithms, *Proc. 7th International Conference on Hydraulic Engineering Software – Hydrosoft 98*, Southampton, UK, p. 131-140.

[3] Lansey, K.E., El-Shorbagy, W., Ahmed, I., Araujo, J., Haan, C.T. (2001) Calibration assessment and data collection for water distribution networks, *Journal of Hydraulic Engineering*, Volume 127, Number 4, 2001, p. 270-279.

[4] ECAC (1999) Calibration guidelines for water distribution modelling, P*roc. AWWA 1999 Imtech Conference*, Seatlle, USA.

[5] Kapelan, Z., Savic, D.A., Walters, G.A. (2003) Multiobjective sampling design for water distribution model calibration, *Journal of Water Resources Planning and Management*, Volume 129, Number 6, 2003, p. 466-479.

[6] Bush, C.A., Uber, J. (1998) Sampling design methods for water distribution model calibration, *Journal of Water Resources Planning and Management*, Volume 124, Number 6, 1998, p. 334-344.

[7] Knopman, D.S., Voss, C.I. (1989) Multiobjective sampling design for parameter estimation and model discrimination in groundwater solute transport, *Water Resources Research*, Volume 25, Number 10, 1989, p. 2245-2258.

[8] Kozelj, D., Šantl, S., Steinman, F., Banovec, P. (2005) Sampling design for calibration of water distribution system models by genetic algorithms, *Proceedings of the Eight International Conference on Computing and Control for the Water Industry*, University of Exeter, UK, p. 173-178.

[9] Goldberg, D.E. (1989) Genetic algorithms in search, optimization and machine learning, *Addison-Wesley Publishing Company*, USA.

[10] Steinman, F., Banovec, P., Šantl, S. (2001) Genetic-algorithms-supported planning of water supply systems, *Journal of Mechanical Engineering*, Volume 47, Number 6, 2001, p. 263-279.

[11] Keedwell, E., Khu, S.T. (2005) A hybrid genetic algorithm for the design of water distribution networks, *Engineering Applications of Artificial Intelligence*, Volume 18, Number 4, June 2005, p. 461-472.

[12] Simpson, A.R., Dandy, C.G. (1994) Genetic algorithms compared to other techniques for pipe optimization, *Journal of Water Resources Planning and Management*, Volume 120, Number 4, 1994, p. 423-443.
[13] Wall, M., Galib (1996) A C++ library of genetic algorithm components, *Mechanical Engineering Department, Massachusetts Institute of Technology*, USA.
[14] Walski, T.M. et al. (1987) Battle of the network models: Epilogue, *Journal of Water Resources Planning and Management*, Volume 113, Number 2, 1987, p. 191-203.
[15] Mallick, K.N., Ahmed, I., Tickle, K.S. Lansey, K.E. (2002) Determining pipe groupings for water distribution network, *Journal of Water Resources Planning and Management*, Volume 128, Number 2, 2002, p. 130-139.
[16] Meier, R.W., Barkdoll, B.D. (2000) Sampling design for network model calibration using genetic algorithms, *Journal of Water Resources Planning and Management*, Volume 126, Number 4, 2000, p. 245-250.

Naslov avtorjev: doc. dr. Primož Banovec
Daniel Kozelj
Sašo Šantl
prof. dr. Franci Steinman
Univerza v Ljubljani
Fakulteta za gradbeništvo in geodezijo
Hajdrihova 28
1000 Ljubljana
primoz.banovec@fgg.uni-lj.si
daniel.kozelj@fgg.uni-lj.si
saso.santl@evj-kabel.net
fsteinma@fgg.uni-lj.si

Authors' Address: Doc. Dr. Primož Banovec
Daniel Kozelj
Sašo Šantl
Prof. Dr. Franci Steinman
University of Ljubljana
Faculty of Civil and Geodetic Engineering
Hajdrihova 28
1000 Ljubljana, Slovenia
primoz.banovec@fgg.uni-lj.si
daniel.kozelj@fgg.uni-lj.si
saso.santl@evj-kabel.net
fsteinma@fgg.uni-lj.si

Prejeto:
Received: 5.5.2005

Sprejeto:
Accepted: 25.10.2006

Odprto za diskusijo: 1 leto
Open for discussion: 1 year

Strojniški vestnik - Journal of Mechanical Engineering 52(2006)12, 835-851
UDK - UDC 62-33:621.5
Izvirni znanstveni članek - Original scientific paper (1.01)

Analiza delovanja pnevmatičnega ventila s predkrmilnim piezoventilom

Analysis of the Operation of Pilot-Stage Piezo-Actuator Valves

Niko Herakovič - Dragica Noe
(Fakulteta za strojništvo, Ljubljana)

Zaradi vse večjih zahtev po boljših dinamičnih lastnostih in manjši porabi energije pnevmatičnih ventilov, je treba nenehno izboljševati sedanje elektromagnetne izvršilnike, obenem pa raziskati možnosti uporabe alternativnih aktuatorjev. Odkar so piezoelektrični izvršilniki, predvsem upogibni, pridobili na preprostosti oz. cenenosti, hitrosti delovanja in zanesljivosti, so v zadnjih letih pritegnili veliko pozornosti tudi za uporabo pri krmiljenju pnevmatičnih ventilov. V okviru predstavljene raziskave je bil razvit predkrmilni ventil z dvema upogibnima piezoelementoma ter prigrajen standardnemu pnevmatičnemu ventilu velikosti ISO 3, 5/2. V prispevku so prikazane bistvene značilnosti piezoelementov, možnosti uporabe le-teh za krmiljeneje pnevmatičnih ventilov in na koncu analiza ventila s predkrmilnim piezoelementom.

(Ključne besede: ventili pnevmatični, analize delovanja, predkrmiljenje ventilov, elementi piezoelektrični)

Due to the ever-growing demands for better dynamic properties and lower energy consumption for pneumatic valves, constant efforts to improve existing electromagnetic actuators are required, while at the same time new possibilities for alternative actuators are being searched for. Since piezoelectric actuators, especially the bender type, have become low-cost, easy to use, faster and more reliable in operation, they have also attracted a lot of attention in pneumatic control-valve applications. The presented study reports on the experimental development of a pilot-stage valve with two bending piezo-elements attached to a standard pneumatic valve of size ISO 3, 5/2. The most important characteristics of piezo-actuators and the possibilities for their use in pneumatic control valves are discussed, and the features of the developed pilot-stage piezo-actuator valve are presented.

(Keywords: pneumatic valves, operation analysis, piezo-controlled hydraulic pilot stage, piezo-elements)

0 UVOD

Pri razvoju ventilov se srečujemo z zahtevami po čim manjših izmerah, dobrih dinamičnih značilkah ter čim manjšo porabo električne energije. Pogosto se zahteva izpolnjevanje vseh treh meril. Tehnične izboljšave pri razvoju pnevmatičnih ventilov pa bo mogoče doseči tako z optimizacijo konstrukcije kakor tudi z novimi načini krmiljenja in uporabo novih materialov [1]. Raziskave na področju razvoja predkrmilnih pnevmatičnih ventilov so pokazale, da je uporaba elektromagnetnih izvršilnikov, kot predkrmilnih ventilov, omejena in je treba iskati nove rešitve. Ugotoviti je mogoče, da dosedanja uporaba piezoelektričnih pogonov v razvoju

0 INTRODUCTION

In the design and development of valves, the requirements that have to be met are the smallest possible dimensions, good dynamic characteristics and the lowest possible electric power consumption. Quite often these three criteria have to be fulfilled. Technical improvements in the development of pneumatic valves can be achieved by optimizing the design as well as introducing new principles of pneumatic control and new materials [1]. Research in the field of pilot-stage pneumatic valves has shown that the use of electromagnetic actuators in the pilot-stage has its own restrictions and that new solutions have to be sought. On the other hand, it can be established that in the development of fluid-power components and fluidnotehničnih komponent in drugih mehatronskih sistemov kaže obetavne rezultate ([2] do [6]).

Razvoj piezoelektričnih izvršilnikov zahteva dobro poznavanje piezotehnike, postopka izdelave piezoelementov ter možnosti, ki jih posamezne izvedbe piezoelementov ponujajo. Pomembna sta tako raztezek in sile, oblike in izmere piezoelementov pa so lahko prilagojene vsakokratni uporabi.

V predkrmilnih ventilih so bili v predhodnih raziskavah uporabljeni predvsem upogibni konzolni piezoelementi ([6],[10] in [18]). Namen naše raziskave pa je analizirati možnosti uporabe mostičnega piezoelementa [1]. Zato je bil okviru raziskave standardni izvedbi pnevmatičnega potnega ventila, namesto magnetnih premikal, prigrajen predkrmilni ventil z mostičnim piezoizvršilnikom, rezultate delovanja oz. značilke ventila pa smo primerjali z elektromagnetnim predkrmilnim ventilom.

1 IZHODIŠČA ZA RAZVOJ VENTILA S PREDKRMILNIM PIEZOVENTILOM

Pnevmatični posredno krmiljeni ventili so zgrajeni iz glavnega ventila, ki usmerja zrak od napajanja k porabniku ter predkrmilnega ventila (pk1 in pk2), ki preklaplja oziroma krmili glavni ventil – gv (sl. 1). Naloga predkrmilnega ventila je spremeniti električno energijo v mehansko delo, oziroma premik zapirnega elementa, ki usmerja krmilni zrak na krmilni priključek glavnega ventila. Na ta način so izmere izvršilnikov predkrmilnega ventila manjše, manjša pa je tudi poraba moči.

V preteklosti je bilo razvitih več načinov pogonov, ki električni signal spremenijo v silo ali premik. Naloga pogona je povezovati električni krmilni obtok s pnevmatičnim, oziroma spremeniti električno energijo v energijo

other mechatronic systems the use of piezoelectric actuators has become very promising ([2] to [6]).

The development of piezoelectric actuators requires a good knowledge of piezo technology, manufacturing procedures and the possibilities offered by their particular designs. Factors that are important to consider are the extension and the force, while the shapes and sizes of piezo elements can be adapted to each particular application.

In pilot-stage valve applications, previous researchers have mainly used bending cantilever piezo-elements ([6],[10] and [18]). The aim of our study was to analyze the use of another possible type, i.e., a bending crossbow piezo-element [1]. For this purpose, a pilot-stage valve with a crossbow piezo-actuator was built to a standard pneumatic directional valve, and the results and the characteristics of the thus obtained valve were compared to an electromagnetic pilot-stage valve.

1 CONSIDERATIONS IN THE DESIGN OF PILOT-STAGE PIEZO-ACTUATOR VALVE

Pneumatic pilot-stage valves consist of the main valve that directs the air from the supply source to the consumer and a pilot-stage component (pk1 and pk2) that switches on/off the main valve (gv), Fig 1. The task of the pilot-stage valve is to convert the electrical energy into mechanical work or displacement of the closing element, which then directs the controlling air onto the control element of the main valve. This kind of design makes it possible for the dimensions of pilot-stage actuators to be smaller and the power consumption to be lower.

In the past, a number of actuator principles for converting an electrical signal into a force or motion have been developed. The task of the actuator is to connect the electrical control circuit with the pneumatic circuit, or, in other words, to convert the electri-

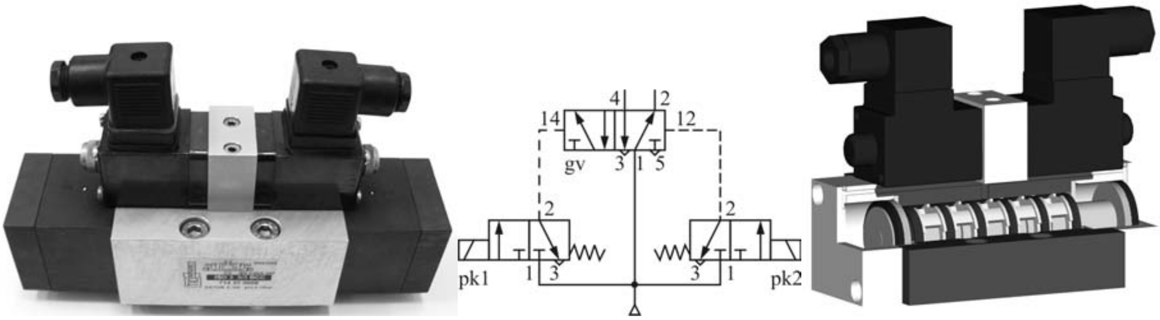

Sl. 1. *Elektromagnetni posredno krmiljeni pnevmatični 5/2 potni ventil [17]*
Fig. 1. *Electromagnetic pilot-stage directional pneumatic valve 5/2 [17]*

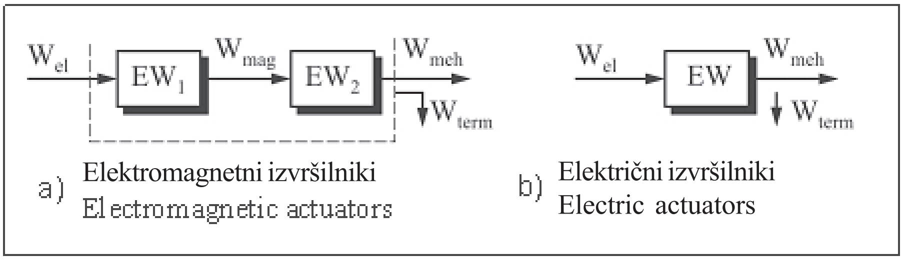

Sl. 2. *Spreminjanje električne energije v mehansko*
Fig. 2. *Conversion of electrical energy into mechanical energy*

stisnjenega zraka. Po načinu delovanja so elektromehanski pretvorniki (EP) razdeljeni v elektromagnetne in električne izvršilnike. Elektromagnetni najprej električno energijo spremenijo v magnetno energijo in nato v mehansko, pri električnih pa je ta sprememba neposredna (sl. 2 a in b).

Vprašanje je, kakšne možnosti ima elektromagnetni izvršilnik v smislu skrajševanja preklopnih časov, zmanjševanja izmer ter zmanjševanja porabe moči. V fizikalnem smislu nastanejo, zaradi magnetne indukcije in vrtinčnih tokov pri vklopu električnega toka, zakasnitve pri preklopu. Preklopni časi so tem krajši, čim manjše so mase gibljivih delov in čim krajši je gib jedra tuljave. Pri najboljši izvedbi elektromagnetnih premikal so preklopni časi v območju 500 μs, za običajne izvedbe ventilov pa je čas preklopa med 10 in 20 ms. Pomembna za uporabnike pa je tudi ponovljivost preklapljanja v vsej dobi trajanja v pričakovanem okolju. Posebni ventili lahko dosežejo ponovljivost tudi pri 100 milijonih gibov ([1], [3], [6] in [7]).

Naslednji ukrepi, ki jih je mogoče zaslediti pri razvoju elektromagnetnih predkrmilnih ventilov, so povezani z zmanjševanjem prostornine pnevmatičnih komponent pri enakih ali celo povečanih pretokih stisnjenega zraka. Trenutno se je zmanjševanje ustavilo pri 10 mm. Nadaljnje zmanjševanje izmer onemogočajo elektromagnetni izvršilniki. Izdelava manjših ventilov je zaradi zahtevnih tehnoloških postopkov manjših elektromagnetov ekonomsko neupravičena. Napredek je mogoče iskati v smeri izvršilnikov na podlagi silicija. Trenutno je tako imenovana mikropnevmatika, pri kateri so izmere pnevmatičnih predkrmilnih ventilov samo nekaj mm, na začetku svojega razvoja. Problem, ki nastane pri zmanjševanju izmer, se kaže dandanes v nesorazmerju pnevmatičnega dela s priključki za zaznavala, pri

cal energy into the energy of compressed air. In terms of operation, electro-mechanical transducers (EP) can be divided into electromagnetic and electrical actuators. The electromagnetic actuators convert electrical energy first into magnetic energy and then into mechanical energy, whereas the electrical actuators transform it directly (Fig 2 a and b).

The potentials of the electromagnetic actuators are questionable when factors such as shorter switchover times, smaller dimensions and lower power consumption are considered. In the physical sense, due to magnetic induction and eddy currents during switching the current on, delays in switchover occur: the shorter the switchover times, the lower are the masses of the moving parts and the shorter is the movement of the core of the coil. In optimal electromagnetic-actuator design solutions, the switchover times are in the range of 500 μs, while for standard valve designs the switchover time ranges between 10 to 20 ms. The switchover repeatability during the life time in a foreseen environment is also important for customers. Special valves may reach a repeatability as high as 100 million strokes ([1], [3], [6] and [7]).

Some efforts in the development of electromagnetic pilot-stage valves are directed into reducing the volume of the pneumatic component at equal or even higher compressed air-flow rates. So far the reductions have stopped at *10 mm*^{3}. A further scale-down of dimensions is not possible because of the electromagnetic actuators. Due to demanding technological procedures the manufacturing of smaller valves is not economically justifiable. However, an advancement could be looked for in the direction of making actuators based on silicon. Currently, the so-called micro-pneumatics, where the dimensions of pneumatic pilot-stage valves reach just a few mm, is still in its early stages. The problem in scaling down the dimensions is in the disproportion between the pneumatic part and the sensor connectors, where the pneumatic part can be

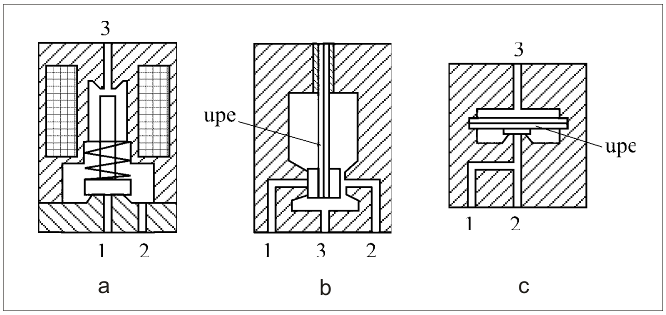

Sl. 3. *Izvedbe predkrmilnih ventilov, a - elektromagnetni, b - z dvoslojnim upogibnim piezoelementom, c - z mostičnim piezoelementom - izvedba z odbojno šobo, upe - upogibni piezoelement*
Fig. 3. *Designs of pilot-stage valves a - electromagnetic, b - two-layer bending piezo-element, c - crossbow piezo-element – flapper nozzle system, upe - bending piezo-element*

katerih je pnevmatični del bistveno manjših izmer od priključkov za zaznavala. Za zdaj tu še ni ustreznih rešitev (M12 priključek je sedaj še nujnost) [6] .

Več razlogov narekuje razvoj učinkovitih elektromehanskih pretvornikov, ki se uporabljajo v vrsti elektronskih naprav in nenazadnje tudi v pnevmatiki. Eden izmed njih je tudi zahteva po energetsko varčnih komponentah in je posledica zahtev po varčevanju energije v vseh vrstah uporab. Razviti so piezoelektrični, elektrouporni, magnetouporni, spominski elementi, elektromagnetni itn. [1]. Za velike dinamične zahteve je piezoelektrični izvršilnik prav gotovo najprimernejši. Prednost piezoelektričnih materialov je v tem, da spreminjajo električno energijo v mehansko in nasprotno skoraj brez izgub (sl. 2).

Med različnimi izvedbami električnih izvršilnikov imajo piezoelektrični največje možnosti za široko in ekonomsko upravičeno uporabo ([4], [6] in [7]). Ker so v pnevmatiki preklopne sile, v primerjavi s hidravliko majhne, so primerni za uporabo predvsem upogibni piezoizvršilniki oziroma elementi. Razvoj piezo materialov in pogonov je v zadnjih letih močno napredoval, tako da je mogoče z uporabo novih materialov in tehnologij izdelati upogibne piezoizvršilnike, primerne za krmilne sile tudi do 100 N ali v posebnih izvedbah do 1kN [15]. V pnevmatiki so se do sedaj v največji meri uporabljali predvsem konzolni upogibni piezoelementi, vendar imajo tudi mostični piezoelementi primerne značilnosti za uporabo pri krmiljenju potnih ventilov (sl. 3).

2 UPOGIBNI PIEZOIZVRŠILNIKI

Piezopojav je lastnost številnih materialov, ki jih najdemo v naravi. Njihova poglavitna značilnost

significantly smaller than the connectors. At the current stage of development there are still no suitable solutions available (an M12 connection is still a necessity) [6].

There is a growing need to develop efficient electro-mechanical transducers that can be used in electronic devices and fluid power systems. One reason for this is the need for energy-saving as a general trend in all kinds of applications. Some of the most recent developments are piezoelectric, magnetoresistive, electromagnetic and shape-memory elements [1]. There is no doubt that for high-dynamic-load applications the piezoelectric actuators are the best choice. The advantage of piezoelectric materials lies in the fact that they convert electrical energy into mechanical and vice versa, almost without any losses (Fig 2).

Among the various kinds of electric actuator, the piezoelectric actuators have the best chance to become widespread and economically justifiable. ([4], [6] and [7]). Since in pneumatic systems the switchover forces are low compared to hydraulic systems, the bending piezo-actuators are the ones that are especially suitable for pneumatic applications. Recently, there has been considerable progress in the development of piezo-materials and piezo-actuators so that with the use of new materials and technologies it is possible to manufacture bending piezo-actuators suitable for control forces up to 100 N, or in cases of special design, even 1 kN [15]. In pneumatic systems, cantilever bending piezo-actuators are mostly used, though the crossbow piezo-actuators also possess properties suitable for use in directional control valves (Fig 3).

2 BENDING PIEZO-ACTUATORS

The piezo effect is a feature of numerous materials found in nature. Their basic characteristic is je ta, da se na kristalu pri mehanski deformaciji, zaradi tlačne ali natezne sile, pojavi električni naboj. Ta pojav je imenovan tudi neposredni piezopojav. Nasprotni pojav, ko se kristal pod vplivom električnega polja deformira – skrči ali raztegne, pa se imenuje inverzni ali povratni piezopojav in je uporaben za premikala oziroma pogone.

that on a crystal subjected to mechanical deformation, as a result of compressive and tensile forces, an electrical charge is created. This effect is also known as the direct piezo effect. The opposite phenomenon, when under the influence of an electric field the crystal deforms, i.e., it contracts or extends, is called the reverse piezo effect. This is used in actuators.

2.1 Osnovna načela delovanja

Za razumevanje povratnega piezopojava, ki sta ga opredelila v letu 1881 Curie in Lippman ([8] in [9]) je treba razumeti *električno polarnost*, katere povzročitelji so *električni dipoli.* Pri tem je električni dipol primerljiv z magnetnim, torej s tako imenovanim elementarnim magnetom vendar v električnem smislu. Dipol je mogoče prikazati z negativnim (- q) in pozitivnim nabojem (+q) in puščico, ki je usmerjena od negativnega k pozitivnemu dipolu. Opisati ga je mogoče z momentom dipola, z vektorjem p, ki je definiran kot zmnožek naboja q in medsebojne oddaljenosti l in je podan v enoti dolžine (sl. 4 a).

Električna polariteta je lahko naravna ali pa nastane pri delovanju električnega polja na nepolarizirane atome - spontana polarizacija. Polarizacija je lahko trajna ali pa po prenehanju delovanja električnega polja izgine. Za razvoj piezopogonov je zanimiva trajna ali permanentna polarnost.

Dipol se v močnem električnem polju E usmeri glede na smer polja. Pri tem deluje na pozitivni del dipola sila F_1 v smeri električnega polja in sila F_2 v nasprotni smeri (sl. 4 b). Dvojica sil se izrazi kot vrtilni moment M, ki je enak zmnožku potenciala p in električnega polja E ($M= p \cdot E$).

2.1 Basic principles of operation

The reverse piezo-effect, first described in 1881 by Curie and Lippman ([8] and [9]), can be explained by the electrical polarity caused by electric dipoles. Here, the electrical dipole is comparable to the magnetic one, i.e., to the so-called elementary magnet, but in the electrical sense. A dipole can be presented with a negative (- q) and positive charge (+ q) and an arrow directed from the negative to the positive dipole. It can be defined by the dipole moment, vector p, defined as the product of the charge q and the distance l between them, Fig 4a.

Electrical polarity can be natural or can occur when an electrical field acts on non-polarized atoms, i.e., spontaneous polarization. Polarization can be permanent or can disappear after the electrical field stops acting. It is the permanent polarization that is of interest in the development of piezo-actuators.

In a strong electric field, $E,$ a dipole aligns with the direction of the electric field. In this way only the positive part of the dipole is acted on by force $F1$ in the direction of the electrical field, and $F2$ in the reverse direction (Fig 4b). The force couple expresses itself as a rotating moment M equal to the product of the potential, p, and the electrical field E ($M = p \cdot E$).

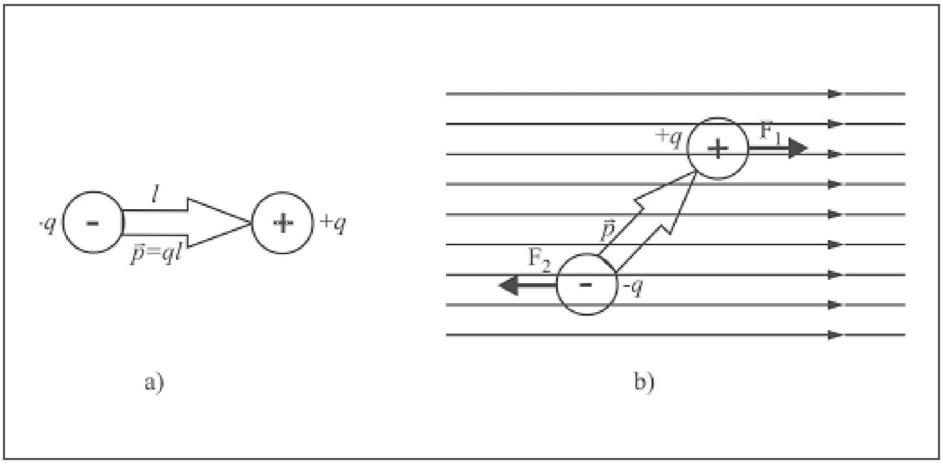

Sl. 4. *Dipol (a) in dipol v električnem polju (b)*
Fig. 4. *Dipole (a) and dipole in the electric field (b)*

Za dipole v dielektriku velja, da so naključno usmerjeni in je material navzven nevtralen. S postavitvijo materiala v električno polje se dipoli ustrezno usmerijo in na površini dielektrika nastane površinski naboj.

Kadar govorimo o dipolih v trdnih telesih, mislimo s tem polarizirane elementarne kristalne mreže. Najbolj znan piezomaterial je kremen, vendar piezopojav pri njem ni dovolj izrazit, sile so majhne in tako ni primeren za krmiljenje pnevmatičnih ventilov. Mnogo primernejši materiali so različne feroelektrične keramike, med njimi barijev titanat (BaTiO3), svinčev titanat, svinčev cirkonat in svinčev cirkonat-titanat (PZT). Fizikalne lastnosti PZT piezokeramike so odvisne od mešanice cirkonija in titanata in dodanih drugih materialov, ki so specifični za posamezne izdelovalce piezoelementov.

Kristaliti PZT so pred polarizacijo centrosimetrično kubični (izotropno), po polarizaciji pa kažejo tetragonalno simetrijo (anizotropna sestava), in sicer v pogojih, ko vrednost temperature ne presega Curie-jeve temperature [9]. Nad to temperaturo kristali izgubijo piezoelektrične lastnosti.

V piezomaterialu, ki je zgrajen iz več osnovnih kristalov, so dipoli umerjeni naključno. Vendar se v materialu najdejo skupine kristalov oziroma dipolov, ki so enako usmerjene. Take skupine so označene kot območja, ki v bistvu ustrezajo makroskopskemu dipolu, saj so znotraj polarizirane. Ker so ta območja ponovno naključno usmerjena, kristal na zunaj ne kaže polarnosti. Če se tak material postavi v močno električno polje nekaj kV na mm dolžine, se območja pričnejo usmerjati, posamezne skupine jeder kristala dobijo enako usmerjenost in jedra rastejo na račun drugih. Z zamrznitvijo polariziranega stanja dobimo piezoelektrični kristal s polarizirano osjo. Pod Curie-

Dipoles in a dielectric fluid have a random sense of direction, and outwardly the material acts as neutral. By placing the material into an electric field, the dipoles align accordingly, and on the surface of the dielectric a surface charge is produced.

Dipoles in reference solids are displayed as polarized elementary crystals in the crystal lattice. A is commonly known, quartz is a piezo-material; however, in quartz the piezo effect is not distinct enough, the forces induced are small, which makes it inappropriate for use in pneumatic valves. Much more suitable materials include some ferromagnetic ceramics, among them barium-titanate (BaTiO3), lead-titanate, lead-zirconate and lead-zirconate-titanate (PZT). The physical properties of PZT piezo-ceramics depend on the proportion of zirconium and titanium and their additions specific for each particular manufacturer of piezo-elements.

Prior to polarization PZT crystallites are axisymmetrical cubes (isotropic), after the polarization, however, they display a tetragonal symmetry (anisotropic structure), and this is in conditions when the temperature does not exceed the Curie temperature [9]. Above this temperature the crystals lose their piezoelectric properties.

In a piezo material made from several basic crystals, the dipoles are directed randomly. However, in the material it is possible to find groups of crystals that have the same direction. These groups are marked as domains and actually correspond to the macroscopic dipole because they are polarized on the inside. Since these domains again are randomly directed, on the outside the crystal does not display any polarity. If such materials are subjected to a strong electric field of a few *kV* per *mm* of length, the domains start aligning themselves, and particular groups in the crystal core become equally directed and these cores start growing at the expense of others. By freezing such a polarized state, a piezoelectric crystal with a polarized axis is obtained. Below the Curie temperature and on removal

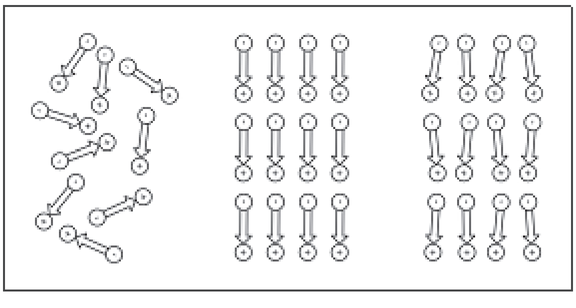

Sl. 5. *Predstavitev posameznih kristalnih zrn in njihovih območij*
Fig 5. *Presentation of crystal grains and their domains*

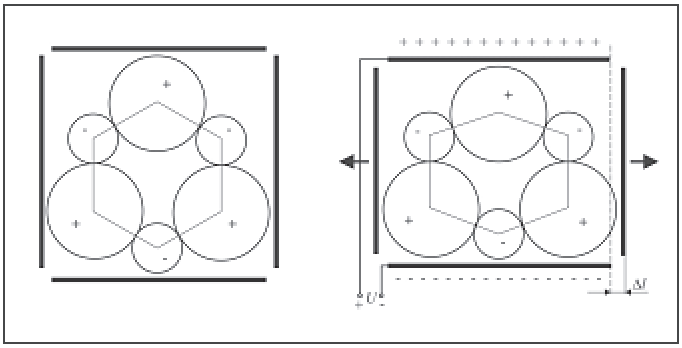

Sl. 6. *Deformacija kristalne rešetke pri postavitvi v električno polje*
Fig. 6. *Deformation of crystal lattice when subjected to electric field*

jevo temperaturo in po odstranitvi električnega polja se dipoli sicer nekoliko razbremenijo, vendar v večini ostanejo v dani usmerjenosti (sl. 5).

Pri ponovni postavitvi piezoelektrične keramike v električno polje se polarizacija območij ponovno ojači in kristal se deformira, oziroma razširi vzdolž osi polarizacije (sl. 6).

Deformacija kristala Δl je odvisna od jakosti električnega polja E oziroma napetosti U in piezo modula d_{ij}, kjer je i smer električnega polja v kartezičnem koordinatnem sistemu in j smer deformacije za dano polarizacijo kristala (sl. 7).

of the electric field, the dipoles discharge slightly, but mainly remain in the given direction (Fig 5).

By putting the piezoelectric ceramic back into the electric field, the polarization of the domains intensifies again and the crystal deforms or extends along the polarization axis (Fig 6).

The deformation of the crystal depends on the intensity of the electric field, *E*, or the voltage, *U,* and piezo-module, dij, where i denotes the direction of the electric field in the Cartesian coordinate system and j the direction of deformation for a given polarization of the crystal (Fig 7).

$$\Delta l = d_{ij} \cdot E \cdot l_o = d_{ij} \cdot l_o \cdot U/l_o = d_{ij} \cdot U \qquad (1).$$

Glede na smer delovanja električnega polja in smer polarizacije se kristal lahko deformira v smeri polarizacije ali pravokotno na polarizacijo. Tako predstavlja piezomodul d_{33} vzdolžno deformacijo kristala v smeri osi z, ko je smer električnega polja enaka smeri prvotne polarizacije, v osi z, piezomodul d_{31} pa prečno deformacijo glede na smer električnega polja, ko je smer polarizacije v osi z in deformacija

With respect to the working direction of the electric field and the direction of polarization, the crystal may deform in the direction of polarization of perpendicularly to it. Thus, the piezo module, d_{33}, represents the longitudinal deformation of the crystal in the direction of the z-axis, when the sense of direction of the electrical field is the same as the direction of the original polarization in the z- axis, and the piezo-module d_{31} presents a transverse deformation with respect to the direction of

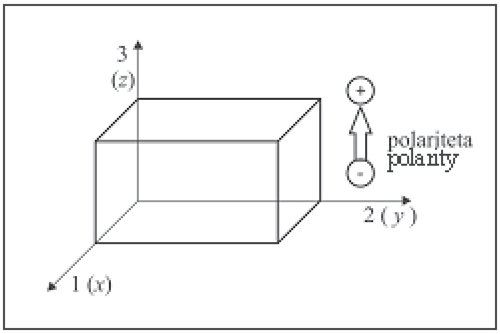

Sl. 7. *Opredelitev indeksov piezomodula*
Fig. 7. *Determination of the subscripts of a piezo module*

pravokotno na os z. Za polikristalno keramiko PZT je vrednost modula d_{33} med vrednostjo 50 in 765 pm/V [11].

Pri izbiri piezoizvršilnikov, primernih za pogon pri pnevmatičnih ventilih, je poleg največjega raztezka aktuatorja Δl treba poznati še največjo dopustno silo F, ki jo lahko piezoizvršilnik doseže, ter točko delovanja glede na najboljšo silo in raztezek. Največja sila, imenovana tudi omejevalna sila, ki se vzpostavi v piezoelementu, ko je ta pod napetostjo in je vpet med dve aboslutno togi površini, ki ne dopuščata raztezka - $\Delta l/l$=0. Sila je odvisna od vzmetne stalnice kristala in deformacije:

the electrical field, when the sense of direction of the polarization is in the z-axis and the deformation is perpendicular to the z-axis. For PZT polycrystalline ceramics the value of the module d_{33} ranges between 50 to 765 pm/V [11].

When selecting piezo-actuators suitable for pneumatic valves, besides the maximum elongation of the actuator, we also need to know the maximum allowable force F a piezo-actuator can reach, and the point of action with respect to the optimal force and extension. The maximum force, called the blocking force, is the force occurring in the piezo element when the latter is under stress and is fixed between two absolutely rigid surfaces allowing no extension, i.e., $\Delta l/l = 0$. The force depends on the spring constant of the crystal and the deformation.

$$F= k_T \cdot d_{ij} \cdot U \qquad (2),$$

kjer je k_T – vzmetna stalnica piezo kristala oziroma količnik togosti, ki je odvisen od vrste parametrov.

Primer delovnega diagrama piezoizvršilnika je podan na sliki 8. S tem diagramom, ki je specifičen za vsak piezoizvršilnik, je mogoče preprosto razbrati delovne točke piezoizvršilnika med obema mejnima vrednostima sile in raztezka. Najboljša točka delovanja vsakega piezoizvršilnika je na polovici zveznice med največjo silo in največjim upogibom oz. raztezkom (sl. 8).

Pri ogrevanju piezomaterialov nad Curie-jevo temperaturo T_c polarizacija kristalov piezoizvršilnika izgine. Podatek je pomemben prav za uporabo v

where k_T is the spring constant of the piezo-crystal or the coefficient of stiffness, depending on a number of parameters.

Figure 8 shows in a graph the optimal operating point of a piezo-actuator. From this force-deflection graph, which is specific for each piezo-actuator, we can easily see the operating points of piezo-actuators lying between the limit values of force and extension. The optimal operating point of each piezo-actuator is in the middle of the connecting line between the maximum force and the maximum deflection or extension (Fig. 8).

When piezo-materials are heated above the Curie temperature, T_c, the polarization of the crystals disappears. This data is important for high-

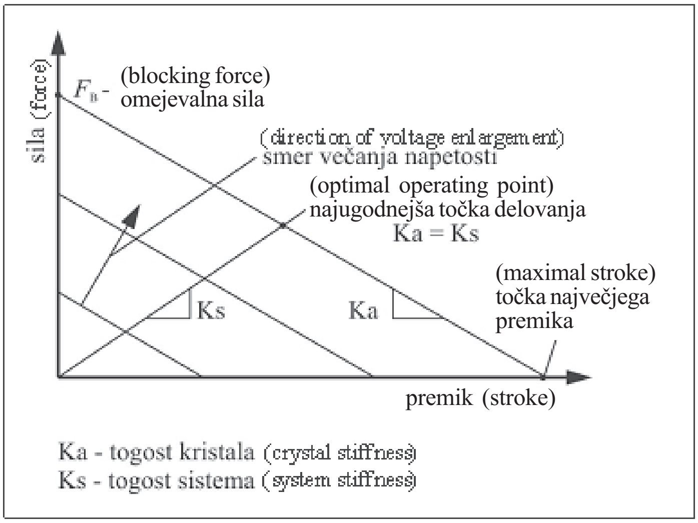

Sl. 8. *Diagram sila - raztezek pri različnih električnih napetostih napajanja*
Fig. 8. *Force-deflection graph in relation to voltage*

delovanju pri povišanih temperaturah. Curie-jeva temperatura za keramični kristal je T_c = 570 °C, medtem ko ima svinčev cirkonijev titanat PZT ($Pb[ZrTi]O_3$) Curie-jevo temperaturo okrog 350 °C. Pri ohlajanju kristal ponovno samodejno polarizira, vendar ne dobimo izrazite usmerjenosti dipolov, zato je treba tak pogonski element ponovno polarizirati.

2.2 Izvedbe upogibnih piezoizvršilnikov

Za krmiljenje pnevmatičnih ventilov je mogoče izbirati med več konstrukcijskimi različicami upogibnih piezopogonov. Najpogosteje sta to enostransko vpet trak ali obojestransko vpeta ploščica (sl. 9). Najpreprostejši upogibni izvršilniki so zgrajeni iz jeklenega traku, na katerega je nanesen (prilepljen) sloj piezomateriala. S priključitvijo električne napetosti se piezokeramični material podaljša, posledica pa je upogib oz. izbočitev nosilca oz. traku.

Upogibni dvoslojni piezoizvršilniki sestoje iz dveh piezokeramičnih ploščic, ki sta vezani zaporedno oziroma vzporedno glede na smer polarizacije (sl. 10). Pri piezoizvršilniku z zaporedno vezavo električno napajanje deluje preko obeh plasti. Vzporedna vezava zahteva dovajanje napetosti na vsako plast ločeno, tako dvoplastni izvršilnik zahteva tri priključke, dva priključka na zunanji elektrodi in en priključek za vmesno plast, ki ločuje oba piezoelementa. Za enak raztezek oz. upogib izvršilnika v vzporedni vezavi je potrebna polovična električna napetost kakor pri zaporedni vezavi.

temperature applications. The Curie temperature for a ceramic crystal is T_c = 570°C, while the lead-zirconium titanate PZT ($Pb[ZrTi]O_3$) has a Curie temperature around 350°C. During cooling down, the crystal is automatically re-polarized; however, the sense of direction of the dipoles is no longer clear, so that such an actuator has to be re-polarized.

2.2 Configurations of bending piezo-actuators

For the operation of pneumatic control valves it is possible to choose among several configurations of bending piezo-actuators. Most often these configurations involve either cantilever bending strips or plates fixed on both ends in a crossbow (Fig 9). The simplest bending actuators are built from a steel strip with a layer of piezo-material deposited (or glued) onto it. When the electrical power is switched on, the piezo-ceramic material extends and the result of this is the bending or deflection of the beam or strip.

A bending two-layer piezo-actuator consists of two piezo-ceramic plates in series or parallel connection with respect to the direction of polarization (Fig. 10) In the series connection the power supply acts across both layers, whereas in the parallel connection the power has to be supplied separately to each layer. Thus, a two-layer actuator requires three power supplies, two on the outer electrode and one for the middle layer, separating both piezo-elements. To reach the same actuator extension or deflection as in the series connection, the required voltage in the parallel connection is halved.

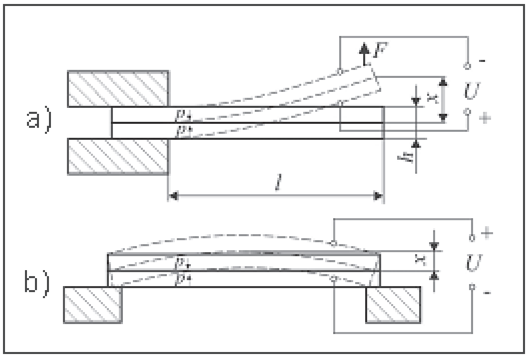

Sl. 9. *Enostransko vpet piezoelement (a) in mostični piezoelement (b)*
Fig. 9. *Cantilever piezo-element (a) and crossbow piezo-element (b)*

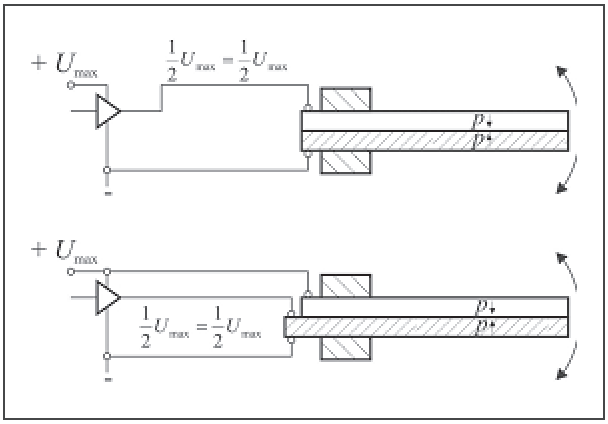

Sl. 10. *Električno napajanje vzporedno in zaporedno vezanih piezoizvršilnikov*
Fig. 10. *Power supply in parallel and series connection*

3 RAZVOJ PREDKRMILNEGA VENTILA S PIEZOELEMENTOM, ŠOBO IN ODBOJNO PLOŠČO

V okviru raziskave je bil razvit nov predkrmilni ventil, ki je bil prigrajen na glavni pnevmatični ventil običajne izvedbe velikosti ISO 3. V predkrmilnem ventilu je bil uporabljen sistem, ki deluje po načelu šoba – odbojna plošča (sl. 11a). Ventil sestavljata dve šobi – nespremenljiva šoba (kš) s premerom $d_{kš}$ in nastavljiva šoba (nš) s premerom $d_{nš}$ ter odbojna plošča (op), ki je oddaljena od nastavljive šobe za razdaljo h in pritrjena na mostični piezoelement. Izvršilnik napaja stisnjen zrak tlaka p_n, ki odteka skozi obe šobi v ozračje in tudi v krmilno komoro pnevmatičnega ventila. S približevanjem odbojne plošče se tlak p_k na izhodu počasi zvišuje, oz. pri oddaljevanju znižuje. Pri tem je bilo treba upoštevati, da mora piezoizvršilnik omogočati dotok zraka na eno stran potnega ventila in odzračitev druge strani (sl. 11b) ter zagotoviti dovolj veliko silo tlaka za prekrmiljenje glavnega ventila kakor tudi ustrezno frekvenco preklopov.

Za določitev najboljšega razmerja premerov obeh šob ($d_{kš}$ in $d_{nš}$) je bilo treba analizirati delovanje predkrmilnega piezoventila. V ta namen je bilo postavljeno preizkuševališče ([12] in [13]) in izvedene meritve poteka tlaka p_k oz. posredno poteka preklopne sile glavnega ventila. Na temelju meritev sta bila določena potreben premik odbojne plošče h in potrebna sila F, ki jo mora zagotoviti piezoelement, da pride do popolnega odzračenja krmilne komore glavnega ventila na eni strani in vzpostavitve dovolj velike preklopne sile oz. tlaka

3 DEVELOPMENT OF A PILOT-STAGE PIEZO-ACTUATOR VALVE WITH A FLAPPER/NOZZLE SYSTEM

In the experimental part of our research, a new pilot-stage valve was developed and built into the main pneumatic valve of a standard configuration size, ISO 3. In the pilot-stage valve a system working on the nozzle/flapper principle was used, Fig 11. The valve consists of two nozzles: the constant nozzle (kš) with a diameter dkš, and an adjustable nozzle (nš) with a diameter dnš. >There is also a flapper (op) distanced from the adjustable nozzle by a distance h and fixed to the crossbow piezo-element. The actuator is fed by compressed air with a pressure p_n, which flows out through both nozzles into the atmosphere, but also into the control chamber of the pneumatic valve. When the flapper is approaching the pressure *pk* at the outlet gradually increases and when the flapper is returning the pressure decreases. Here, it was necessary to consider that the piezo-actuator has to enable air inflow to one side of the directional valve and air relief on the other side (Fig 11) and provide a large enough pressure for piloting the main valve as well as a suitable switchover frequency.

To determine the optimal diameter ratio of both nozzles ($d_{kš}$ / $d_{nš}$) it was necessary to analyze the operation of the pilot-stage piezo-actuators. For this purpose a test rig was set up ([12] and [13]) to measure and observe the histories of the pressure p_k and the switchover force of the main valve. The measurements provided a basis for the determination of the necessary flapper displacement, h, and the necessary force, *F,* that have to be provided by the piezo-element to achieve complete air relief in the control chamber of the main valve, on the one side, and a large enough switchover

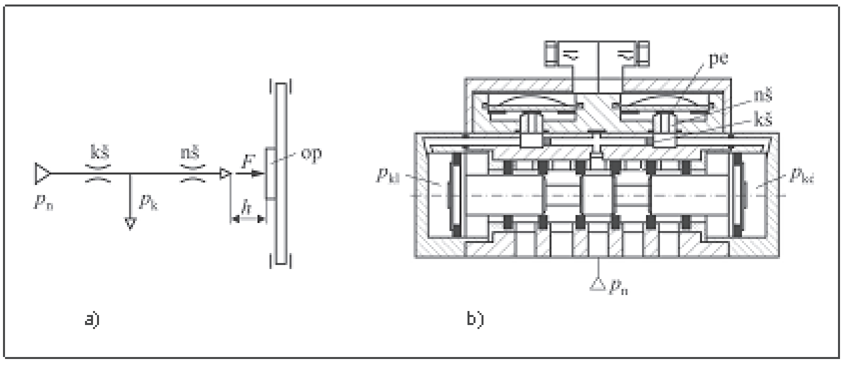

Sl. 11. *Shematični prikaz sistema šoba - odbojna plošča (a) in glavni ventil s predkrmilnima piezoventiloma, ki delujeta po načelu šoba - odbojna plošča, v prerezu (b)*

Fig. 11. *a) Schematic of the nozzle-flapper system; b) the main valve with the pilot-stage piezo-actuators, flapper/nozzle design, cross section*

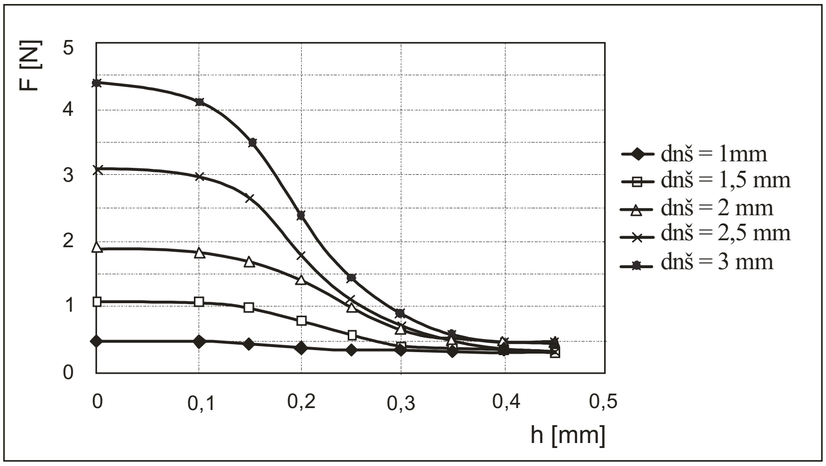

Sl. 12. *Potek odvisnosti sile F od odmika odbojne plošče in premera nastavljive šobe*
Fig. 12. *Force, F, versus flapper displacement for various adjustable nozzle diameters*

v krmilni celici na drugi strani bata glavnega ventila. Na sliki 12 so prikazani rezultati meritev tlaka p_k oz. sile F v odvisnosti od odmika odbojne plošče h od nastavljive šobe pri različnih razmerjih premerov obeh šob (kš in nš).

Poteki sile F pri različnih premerih nastavljive šobe so značilni in kažejo odvisnost sile F od odmika odbojne plošče h. Rezultati kažejo, da se sila F prične zmanjševati pri odmiku odbojne plošče h= 0,1 mm (sl. 12). Hitrost zmanjševanja sile se z večanjem premera šobe veča. Sila F se pri odmiku h=0,4 mm zmanjša na vrednost 0,5 N, neodvisno od premera nastavljive šobe. Iz tega je mogoče sklepati, da v krmilni celici ostaja še vedno tlak v vrednosti okrog 1 bar. Ugotovimo tudi, da je največja sila pri premeru nastavljive šobe 3 mm pod 4,5 N. Pri manjših premerih šob se sila tlaka na odbojno ploščo zmanjšuje.

Na potek preklapljanja ventila neposredno vplivata obe šobi v predkrmilnem ventilu ter odmik zaslonke h. Raziskava je pokazala, da na delovanje pnevmatičnega potnega ventila značilno vpliva razmerje med premerom nespremenljive šobe in premerom spremenljive šobe. Izpolnjen mora biti pogoj, da je $d_{kš} < d_{nš}$. Številne meritve so pokazale, da je za dani primer najugodnejše delovanje piezopremikala pri premeru $d_{kš}$ = 1,6 mm in $d_{nš}$ = 2,5 mm do $d_{nš}$ = 3 mm ([12] in [13]).

Za določitev piezoelementa in njegovih značilk je treba opredeliti še razmere pri praznjenju in polnjenju krmilnih celic glavnega ventila v povezavi s premikom odbojne plošče h in sile F s katero deluje curek zraka pri iztoku iz $d_{nš}$ na mostični piezoelement.

force or pressure in the control chamber on the other side of the piston of the main valve. Fig 12 shows the measured results of the pressure, p_k, or force, F, versus the flapper displacement, h, from the adjustable nozzle at various diameter ratios of both nozzles (kš and nš).

The successive changes of the force, F, at various diameters of the adjustable nozzle are characteristic and show the dependence of force, F, on the flapper displacement, h. The results show that the force, F, starts falling at the flapper displacement h = 0.1 mm (Fig 12). The rate at which the force is falling increases with increasing nozzle diameter. At the displacement h = 0.4 mm, the force, F, falls to 0.5 N, irrespective of the diameter of the adjustable nozzle. From this we can conclude that in the control chamber there still remains a pressure of about 1 bar. It can also be seen that the maximum force at the adjustable nozzle diameter 3 mm is below 4.5 N. At smaller nozzle diameters the pressure acting on the flapper is falling.

The switchover of the valve is directly dependent on the sizes of both nozzles in the pilot-stage valve and the flapper displacement, h. Our research has shown that the operation of a pneumatic directional valve is largely influenced by the ratio between the constant nozzle diameter and the adjustable nozzle diameter. For a successful operation the condition $d_{kš} < d_{nš}$ has to be fulfilled. Numerous measurements have shown that for the studied case, the actuator operates best at a diameter $d_{kš}$ = 1,6 mm and $d_{nš}$ = 2,5 mm to $d_{nš}$ = 3 mm ([12] in [13]).

To determine the piezo element characteristics, it is also necessary to measure the relationships between the supply and relief of the main chamber and the flapper displacement, h, and force, F, with which the air jet acts at the nozzle outlet (*dnš*) onto the crossbow piezo element.

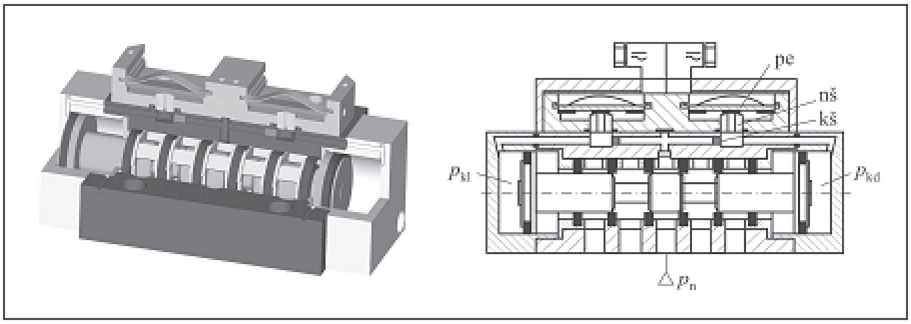

Sl. 13. *Pnevmatični ventil ISO 3, 5/2 s predkrmilnim piezoventilom*
Fig 13. *Pneumatic valve ISO 3, 5/2 with a pilot-stage piezo-actuator.*

Dana meritev je temelj za izbiro piezoelementa in določitev njegove najboljše delovne točke. Sila piezoelementa mora biti večja od sile tlaka. Temelj za izbiro piezoelementa sta tako potreben gib h oziroma deformacija piezoelementa in sila, ki jo mora piezoelement zagotavljati. Sklepati je mogoče, da mora upogibni piezoelement omogočati gib med 0,1 in 0,4 mm in zagotavljati silo, večjo od 5 N, če želimo doseči zanesljivo delovanje ventila. Na podlagi rezultatov uvodne raziskave je bil izbran piezoelement [16] z največjim upogibom Δx = 250 μm, z največjo silo F = 35 N pri U = 200 V enosmerne napetosti.

Na sliki 13 je prikazan prirejen glavni potni ventil velikosti ISO 3, 5/2 s prigrajenim predkrmilnim piezoventilom. Raziskava možnosti uporabe piezoizvršilnikov z upogibnimi elementi je pokazala, da je za krmiljenje 5/2 potnega ventila mogoče uporabiti na novo razviti predkrmilni ventil z upogibnim piezoelementom, ki deluje po načelu šoba - odbojna plošča. V predkrmilnem ventilu sta uporabljena dva mostična piezoelementa (sl. 3c, 9b in 13) ([16] in [17]). Vod napajalnega tlaka p_n je speljan iz glavnega napajalnega priključka glavnega potnega ventila. Napajalni zrak tako teče skozi nespremenljivo šobo do spremenljive šobe. V mirujoči legi sta oba piezoelementa neobremenjena, zrak teče iz obeh šob v ozračje. Pri vklopu enega izmed predkrmilnih ventilov se piezoizvršilnik upogne in se premakne proti šobi za premik h. Zaradi oviranja iztekanja zraka v krmilnem prostoru se tlak p_k zviša. Pri ustrezno veliki sili tlaka v krmilnem prostoru se ventil premakne v novo lego.

4 RAZULTATI MERITEV IN ANALIZA

4.1 Preizkuševališče

Za potrebe izvedbe meritev značilk ventila je bilo postavljeno preizkuševališče, kar je prikazano

This measurement serves as the basis for the selection of the piezo-element and the determination of its optimal operating point. The force of the piezo-element has to be greater than the force resulting from the pressure. The basis for the selection is thus the necessary displacement, h, or the deformation of the piezo-element and the force it has to ensure. It is possible to conclude that a bending piezo-element has to enable a deflection of between 0.1 to 0.4 mm and ensure a force greater than 5 N for reliable operation. On the basis of the results of our preliminary research, a piezo-element was selected with a maximum deflection of Δx = 250 μm, maximum force F = 35 N at U = 200 V DC.

Fig 13 shows the main directional valve of size ISO 3, 5/2 with a pilot-stage piezo-actuator. The research into the possibilities of using piezo-actuators with bending elements has shown that for controlling a 5/2 directional valve it is possible to use the discussed crossbow piezo-element with a flapper/nozzle system. In the pilot-stage two such crossbow elements were used (Fig 3c, 9b and 13) ([16] in [17]). The supply pressure, pn, is led from the main power supply on the main directional valve. The supply air flows through the constant nozzle to the adjustable nozzle. At standstill both piezo-elements are unloaded and the air flows from both nozzles into the atmosphere. When switching on one of the pilot-stage valves, the piezo-actuator bends and moves towards the nozzle by a displacement h. Due to greater blockage of the air outflow, the pressure, p_k, in the chamber rises. When the pressure in the chamber is big enough, the valve is switched over into a new position.

4 ANALYSIS OF MEASUREMENT RESULTS

4.1 Test rig

A test rig was set up to carry out the measurements of the valve's characteristics. A photograph of the rig is

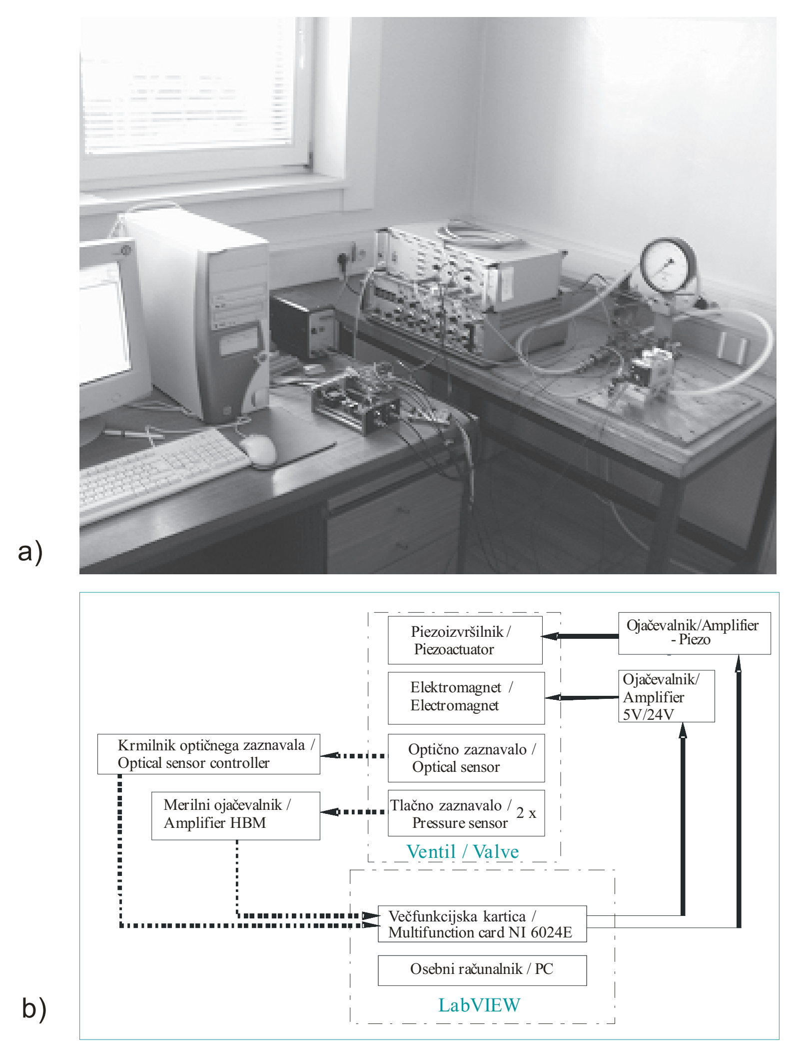

Sl. 14. *a) Preizkuševališče, b) shema merilne verige*

Fig. 14. *a) A photograph of the test rig, b) block diagram of the measuring chain*

na sliki 14a. Verižna shema merilne verige je prikazana na sliki 14b. Poteki tlakov v obeh celicah so bili merjeni s piezomerilniki tlakov ([13] in [14]), lega gibljivega dela glavnega ventila pa s svetlobnimi mejnimi stikali, ki omogočajo zaznavanje le končnih leg bata ventila, medtem ko vmesnih leg ni mogoče meriti. Potek preizkušanja je bil voden in rezultati so vrednoteni v okolju LabVIEW.

4.2 Analiza delovanja

Temelj za uspešen razvoj pnevmatičnega ventila s piezoventilom je potrebni potek tlaka v obeh krmilnih celicah pri različnih premerih nespremenljive

shown in Fig 14a, while a block diagram of the measuring chain is presented in Fig. 14b. The histories of the pressures in both chambers were measured with piezo pressure gauges [13, 14], and the position of the moving part of the main valve with light limit switches, sensing only the final positions of the valve piston, while the intermediate positions could not be measured. The testing procedure was guided and the results evaluated in the LabVIEW environment.

4.2 Analysis of operation

The basis for the successful development of a pneumatic valve with a piezo-actuator is to be able to produce the required continuous changes of presin spremenljive šobe pri napajalnem tlaku p_n = 6 bar. Rezultati meritev potekov tlakov pri običajnem elektromagnetnem ventilu so prikazani na sliki 15. Poteki tlakov so značilni in kažejo, da se v krmilni celici pri preklopu tlak p_{kL} na napajalni (tlačni) strani najprej hitro zviša, nato pa zniža in ob koncu preklopa ventila ponovno zviša na vrednost, ki je enaka napajalnemu tlaku. Sočasno se na drugi, odzračeni strani, tlak p_{kD} hitro zniža in ob koncu preklopa doseže vrednost pod p_{kD} = 1 bar, praktično p_{kD} = 0 bar. Iz diagrama je mogoče določiti tudi čas zakasnitve po vklopu predkrmilnega ventila, čas preklopa predkrmilnega ventila t_{pv}, čas preklopa glavnega ventila t_{gv} ter skupni čas preklopa t_p. Čas preklopa določa frekvenco ventila.

Na velikost potrebne sile za preklop in s tem krmilnega tlaka - p_{kL}, vplivajo masa gibljivega dela ventila m, sila trenja F_{tr} ter višina tlaka na nasprotni strani ventila p_{kD}. Gibljivi del ventila se premakne v novo lego, ko je sila tlaka na eni strani večja od vsote vseh sil, ki delujejo v nasprotni smeri gibanja.

Na sliki 16 so prikazani rezultati meritev tlakov v okolju LabVIEW za razviti ventil s predkrmilnim piezoventilom. Pri napajalnem tlaku p_n = 5 bar je potek značilen, v levi celici se tlak p_{kL} hitro zviša in nato zniža, ob koncu giba pa se ponovno zviša na največjo vrednost. Odzračitev nasprotne celice je hitra, vendar je vrednost tlaka v celici ob koncu giba bata ventila še vedno

sure in both chambers at different diameters of the constant and adjustable nozzles at the supply pressure p_n = 6 bar. The results of the measurements of pressure history in the standard electromagnetic valve are shown in Fig 15. The pressure histories are characteristic and show that on switchover in the control chamber the pressure, p_{kL}, on the supply side (pressure side) first rises steeply and then falls, and then at the end of the switchover rises again to a value equal to the supply pressure. Simultaneously, on the other air-relief side, the pressure, p_{kD}, falls and at the end of the switchover reaches a value below p_{kD} = 1bar, practically p_{kD} = 0 bar. From the graph we can also determine the switchover time of the pilot-stage valve, t_{pv}, the switchover time of the main valve, t_{gv}, and total switchover time, t_p. This defines the frequency of the valve.

The magnitude of the force necessary for switching-over, i.e., the control pressure, p_{kL}, depends on the mass of the moving part of the valve, m, friction force, F_{tr}, and the pressure on the opposite side of the valve, p_{kD}. The moving part of the valve moves into a new position when the pressure force on one side is greater that the sum of all the forces acting in the opposite direction.

Fig. 16 shows the results of measurements of pressures in the LabVIEW environment for the developed pilot-stage piezo-actuator valve. At the supply pressure, p_n = 5 bar, the pressure changes are typical. In the left chamber the pressure, p_{kL}, rises steeply and then falls, and at the end of the stroke rises again to its maximum vale. The air relief on the opposite side is fast; however, at the end of the piston stroke the value

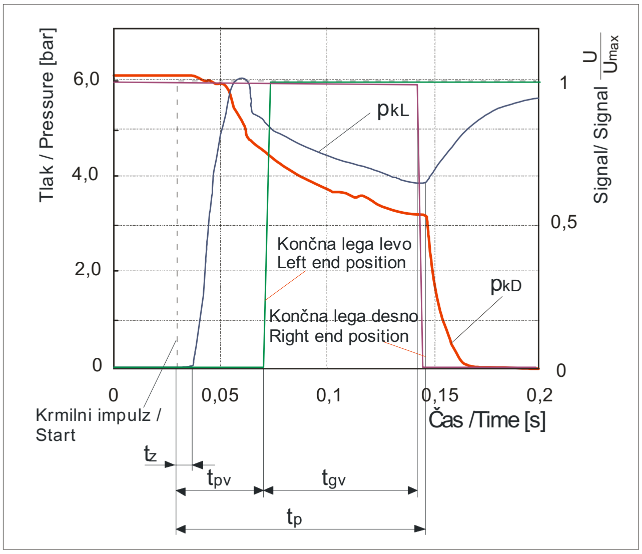

Sl. 15. *Poteki tlakov in značilke preklopa ventila*
Fig. 15. *Pressure histories and characteristics of valve switchover*

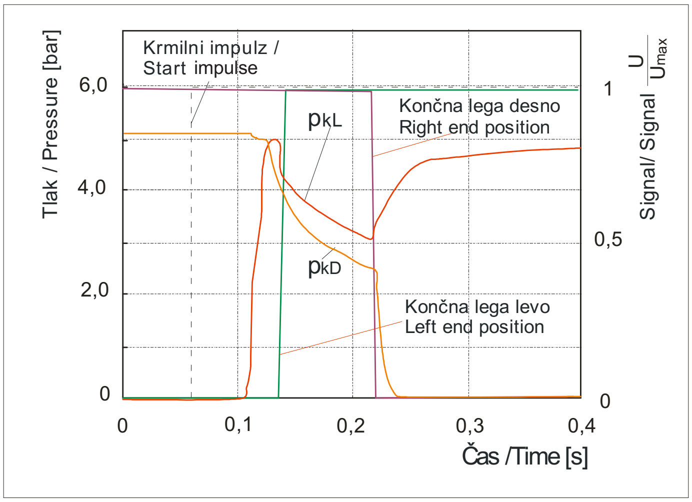

Sl. 16. *Odvisnost posameznih časov od višine tlaka pri ventilu s piezopogonom*
Fig. 16. *Characteristic times versus pressure values in a piezo-actuator valve*

p_{kD} =2,5 bar, kar dejansko zmanjšuje hitrost preklopa ventila.

Lastnosti ventila s piezopogonom in s sistemom šobe odbojne plošče je mogoče dobro ponazoriti z odvisnostjo časov preklopa - postavitve bata ventila iz začetne v končno lego in časov zakasnitve giba bata pri različnih napajalnih tlakih (sl. 17). Rezultati kažejo pričakovano povezavo med časi preklopa ventila in zakasnitve z višino napajalnega tlaka, vendar se je izkazalo, da višina napajalnega tlaka ne vpliva odločilno na čase preklopa ventila.

Mejno število preklopov prikazanega ventila je največje število gibov, ki jih gibljivi del ventila lahko opravi ob največji amplitudi, to pomeni, da se popolnoma premakne iz začetne v končno lego in nazaj. Za opazovani ventil s piezopogonom je mejna frekvenca 4,35 Hz in je

of the pressure in the chamber is still p_{kD} = 2.5 bar, which actually lowers the switchover rate.

The characteristics of a piezo-actuator valve with a nozzle-flapper system can be well illustrated by the relationship between the switchover times, i.e., the times necessary for the valve piston to get from the initial into its final position, the piston stroke delay times and the different supply pressures, Fig 17. The results display an expected relationship between the valve switchover times, the delay times and the supply pressure values; however, it was found that the supply pressure value does not significantly influence the valve switchover time.

The limiting number of switchovers of the developed piezo-valve represents the highest number of strokes that the moving part of the valve can perform at maximum amplitude, i.e., the fully completed motion from the initial into the final position and back. The piezo-drive valve under observation had a limit frequency of

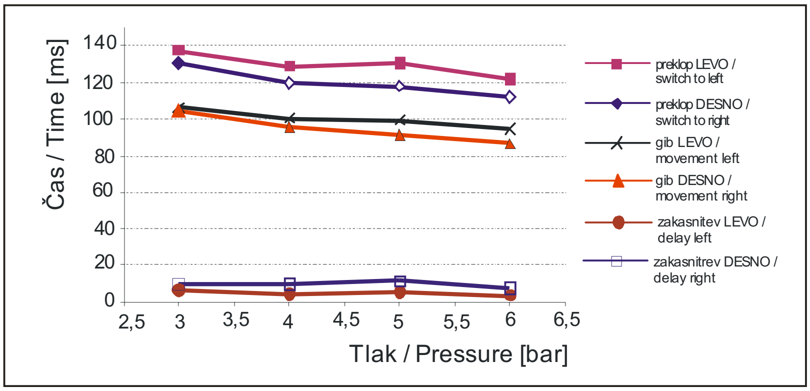

Sl. 17. *Odvisnost posameznih značilnih časov ventila pri različnih napajalnih tlakih*
Fig 17. *Characteristic times of the valve versus supply-pressure values*

bila določena iz odziva ventila na vhodni pravokotni signal. Seveda na mejno frekvenco poleg pogonskega dela vplivata še masa gibljivega dela ventila, trenje med gibljivimi in negibljivimi deli ventila ter pretočne in tlačne sile v ventilu.

5 SKLEP

Razvoj pnevmatičnih komponent v svetu terja nenehno optimiranje sedanjih in tudi razvoj novih komponent. Eno izmed možnosti razvoja novih ventilov in optimiranja sedanjih je vsekakor uporaba drugačnih, predvsem piezoizvršilnikov za krmiljenje ventilov.

Na podlagi teoretičnih izhodišč in meritev pnevmatičnega ventila je mogoče sklepati, da uporaba upogibnih piezoelementov v predkrmilnih potnih ventilih ponuja vrsto prednosti pred elektomagnetnimi izvršilniki. Poleg konzolnih upogibnih izvršilnikov je mogoče uporabiti za preklapljanje ventila tudi mostično izvedbo v sistemu šoba odbojna plošča, kar je bilo izvedeno tudi v tej raziskavi.

Razviti predkrmilni izvršilnik je prigrajen k običajnemu potnemu ventilu velikosti ISO 3, 5/2, kar omogoča tudi primerjave med elektromagnetnim in piezoizvršilnikom. Meritve so pokazale, da ima prototipna izvedba ventila preklopne frekvence v mejah, kakršne imajo primerjalni elektromagnetni ventili.

Mejne frekvence so dovolj velike tudi za hitre delovne kroge. Ustrezne konstrukcijske rešitve in integracija napajalne elektronike bo v nadaljevanju omogočila gradnjo manjših in hitrejših ventilov.

4.35 Hz, which was determined from the valve response to the rectangular signal. It is, of course, understood that, apart from the driving part, the limit frequency is influenced by the mass of the moving part of the valve, the friction between the moving and inert parts of the valve, the flow force and the pressure in the valve.

5 CONCLUSION

Trends in the development of fluid power systems dictate continuous efforts to optimise the existing components and develop new ones. One of the possible developments in this area is the use of alternative piezo-actuators for piloting valves.

On the basis of a theoretical study and experimental measurements it is possible to conclude that the use of bending piezo elements in the pilot-stage of directional valves offers a number of advantages over electromagnetic actuators. Besides the cantilever configuration, also the crossbow flapper nozzle design can be successfully used, which was also realized in this research.

The developed pilot-stage actuator is a unit built to the standard directional valve ISO 3 5/2, offering a comparison between the electromagnetic and piezo-actuators. The measurements have shown that the prototype design has switchover frequencies ranging within the limits that are also characteristic for electromagnetic valves.

The limit frequencies are high enough to allow for rapid working cycles. In future, better design solutions and the integration of power-supply electronics will enable smaller valve sizes and faster operation.

6 LITERATURA
6 REFERENCES

[1] Herakovič N., Noe D. (1998) Nova generacija energetsko varčnih pnevmatičnih ventilov. *Ventil,* letnik 4, št. 4, str. 210-214.

[2] O+P-Gesprächsrunde (2002) Aktoren für Ventile und ihre Peripherie, *O+P Ölhydraulik und Pneumatik*, 46 (2002) Nr. 11-12, Str. 640-689

[3] Herakovič N. (1999) Die Untersuchung des Nutzung des Piezoeffektes zur Ansteuerung fluidtechnischer Ventile, *Verlag Meinz*, Aachen.

[4] Matten N., Ohmenhäuser M. (1994) Stetigwirkendes Wegeventil mit piezoaktuatorischem Stellelement. *Ölhydraulik und Pneumatik*, Vol. 38, Nr. 6, Seite 350-355.

[5] Herakovič N. (1995) Piezoaktorbetätigung für ein einstufiges hochdynamisches Servoventil. *Ölhydraulik und Pneumatik*, Vol. 39, Nr. 8, Seite 601-605.

[6] Murenhoff H. (2003) Trends in Ventilentwicklung, *O+P Ölhydraulik und Pneumatik*, Nr. 47 (2003), Str. 226-241.

[7] Wennmacher G., Yamada H. (1993) Prototyp eines dynamischen Schnellschaltventils mit piezoelektrischer Ansteuerung. *Ölhydraulik und Pneumatik*, Vol. 37, Nr. 10, Seite 794-797.
[8] N.N. Physik Instrumente (PI) Katalog.
[9] N.N. Piezooxide (PXE), Eigenschaften und Aufwendungen, Valvo, Philips 1.Auflage, Juli 1988.
[10] Loesel M. (2003) Klein- und Versteuerventile, Steuerung neutraler und aggressiver Fluide, *O+P Ölhydraulik und Pneumatik*, 47 (2003) Nr. 5, Str. 360-362.
[11] http://users.telenet.be/educypedia/electronics/sensorspiezo.htm
[12] Kezele N. (2001) Določitev karakteristik pnevmatičnih potnih ventilov. Diplomska naloga, *Fakulteta za strojništvo, Univerza v Ljubljani*, Ljubljana.
[13] Slamnik G. (2002) Razvoj krmiljenja pnevmatičnega ventila s piezoaktuatorjem. Diplomska naloga, F*akulteta za strojništvo, Univerza v Ljubljani*, Ljubljana.
[14] Fabjan R. (2003) Določitev dinamičnih karakteristik pnevmatičnih potnih ventilov. Diplomska naloga, *Fakulteta za strojništvo, Univerza v Ljubljani*, Ljubljana.
[15] www.face-int.com/pdf/whtpaper.pdf
[16] Podatki podjetja Ceramtec
[17] Katalog podjetja TIO
[18] Hoerbiger katalog

Naslov avtorjev: doc. dr. Niko Herakovič
prof. dr. Dragica Noe
Univerza v Ljubljani
Fakulteta za strojništvo
Aškerčeva 6
1000 Ljubljana
niko.herakovic@fs.uni-lj.si
dragica.noe@fs.uni-lj.si

Authors' Address: Doc. Dr. Niko Herakovič
Prof. Dr. Dragica Noe
University of Ljubljana
Faculty of Mechanical Eng.
Aškerčeva 6
1000 Ljubljana, Slovenia
niko.herakovic@fs.uni-lj.si
dragica.noe@fs.uni-lj.si

Prejeto:
Received: 7.3.2006

Sprejeto:
Accepted: 22.6.2006

Odprto za diskusijo: 1 leto
Open for discussion: 1 year

Strojniški vestnik - Journal of Mechanical Engineering 52(2006)12, 852-862
UDK - UDC 681.511:517.9
Izvirni znanstveni članek - Original scientific paper (1.01)

Programljivi logični krmilniki na temelju rešitve algebraične Riccatijeve enačbe

Programmable Logic Controllers Based on the Algebraic Riccati Equation Solution

Primož Podržaj - Zoran Kariž
(Fakulteta za strojništvo, Ljubljana)

V prispevku je predstavljena sinteza podoptimalnega krmilnika, ki sloni na rešitvi algebraične Riccatijeve enačbe (ARE). Predstavljen je numerični postopek, s katerim lahko pridemo do te rešitve. V praksi se parametri krmiljenega sistema mnogokrat precej razlikujejo od tistih v ARE. V tem primeru sta vprašljivi optimalnost in celo stabilnost krmilnega sistema. Zelo uporabno bi torej bilo, če bi lahko zasnovali prilagodljivi linearni podoptimalni krmilnik. Tak krmilnik bi bil zmožen odkriti spremembe v parametrih sistema in prirediti parametre.

(Ključne besede: sistemi prilagodljivi, enačbe Riccatijeve, krmilniki logični, krmilniki programljivi, algoritmi numerični)

This paper deals with the synthesis of a suboptimal controller, based on the solution of the algebraic Riccati equation (ARE). The numerical procedure for obtaining the solution is presented. In applications the controlled system parameters often differ from the ones used in the ARE. In this case the optimality of the control system and even its stability are questionable. Therefore, it would be very useful to design an adaptive linear suboptimal controller. Such a controller should be able to detect changes in the system parameters and adjust its parameters.

(Keywords: adaptive systems, Riccati equations, programmable logic controllers, numerical algorithms)

0 UVOD

Linearni časovno neodvisni sistem (LČN) z diferencialno enačbo stanj:

0 INTRODUCTION

A linear time-invariant (LTI) system with the state differential equation:

$$\dot{x}(t) = Ax(t) + Bu(t) \quad (1),$$

prikazan na sliki 1 je optimalen, če mu je dodana povratna zveza:

shown in Figure 1 is said to be optimal if the feedback:

$$u(t) = -F(t)x(t)$$

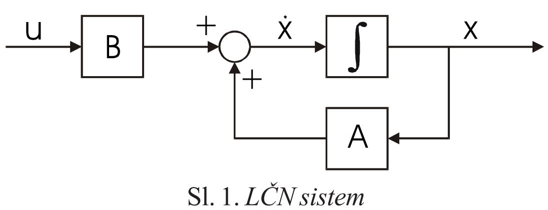

Sl. 1. *LČN sistem*
Fig. 1. *LTI system*

tako, da je integralski kriterij:

is added in such a way that the following cost functional:

$$\int_{t_0}^{t_1}\left[x^T(t)R_1(t)x(t)+u^T(t)R_2(t)u(t)\right]\cdot dt + x^T(t_1)P_1x(t_1)$$

najmanjši. Pri tem so:

- $R_1(t)$ in $R_2(t)$ pozitivno definitni simetrični matriki za $t_0 = t = t_1$,
- P_1 pozitivno poldefinitna simetrična matrika.

Pokazati se da [1], da je treba za minimizacijo funkcionala rešiti naslednjo matrično Riccatijevo enačbo (MRE):

is minimized. This means that

- $R_1(t)$ and $R_2(t)$ are positive definite symmetrical matrices for $t_0 = t = t_{1,}$
- P_1 is a positive semi-definite symmetrical matrix

It can be shown [1], that in order to minimize the cost functional the following matrix Riccati equation (MRE) has to be solved:

$$\dot{P}(t) = R_1 - P(t)BR_2^{-1}B^T P(t) + P(t)A + A^T(t)P$$

Če rešitev MRE konvergira, potem je limita:

If the solution of the MRE converges, then the limiting solution:

$$P = \lim_{t\to\infty} P(t)$$

rešitev naslednje algebraične Riccatijeve enačbe (ARE):

is the solution of the following algebraic Riccati equation (ARE):

$$R_1 - PBR_2^{-1}B^T P + PA + A^T P = 0$$

Krmilnik, ki je zasnovan na temelju te rešitve, se imenuje podoptimalni krmilnik.

The controller based on this solution is called a suboptimal controller.

1 OPIS PROBLEMA

Podoptimalni krmilniki se veliko uporabljajo. Dejstvo pa je, da se lastnosti krmiljenega objekta, dane z matriko A, spreminjajo s časom zaradi staranja in spremenljivih delovnih razmer, čeprav se predpostavlja, da so časovno neodvisne. Matrika A je lahko časovno neodvisna, če opazujemo tipični čas prehodne funkcije krmilnega sistema, toda je časovno odvisna med dobo trajanja sistema. Če se dejanska matrika stanja A_R razlikuje od tiste, ki smo jo uporabili v ARE (matrika A) za Δ, se lahko pojavijo težave.

1 PROBLEM FORMULATION

Suboptimal controllers are frequently used. However, it is a fact that the properties of the controlled system given in matrix A change over time, due to ageing and different working conditions etc., even though they are assumed to be time-invariant. The matrix A may be time-invariant if we consider a typical transient response time of a system, but it is time variant during the lifetime of the system. Many problems can be encountered if the real system matrix, A_R, which differs from the one used in the ARE (matrix A) by the amount Δ, is introduced.

$$A_R = A + \Delta \quad ; \qquad \Delta = \begin{bmatrix} \delta_{11} & \cdots & \delta_{1n} \\ \vdots & \ddots & \vdots \\ \delta_{n1} & \cdots & \delta_{nn} \end{bmatrix}$$

Zaradi tega se izgubi podoptimalnost sistema. V mnogih primerih je vprašljiva celo njegova stabilnost. Zaželeno bi torej bilo, da se zgradi krmilnik, ki bi lahko:

- določil dejansko matriko stanja A_R,
- rešil ARE na podlagi dejanske matrike stanja A_R.

Consequently, the system's suboptimal performance is lost. Even its stability may be questionable in many cases. Therefore, it is desirable to design a controller capable of:

- determining the real system matrix, A_R,
- solving the ARE considering the real system matrix, A_R,

2 DOLOČEVANJE DEJANSKE MATRIKE STANJA A_R

Celoten postopek določevanja dejanske matrike stanja A_R je razdeljen na dva koraka, in sicer v odvisnosti od tega ali matrika stanja A_R ni poznana (prvi korak), ali pa je vsaj približno poznana (drugi korak).

2 DETERMINING THE REAL SYSTEM MATRIX, A_R

The whole procedure for determining the real system matrix, A_R, is divided into two steps, depending on whether the system matrix, A_R, is not known at all (first step) or is approximately known (second step).

2.1 Prvi korak

Če v enačbi (1) uporabimo dejansko matriko stanja v prvem koraku, dobimo:

2.1 First step

When the real system matrix, A_{R1}, is used in the first step, Equation (1) implies the following equality:

$$\dot{x}(t) - Bu(t) = A_{R1}x(t) \tag{2}$$

Matrika stanja A_{R1} pomeni linearno preoblikovanje vektorskega prostora $\Re^n$ v vektorski prostor $\Re^n$ in je enolično določena z baznimi vektorji prostora $\Re^n$. Torej je za določitev elementov sistemske matrike treba najti n linearno neodvisnih vektorjev stanj in njihove slike. Predpostavimo, da lahko merimo vse komponente vektorja stanj x in da je med fazo branja vhodni signal signal u enak 0 (sl. 2).

Uporabljena je bila tudi predpostavka, da je mogoče izračunati odvode vseh komponent vektorja stanja. Postopek, ki ga lahko uporabimo v ta namen, je opisan na primer v [8] in [9]. Levo stran enačbe (2) lahko torej določimo za vsak čas t. Recimo, da krmilnik med fazo branja (u=0) za nek čas vzorčenja t_S prebere $x(0^+)$, $x(T_S)$, $x(2T_S)$ in tako naprej, dokler ne najde n linearno neodvisnih vektorjev stanj $x_1, x_2, \ldots, x_n$. Potem lahko oblikujemo naslednji matriki:

The system matrix, A_{R1}, represents a linear transformation of the space $\Re^n$ into the space $\Re^n$ and is uniquely determined by the images of the vectors on the basis of $\Re^n$. Therefore, in order to determine the elements of the system matrix we only need to find n linearly independent state vectors x and their images. Let us suppose that all the components of the state vector x can be measured, and that during the acquisition phase the control signal u equals 0 (Fig. 2).

Another supposition, that the derivatives of all the components of the state vector x can be calculated, was also made. The procedure, which might be used in this case, is given for example in [8] and [9]. Therefore the left-hand side of Equation (2) can be determined at any time t. Now, let us say that the controller reads $x(0^+)$, $x(T_S)$, $x(2T_S)$ and so on during the acquisition phase (u=0) for a specified sampling time T_S, until n linearly independent state vectors $x_1, x_2, \ldots, x_n$ are found. Then, the following matrices can be formed:

$$\dot{X} = \left[\dot{x}_1 \;\; \dot{x}_2 \;\; \cdots \;\; \dot{x}_n\right] \quad ; \quad X = \left[x_1 \; x_2 \cdots \; x_n\right]$$

Dejansko matriko stanja A_{R1} lahko torej določimo iz naslednje enačbe:

Therefore, the real system matrix, A_{R1}, can be determined by the following equation:

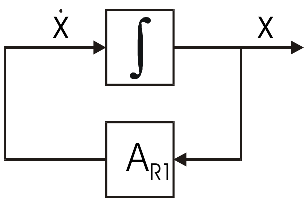

Sl. 2. *Prvi korak, faza branja*
Fig. 2. *First-step acquisition phase*

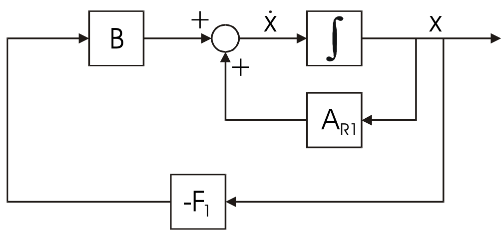

Sl. 3. *Prvi korak, delovna faza*
Fig. 3. *First-step working phase*

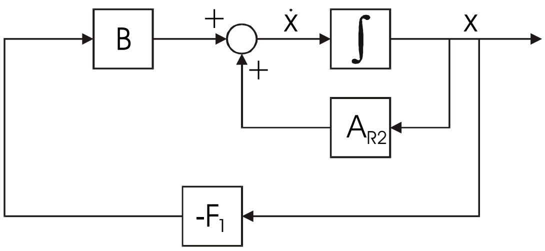

Sl. 4. *Drugi korak, faza branja*
Fig. 4. *Second-step acquisition phase*

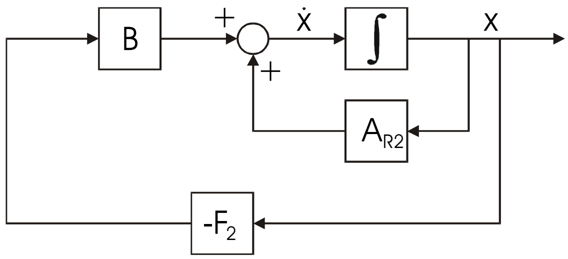

Sl. 5. *Drugi korak, delovna faza*
Fig. 5. *Second-step working phase*

$$A_{R1} = \dot{X} \cdot X^{-1}$$

Z določeno matriko stanja A_{R1} lahko pridemo do rešitve Riccatijeve enačbe. Njena rešitev P_1 se nato uporabi za določitev ustrezne povratne matrike F_1. S tem se faza branja konča. Sistem brez povratne zveze je spremenjen v sistem s povratno zvezo, prikazan na sliki 3.

Ta postopek je treba izvesti le prvič, ko uporabimo tak tip krmilnika na sistemu, o katerem ne vemo ničesar, razen razsežnosti vektorja stanj. Če je matrika stanja A_R (A_{R1}) vsaj približno poznana, potem je pametneje uporabiti povratno matriko F_1, ki ustreza tej matriki stanja in nadaljevati z drugim korakom.

After the system matrix, A_{R1}, is determined, the Riccati equation can be solved. Its solution P_1 is then used to find the appropriate feedback matrix, F_1. At this moment the acquisition phase is ended and the working phase starts. The open-loop system is changed to the closed-loop system shown in Figure 3.

But this procedure only needs to be implemented the first time we use this type of controller on a system we know nothing about, except the number of states. If the system matrix, A_R (A_{R1}), is known approximately, then it is better to use the feedback matrix F_1 associated with this system matrix and proceed immediately to the second step.

2.2 Drugi korak

Ko je matrika stanja določena (ali pa je uporabljena približna), je treba analizirati sistem s povratno zvezo, prikazan na sliki 4.

Med fazo branja je uporabljena povratna matrika F_1 iz prvega koraka. Dejanska matrika stanja je tekoča in ima zato indeks 2. Sistem opišemo z diferencialno enačbo:

2.2 Second step

Once the system matrix has been determined (or an approximate matrix has been used), the closed-loop system shown in Figure 4 should be analyzed.

During the acquisition phase the feedback matrix F_1 from the first step is used. The real system matrix, however, is current and therefore has index 2. The system is described by the differential equation:

$$\dot{x}(t) = \left(A_{R2} + BF_1\right)x(t)$$

Krmilnik mora tako kot v prvem koraku prebrati $x(0^+)$, $x(T_S)$, $x(2T_S)$ in tako naprej. Nato sestavimo matriki X in $\dot{X}$. Realno sistemsko matriko v drugem koraku A_{R2} lahko po končani fazi branja v drugem koraku določimo na podlagi naslednje enačbe:

The controller has to read $x(0^+)$, $x(T_S)$, $x(2T_S)$ and so on, as in the first iteration. Then the matrices X and $\dot{X}$ can be formed. The real system matrix in the second step, A_{R2}, can then be determined after the acquisition phase of the second step is ended, according to the following equation:

$$A_{R2} = \dot{X}X^{-1} - BF_1$$

Ko je nova povratna matrika F_2 določena, se lahko začne delovna faza v drugem koraku. Končni blokovni diagram je prikazan na sliki 5.

Drugi korak se nato iterativno ponavlja.

After the new feedback matrix F_2 is determined the working phase of the second step can begin. The associated block diagram is shown in Figure 5.

The second step is then iteratively continued.

3 REŠEVANJE ARE

Uporabljeni sta bili dve metodi reševanja ARE, in sicer:
- Metoda z uporabo enačb Ljapunova,
- Potterjeva metoda.

3.1 Metoda z uporabo enačb Ljapunova

Ta metoda se je izkazala za dokaj počasno in zato ne bo opisana. Podroben opis je podan v [6] in [7].

3.2 Potterjeva metoda

Ta metoda je bila uporabljena za reševanje ARE. Sestavimo matriko M_r reda 2x2 [1]:

3 SOLUTION OF THE ARE

Two methods for solving the ARE were considered:
- a method using Lyapunov equations
- Potter's method

3.1 Method using Lyapunov equations

This method turned out to be rather slow and will therefore not be described. A detailed description can be found in [6] and [7].

3.2 Potter's method

This method was used in order to solve the ARE. Let us consider the following 2x2 matrix M_r [1]:

$$M_r = \begin{bmatrix} A & -B \cdot R_2^{-1} \cdot B^T \\ -R_1 & -A^T \end{bmatrix}$$

Matriko R_1 lahko zapišemo v obliki:

The matrix R_1 can be expressed as:

$$R_1 = H \cdot H^T$$

Če je matrična dvojica:
- (A,B) ustaljiva in
- (A,H) pregledljiva,

If the matrix pair:
- (A,B) is stabilizable
- (A,H) is observable

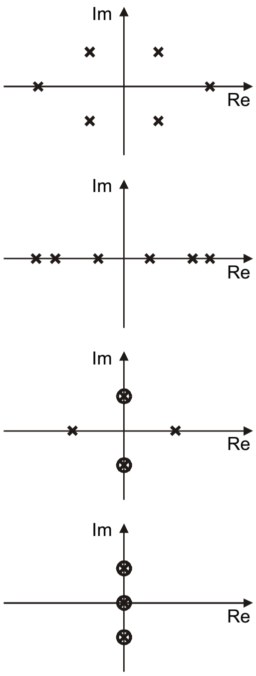

Sl. 6. *Mogoče razporeditve lastnih vrednosti matrike reda 6x6*
Fig. 6. *Possible eigenvalue locations of a 6x6 matrix*

potem se vse lastne vrednosti matrike M_r pojavljajo v dvojicah (λ_i,$-\lambda_i$). Nekaj mogočih primerov je prikazanih na sliki 6.

Naj bo lastni vektor ali korenski vektor y_i matrike M_r, ki ustreza lastni vrednosti λ_i z negativno realno komponento, oblike:

then all the eigenvalues of matrix M_r appear in pairs (λ_i,$-\lambda_i$). Some possible examples are shown in Figure 6.

Let the eigenvector or generalized eigenvector y_i of the matrix M_r corresponding to λ_i, which has a negative real part, be:

$$y_i = \begin{bmatrix} u_i \\ v_i \end{bmatrix}$$

Potem se rešitev ARE dobi z [5]:

Then, the solution of the ARE is given by [5]:

$$P = \left[v_1,\cdots,v_n\right]\cdot\left[u_1,\cdots,u_n\right]^{-1}$$

3.2.1 Izračun lastnih vrednosti in lastnih vektorjev

Da pridemo do rešitve ARE, je najprej treba dobiti lastne vektorje matrike M_r. Ta postopek se največkrat izvede v štirih korakih, in sicer:

- z balansiranjem matrike [4],
- s preoblikovanjem matrike v Hessenbergovo [3],
- s QR algoritmom [3],
- z izračunom lastnih vektorjev [3].

3.2.1 Calculation of the eigenvalues and eigenvectors

In order to solve the ARE we must find the eigenvectors of the M_r. This procedure is usually done in four steps, by:

- matrix balancing [4],
- reducing a matrix to the Hessenberg form [3],
- performing the QR algorithm [3],
- computing the eigenvectors [3].

4 ZGRADBA SISTEMA

4.1 Zgradba krmilnika

Uporabljen je bil programljivi logični krmilnik SIEMENS S7-300 s funkcijskim modulom FM 356-4 in dodatnimi vhodno izhodnimi enotami (slika 7).

4 SYSTEM DESIGN

4.1 Controller design

As an application of the introduced method the controller was built using the SIEMENS S7-300 programmable logic controller along with the FM 356-4 function module and several interface (input and output) modules (Figure 7).

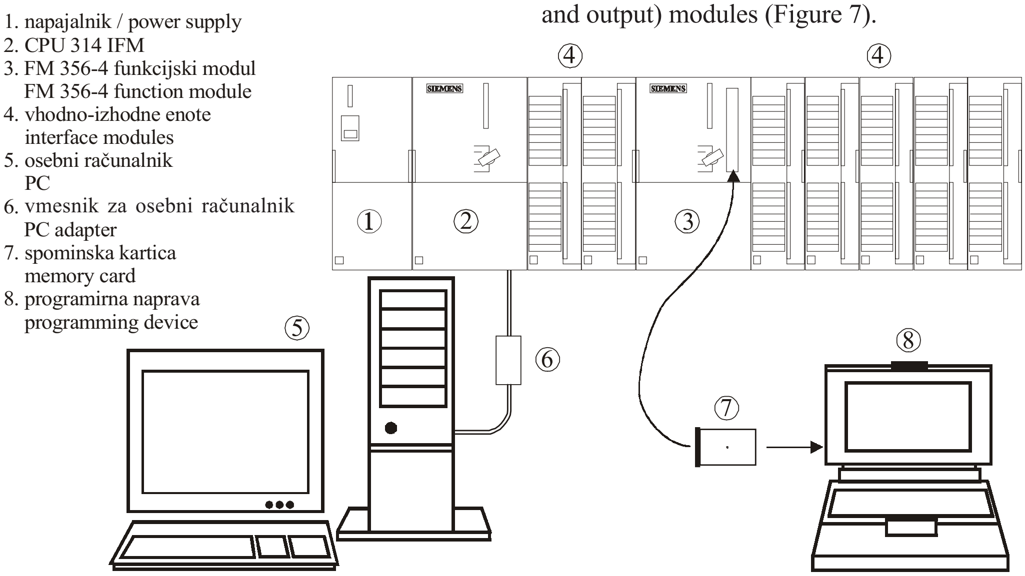

Sl. 7. *Programljivi logični krmilnik z osebnim računalnikom*
Fig. 7. *PLC with supporting PC*

Spominska kartica EPROM se uporablja za vgradnjo in zagon operacijskega sistema ter za nalaganje uporabniškega programa. Za vgradnjo opravilnega sistema na spominsko kartico je potrebna posebna programirna naprava. Uporabniški program pa se lahko spreminja in shranjuje z uporabo osebnega računalnika in vmesnika zanj, ki je priključen na osrednjo procesno enoto (CPU). Program se naloži v CPU, ki je prek vodila (BUS) povezan s funkcijskim modulom (FM).

A flash EPROM memory card is used to install and boot the operating system and to load the user software. A special programming device is needed to install the operating system on the memory card. The user software, on the other hand, can be modified and saved with the PC along with the appropriate PC adapter, which is connected to the CPU. The software is downloaded to the CPU, which is connected to the function module (FM) via a backplane BUS.

4.2 Modeliranje krmiljenega sistema

Za simulacijo krmiljenega objekta je bil uporabljen iterativni analogni računalnik Meda 41TC.

4.2 Controlled system modelling

A Meda 41TC iterative analogue computer was used to simulate the controlled system.

5 REZULTATI

Kot primer je prikazan sistem z matrikama:

5 RESULTS

As an example, a system with the following matrices:

$$A_R = \begin{bmatrix} 1 & 1 & 4 \\ 2 & 3 & 1 \\ 4 & 2 & 5 \end{bmatrix} \quad ; \quad B = \begin{bmatrix} 2 \\ 1 \\ 3 \end{bmatrix} \tag{3}$$

in začetnim pogojem:

and the initial condition:

$$x(0) = \begin{bmatrix} 3 \\ -3 \\ 6 \end{bmatrix}$$

Matriki R_1 in R_2 v integralskem kriteriju sta:

was used. The matrices R_1 and R_2 in the cost functional were:

$$R_1 = \begin{bmatrix} 3 & 1 & 2 \\ 1 & 2 & 1 \\ 2 & 1 & 2 \end{bmatrix} \quad ; \quad R_2 = [1]$$

Odgovor prilagodljivega podoptimalnega krmilnika (tri komponente vektorja stanj) v prvem koraku za T_s=0,1 je prikazan na sliki 8. Dejanska matrika stanja A_R je bila na analognem računalniku namerno modelirana tako, da je sistem brez povratne zveze nestabilen. Zaradi tega je na sliki 8 jasno vidna faza branja. Rezultate lahko primerjamo z odgovorom linearnega podoptimalnega krmilnika, katerega povratna matrika F ustreza matriki A_R (sl. 9). Očitno je, da je v primeru, ko je povratna matrika F v neprilagodljivem krmilniku točna, le-ta boljši od podoptimalnega. Do sprememb pa pride, če se matrika stanja A, za katero je izračunana povratna matrika F, le malo razlikuje od dejanske sistemske matrike A_R. Recimo, da je dejanska matrika stanja A_R enaka kakor v enačbi (3), povratna matrika neprilagodljivega krmilnika pa je izračunana za matriko A, definirano v enačbi (4).

The response of an adaptive suboptimal controller (three components of the state vector) during the first step for T_s=0.1 is shown in Fig. 8. The real system matrix, A_R, was deliberately modelled on an analogue computer in such a way that the open-loop system is unstable. Therefore, the acquisition phase can clearly be seen in Fig. 8. These results can be compared to the response of a linear suboptimal controller whose feedback matrix F is associated with the matrix A_R (Fig. 9). It is obvious that an adaptive controller does not perform as well as a non-adaptive controller if the feedback matrix in the non-adaptive controller is accurate. The situation changes, however, if the system matrix A with which the feedback matrix of an non-adaptive controller is associated differs from the real system matrix, A_R, only slightly. Let us say that the real system matrix, A_R, is the same as in Eq. (3), but the non-adaptive controller's feedback matrix is associated with the matrix A defined in Eq. (4).

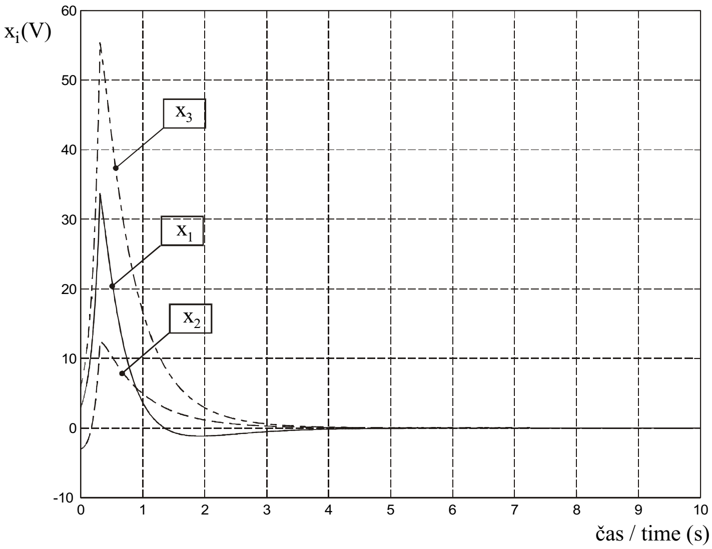

Sl. 8. *Odgovor prilagodljivega linearnega podoptimalnega krmilnika*
Fig. 8. *The response of an adaptive linear suboptimal controller*

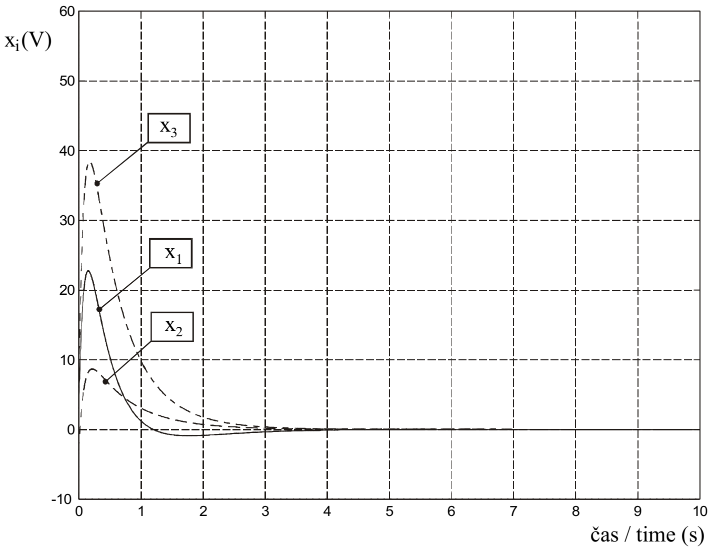

Sl. 9. *Idealni odgovor neprilagodljivega linearnega podoptimalnega krmilnika*
Fig. 9. *Ideal non-adaptive linear suboptimal controller response*

$$A = \begin{bmatrix} 1 & 1,1 & 4,1 \\ 2 & 3,1 & 1,1 \\ 4 & 2 & 4,8 \end{bmatrix} \qquad (4).$$

Odgovor neprilagodljivega krmilnika za ta primer je prikazan na sliki 10.

Sklepamo lahko, da se obnašanje neprilagodljivega linearnega podoptimalnega krmilnika že pri majhnih spremembah parametrov sistema hitro poslabšuje. Kriterijski integral za vse tri primere (prilagodljivi podoptimalni (AS), idealni neprilagodljivi (IN), realni neprilagodljivi (RN)) je prikazan na sliki 11.

The response of the non-adaptive linear controller for such a case is shown in Figure 10.

We can conclude that with only a slight change in the system parameters the performance of the non-adaptive linear suboptimal controller deteriorates rapidly. The cost functionals for all three cases (adaptive suboptimal (AS), ideal non-adaptive (IN), real non-adaptive (RN)) are shown in Figure 11.

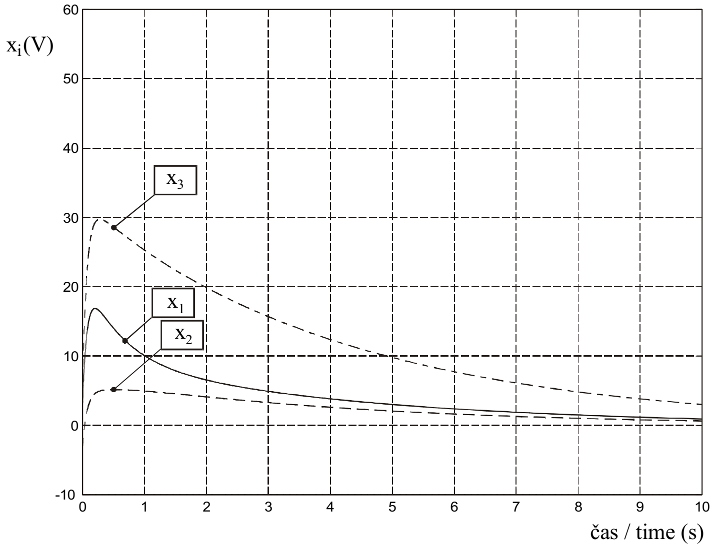

Sl. 10. *Realni odgovor neprilagodljivega linearnega podoptimalnega krmilnika*
Fig. 10. *Real non-adaptive linear suboptimal controller response*

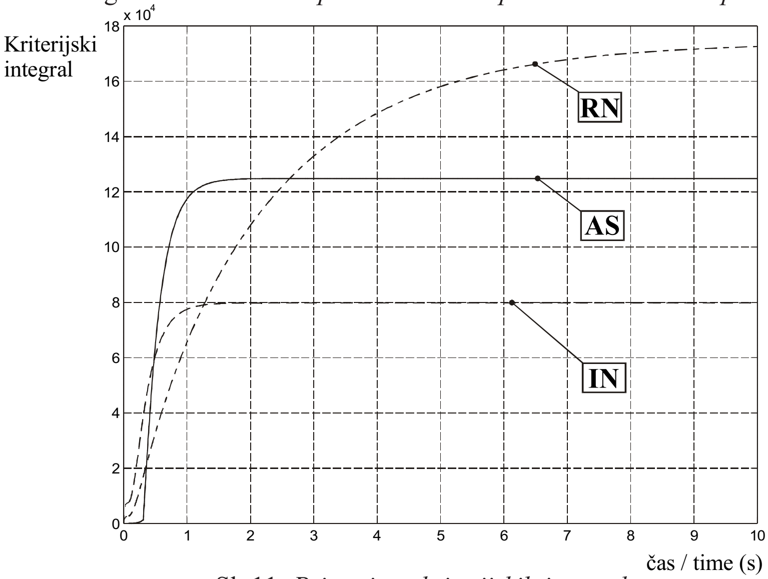

Sl. 11. *Primerjava kriterijskih integralov*
Fig. 11. *Comparison of the cost functionals*

Jasno je, da se obnašanje prilagodljivega linearnega podoptimalnega krmilnika spreminja v povezavi s časom vzorčenja T_S, še posebej, če je sistem brez povratne zveze nestabilen, kajti med fazo branja v prvem koraku le-te ni. Slika 12 prikazuje kriterijske funkcionale za različne čase vzorčenja (od T_S=0,025s do T_S=0,125s s korakom 0,025s).

Jasno je, da je treba za izboljšano obnašanje zmanjšati čas vzorčenja T_S. To je mogoče v teoriji in do neke mere tudi na analognem računalniku. V praksi pa lahko pride do problemov, ker se prebrani vektorji stanj zaradi

It is to be expected that the performance of an adaptive linear suboptimal controller varies with sampling time, T_S, especially if the open-loop system is unstable, because during the acquisition phase of the first step, there is no feedback. Figure 12 shows cost functionals depending on different sampling times (from T_S=0.025s to T_S=0.125s with a 0.025s step).

It is obvious that in order to improve the performance of the controller we must decrease the sampling time, T_S. This can be easily done in theory and to some extent on the analogue computer. In practice, on the other hand, problems may occur because the acquired

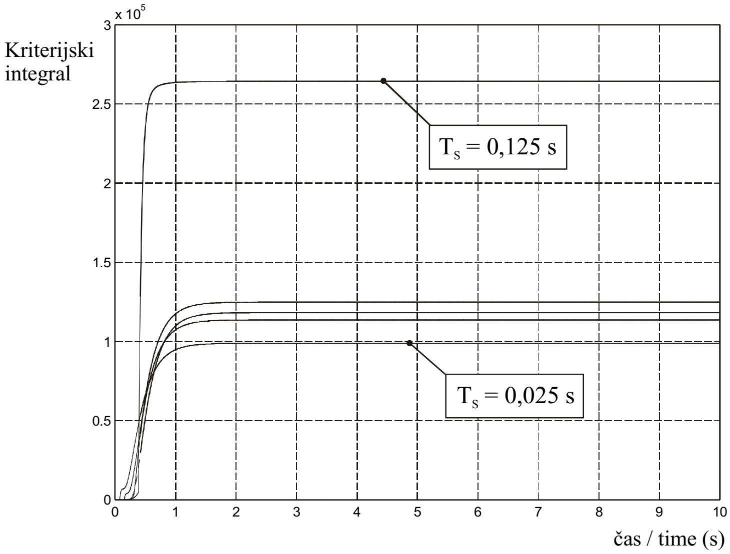

Sl. 12. *Primerjava časov vzorčenja*
Fig. 12. *Cost functional versus sampling time*

šumov ne izražajo v pravi dejanski sistemski matriki A_R. Ti učinki se povečujejo, ko gremo s časom vzorčenja proti 0.

state vectors during the acquisition phase do not result in the correct real system matrix, A_R, due to the noise and other disturbances. These effects are magnified as the sampling time approaches 0.

6 SKLEP

Jasno so bile prikazane prednosti prilagodljivega linearnega podoptimalnega krmilnika pred neprilagodljivim. Te prednosti se povečujejo s povečanimi odstopanji v parametrih sistema. V tem primeru prilagoldjivi krmilnik ohrani svoje zmožnosti. Obnašanje neprilagodljivega krmilnika pa se hitro poslabša.

Če matrike stanja ne poznamo, imamo med fazo branja v prvem koraku sistem brez povratne zveze. Obnašanje sistema je torej odvisno od trajanja te faze, le-to pa od časa vzorčenja. Nadaljnje raziskave je torej treba osredotočiti na določevanje optimalnega časa vzorčenja za različne jakosti šuma.

6 CONCLUSION

The advantages of an adaptive linear suboptimal controller over a non-adaptive controller have been clearly demonstrated. These advantages increase when deviations in the system parameters become larger. In this situation, the adaptive linear suboptimal controller maintains its capability. The performance of a non-adaptive controller, on the other hand, deteriorates rapidly.

However, if the approximate system matrix is not known in advance, we are basically operating the open-loop system during the first-step acquisition phase. The overall performance is therefore dependent on the duration of this phase, which further depends on the sampling time. Further research should, therefore, focus on a determination of the optimal sampling time with regard to the presence of different levels of noise.

7 LITERATURA
7 REFERENCES

[1] H. Kwaakernak, R. Sivan (1972) Linear optimal control systems, *John Wiley & Sons Inc.*
[2] F. L. Lewis (1988) Optimal control, *John Wiley & Sons Inc.*
[3] David M. Young, Robert Todd Gregory (1973) A survey of numerical mathematics, *Addison—Wesley Publishing Company.*
[4] J. H. Wilkinson, C. Reinsch (1973) Die Grundlehren der mathematischen Wissenschaften: Linear Algebra, *Springer Verlag.*

[5] Katsuhisa Furuta, Akira Sano, Derek Atherton (1988) State variable methods in automatic control, *John Wiley & Sons Inc.*
[6] E. J. Davison, F. T. Man (1968) The numerical solution of A'Q+QA=-C, *IEEE Transactions on Automatic Control*, August, str.: 448-449.
[7] David L. Kleinman (1968) On an iterative technique for Riccati equation computations, *IEEE Transactions on Automatic Control*, February, str.: 114-115.
[8] В.А.Бесекерский, В.В.Изранцев (1987) Системы автоматического управления с микроЭВМ, *«Наука»*
[9] Н.Н.Иващенко (1978) Автоматическое регулирование, *«Машиностроение»*

Naslov avtorjev: dr. Primož Podržaj
doc. dr. Zoran Kariž
Univerza v Ljubljani
Fakulteta za strojništvo
Aškerčeva 6
1000 Ljubljana
primoz.podrzaj@fs.uni-lj.si
zoran.kariz@fs.uni-lj.si

Authors' Address: Dr. Primož Podržaj
Doc. Dr. Zoran Kariž
University of Ljubljana
Faculty of Mechanical Eng.
Aškerčeva 6
1000 Ljubljana, Slovenia
primoz.podrzaj@fs.uni-lj.si
zoran.kariz@fs.uni-lj.si

Prejeto:
Received: 12.4.2005

Sprejeto:
Accepted: 25.10.2006

Odprto za diskusijo: 1 leto
Open for discussion: 1 year

Strojniški vestnik - Journal of Mechanical Engineering 52(2006)12, 863-872
UDK - UDC 621.436:621.43.06
Izvirni znanstveni članek - Original scientific paper (1.01)

Raziskava učinkov različnih stopenj vračanja izpušnih plinov na temperaturo plamena in nastanek saj pri uporabi dizelskega goriva z različnimi T90 temperaturami destilacije

Experimental Study of the Effects of Different Exhaust Gas Recirculation Ratios on the Flame Temperature and Soot Formation when Using Diesel Fuels With Different T90 Distillation Temperatures

Danilo Nikolić[1] - Radoje Vujadinović[1] - Norimasa Iida[2]
([1]University of Montenegro, Podgorica, Montenegro; [2] KEIO University, Yokohama, Japan)

V študiji, opisani v tem prispevku, smo preizkušali krmiljenje dušikovega oksida (NOx) in nastanek saj. Kot razredčilo, pri simulaciji kroženja izpušnih plinov, smo uporabili ogljikov dioksid (CO_2) vsebnosti 4,3%, 9,5 in 14,3%, kar pomeni vsebnosti kisika (O_2) 20%, 19% in 18%. V nadaljevanju smo uporabili tri različna dizelska goriva z različnimi T90 temperaturami destilacije. Lastnosti goriva smo zavarovali pred vplivi vsebnosti aromatov, žvepla in cetanskega števila. Za simulacijo dizelskega zgorevanja smo uporabili hitrokompresijski motor z enim cilindrom. Postopek vžiga in zgorevanje pri vbrizgavanju dizelskega goriva smo opazovali s pomočjo hitrega neposrednega fotografiranja. Temperaturo plamena (kazalnik nastanka NO) in faktor KL (kazalnik vsebnosti saj v vbrizgu dizelskega goriva) smo analizirali z uporabo dvobarvne metode. Preizkus je pokazal, da se s povečanjem vsebnosti CO_2 v dovodu zmanjšata najvišja temperatura plamena in nastajanje saj. Prav tako so rezultati pokazali, da pri vsebnosti CO_2 = 4,3% v dovodu, T90 temperatura destilacije nima posebnega vpliva na najvišjo temperaturo plamena in nastanek saj.

(Ključne besede: gorivo dizelsko, plini izpušni, nastanek saj, temperatura destilacije)

In this paper the diesel in-cylinder control of nitrogen oxide (NOx) and soot formation was tested. Carbon dioxide (CO_2) was used as a diluent to simulate the exhaust-gas recirculation (EGR) process at ratios of 4.3%, 9.5% and 14.3%, thus making oxygen (O_2) concentrations of 20%, 19% and 18% respectively. In addition, three diesel fuels with different T90 distillation temperatures were used. The fuel parameters were isolated from the influence of the aromatics content, sulfur content, and cetane number. A single-cylinder rapid compression machine (RCM) was used to simulate the diesel-type combustion. The ignition and combustion processes of the diesel-fuel spray were observed using high-speed direct photography. The flame temperature (an indication of NO formation) and KL factor (an indication of the soot concentration inside the diesel-fuel spray) were analyzed using the two-color method. The study demonstrated that with an increase of the CO_2 concentration in the intake charge, the maximum flame temperature and the soot formation decrease. Also, when there was a CO_2=4.3% concentration in the intake charge, the results showed no significant influence of the diesel-fuel T90 distillation temperature on the maximum flame temperature and the soot formation.

(Keywords: diesel fuels, exhaust gas recirculation (EGR), distillation temperature, rapid compression machine)

0 INTRODUCTION

The environmental impact of motor vehicles is of great concern worldwide. In particular, the contribution to atmospheric pollution from motor vehicles points to the need to reduce vehicular emissions. Relative to the spark-ignited internal combustion engine, the diesel engine emits large quantities of particulate matter (PM) and nitrogen oxide (NOx). It is difficult to reduce both of these pollutants at the same time because of their trade-off. Diesel emission-reduction strategies can be divided into two main types: in-cylinder control and after-treatment. In-cylinder control implies changes to the design of the engine and diesel-fuel reformulation, with the former providing more opportunities to reduce emissions [1].

Exhaust-gas recirculation (EGR) is an effective in-cylinder technique that reduces NOx because it lowers the maximum flame temperature. But the application of EGR can also adversely affect the quality of the lubricating oil, the engine durability and produce higher unburned hydrocarbon (HC) and PM exhaust emissions, resulting from the lower oxygen (O_2) concentration. The influence of EGR on exhaust emissions can be efficiently simulated by the addition of carbon dioxide (CO_2) to the intake charge. Ladommatos et al. [2] identified three major effects of introducing CO_2 into the intake charge of a diesel engine: the dilution effect, the chemical effect, and the thermal effect. The dilution effect, which represents the reduction in O_2 and nitrogen (N_2) fractions in the intake charge due to the replacement with CO_2, was shown to be the most significant, having an influence on both the combustion process and exhaust emissions. With the increase of CO_2 in the intake charge, the ignition delay periods increase ([3] to [7]), the NOx formation decreases ([4] to [7]), while soot formation in some cases increases ([8] and [5]) and in other cases decreases ([4] and [6]).

Many studies have been carried out to assess the effect of the fuel properties on diesel emissions. These studies showed that the fuel properties, such as the cetane number, the aromatic content and type, the distillation temperature, the density, and the viscosity, are the most influential on the combustion process and exhaust emissions. Many papers ([9] to [13]) have investigated the influence of the T90 distillation temperature of diesel fuels on exhaust emissions. Most of them reported an increase of NOx and PM emissions with the increase in the T90 distillation temperature.

The aim of this study was to show the combined effects of the EGR and T90 distillation temperatures of diesel fuel on the formation of NOx and soot inside the combustion chamber. A rapid compression machine (RCM) was used to simulate diesel combustion, having a single fuel-spray injection in the high-temperature and high-pressure atmosphere of the surrounding gas. The RCM is capable of a diesel-fuel spray-combustion investigation with minimized influences of some parameters specific to a high-speed diesel engine. The ignition and the combustion processes of diesel-fuel spray were observed using high-speed direct photography. The flame temperature (an indication of NO formation) and KL factor (an indication of soot formation) were analyzed with the two-color method. The two-color method is based on the continuous radiation of soot particles during the burning diesel-fuel spray.

1 TEST EQUIPMENT AND CONDITIONS

The RCM, Figure 1, used in this study for the simulation of the diesel-combustion process is a duplicated single-diesel-type compression cycle after the combustion process, which is carried out in the environment of a constant volume with high temperature and high pressure. The RCM is a pancake-type combustion chamber with a diameter of 145 mm and a thickness of 48 mm, as illustrated in Figure 2. The single fuel spray from one nozzle hole was injected straight down and did not collide with the walls of the combustion chamber. The piston stroke during compression is 692mm. The ratio and the time of compression are 15.5 and 200ms, respectively.

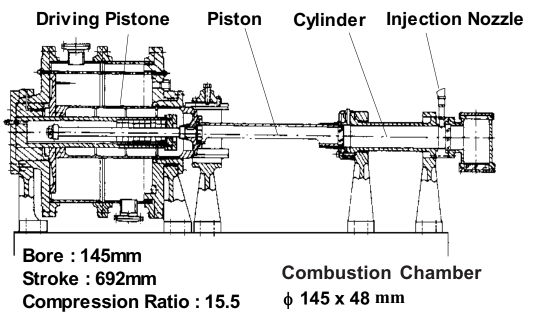

Fig. 1. *The Rapid Compression Machine*

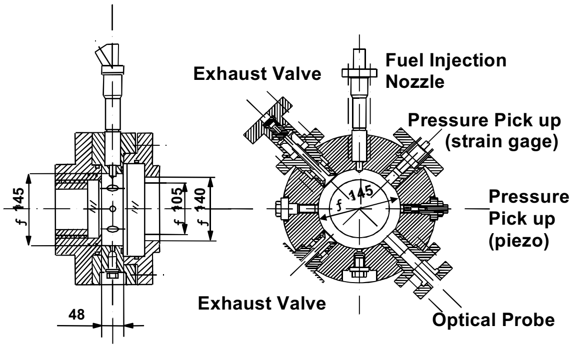

Fig. 2. *The RCM combustion chamber*

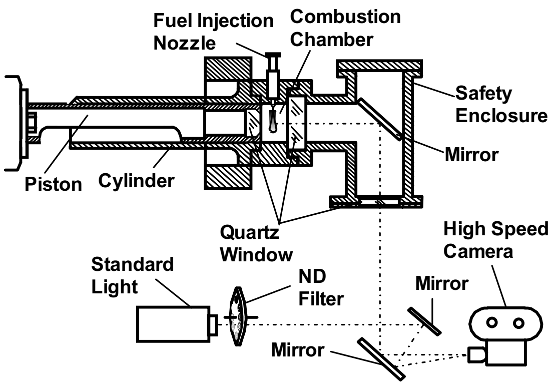

Fig. 3. *Optical arrangement*

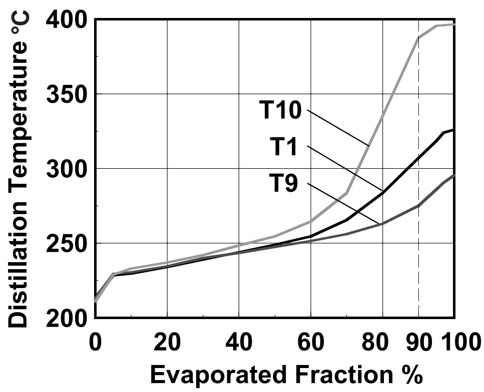

Fig. 4. *Distillation curves of the test fuels*

The in-cylinder pressure inside the RCM combustion chamber was measured with a piezo-electric sensor.

Observations and optical measurements were performed via the quartz windows installed on both the piston and the cylinder head. The image of the flame shape passed through the quartz window was reflected from two plane mirrors (one in the safety box and the other outside) and was caught by the high-speed camera. The speed of the high-speed camera is 5000 flashes per second (FPS) (Model: NAC 16 HD; Shutter constant: 5). The film used was Kodak VISION 500T 7279 (16 mm). Figure 3 shows the optical arrangement of the high-speed photography. The image of a halogen lamp, with a known luminous temperature, was also recorded on each frame as a standard light source for the two-color method analysis. This lamp was positioned at the optical distance from the camera that was equal to the fuel-spray flame.

This study involved high-speed direct photography of the luminous flames, a combustion analysis from pressure diagrams, and flame-temperature and KL-factor analyses by the two-color method applied to the color image of the luminous flames.

CO_2 was used as a diluent to simulate the EGR process at the ratios of 4.3%, 9.5% and 14.3%, thus making O_2 concentrations of 20%, 19% and 18%, respectively. Table 1 shows the composition and the state of the intake charge (gas). Table 2 shows the experimental conditions.

In the experiment, three JCAP (Japanese Clean Air Project) fuels were used, T1, T9, and T10, each with a different T90 distillation temperature. The influence of the T90 was isolated from the influences of the aromatics content (0%), the sulfur content (0%), and the cetane number. Some types of n-paraffins and i-paraffins were mixed to keep the cetane number constant. Table 3 shows the main properties of the test fuels, while Figure 4 shows their distillation curves.

Figure 5 shows the chromatogram data analyzed by Miwa [14]. The fuels with a higher T90 contain heavier elements.

Table 1. *Composition and state of the intake charge*

	O_2 vol %	CO_2 vol %	N_2 vol %	Ar vol %	T_{in} K	T_0 K	P_{in} MPa	P_0 MPa
Air + CO_2	21	0	78	1	353	905±5	0.1	3.0±0.1
	20	4.3	74.2	0.95	353	895±5	0.1	3.0±0.1
	19	9.5	70.5	0.91	353	885±5	0.1	3.0±0.1
	18	14.3	66.8	0.86	353	875±5	0.1	3.0±0.1

Table 2. *Experimental conditions*

Max. Inj. Pressure	P_{inj}	70 MPa
Nozzle Hole Diameters	d	0.18 mm
Fuel-Injection Period	T_{inj}	4.0±0.1 MPa
Injection Equipment		JERK type Fuel Pump
Injection-valve Opening pressure	P_{op}	23 MPa

Table 3. *Properties of the test fuels*

Fuel properties	unit	**T1**	**T9**	**T10**
Density @15°C	g/cm^3	0.7880	0.7852	0.7916
Viscosity@30°C	mm^2/s	3.630	3.322	4.946
Cetane Number		48.8	48.6	48.5
Distillation				
IBP	°C	213.5	213.0	211.0
10%	°C	229.5	230.5	233.0
50%	°C	249.0	247.5	254.5
90%	°C	307.0	275.0	387.5
EP	°C	326.0	295.5	396.5
Sulfur	mass %	0	0	0
Mean Molecular Weight		206	202	219
Lower Calorific Value	J/g	43910	43920	43970
C/H Ratio	(atom/ atom)	0.476	0.479	0.479
n-Paraffin	% (v/v)	36	35	24
i-Paraffin	% (v/v)	57	59	70
Naphthene	% (v/v)	7	6	6
Total-Aromatics	% (v/v)	0	0	0

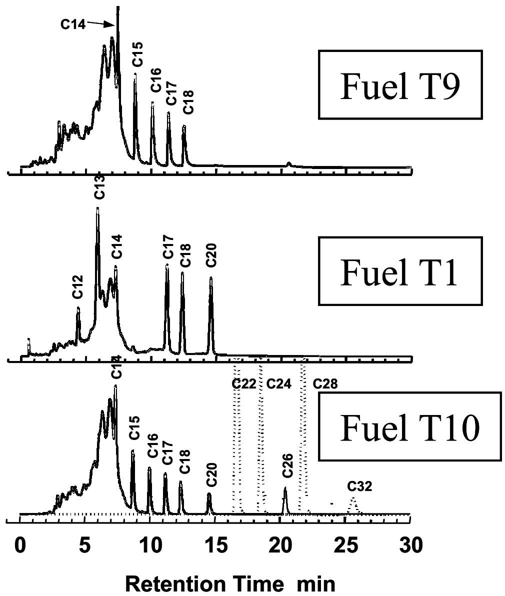

Fig. 5. *Chromatograms of the test fuels*

Figure 6 shows the time histories of the in-cylinder pressure and temperature when only air was compressed. The fuel injection was set to begin at 60 ms after the RCM drive piston reached its top position.

After the in-cylinder pressure reaches its maximum at the top dead center (TDC) and constant-volume conditions begin, the in-cylinder pressure gradually declines due to heat losses and gas leakages. T_o and p_o are the in-cylinder temperature and pressure at the time of the fuel injection.

1.1 Definition of the ignition delay time and the characteristic combustion times

Figure 7 shows a typical example of the in-cylinder pressure rise at the time of the fuel injection and during combustion, and the fuel-injection pressure and the needle-lift histories. When the fuel was injected, mixture cooling occurred and the in-cylinder pressure decreased more rapidly. The time from the start of the fuel injection to the start of the heat release was defined as the ignition delay time

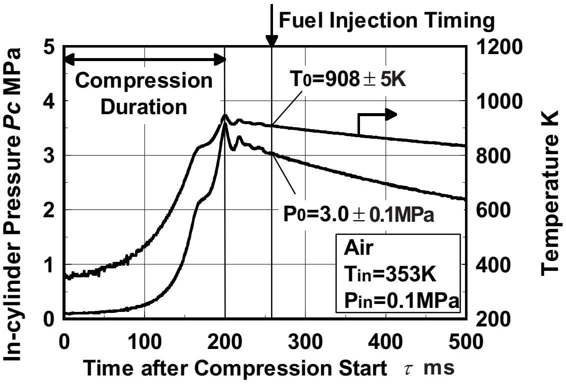

Fig. 6. *Typical in-cylinder pressure and temperature histories for the RCM*

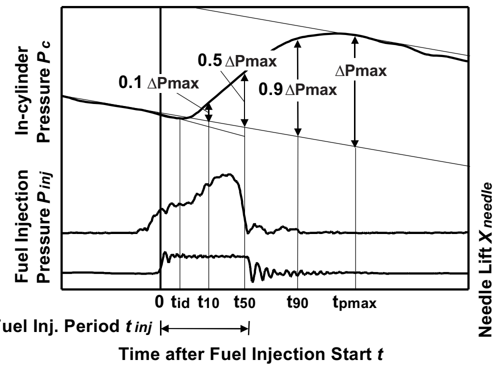

Fig. 7. *Model of in-cylinder pressure, fuel-injection pressure and needle lift*

t_{id}, while the time from the start of the fuel injection to the peak of in-cylinder pressure was defined as t_{Pmax}.

The in-cylinder pressure increase was defined as ΔP_{max}, and the times to reach 10%, 50% and 90% of the peak pressures (ΔP_{max}) were defined as t_{10}, t_{50} and t_{90}, respectively. Because the equivalence ratio was rather small, the specific heat during combustion was assumed to be nearly constant, and thus the burnt-fuel fraction and the pressure increase were considered almost proportional. Therefore, t_{10}, t_{50} and t_{90} could be considered as 10%, 50% and 90% of the burned-fuel timings. The time from the start of the fuel injection to the first appearance of the luminous flame was defined as t_{fa}, and the time of the luminous flame's disappearance was defined as t_{fd}.

2 RESULTS AND DISCUSSION

Figure 8 shows examples of two-dimensional direct photograph images of the T10 fuel-spray combustion for all the test conditions. With the increase of the CO_2 concentration in the intake charge, the luminous flame area and the intensity of the flame decrease. A similar trend appears for the T1 and T9 fuels.

Figure 9 shows pressure diagrams for all the test conditions and the test fuels. During compression and at the time of the fuel injection, the pressure of the intake charge (gas mixture) decreases as the CO_2 concentration increases, maintaining lower pressures during the whole combustion period. This pressure decrease with the increase of the CO_2 concentration in the intake charge is the reason for

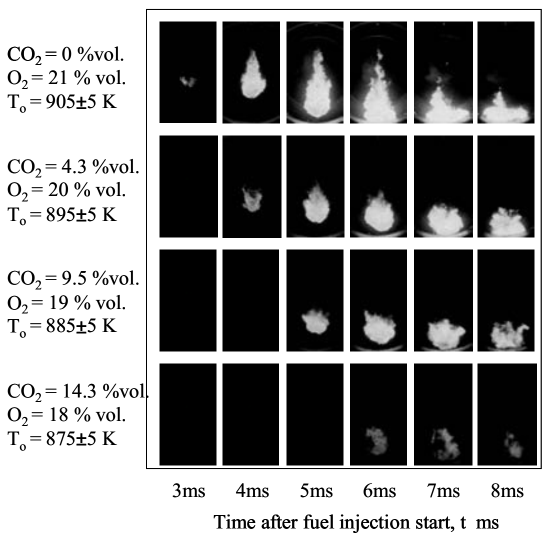

Fig. 8. *Examples of direct photograph images of diesel-fuel spray combustion (fuel T10)*

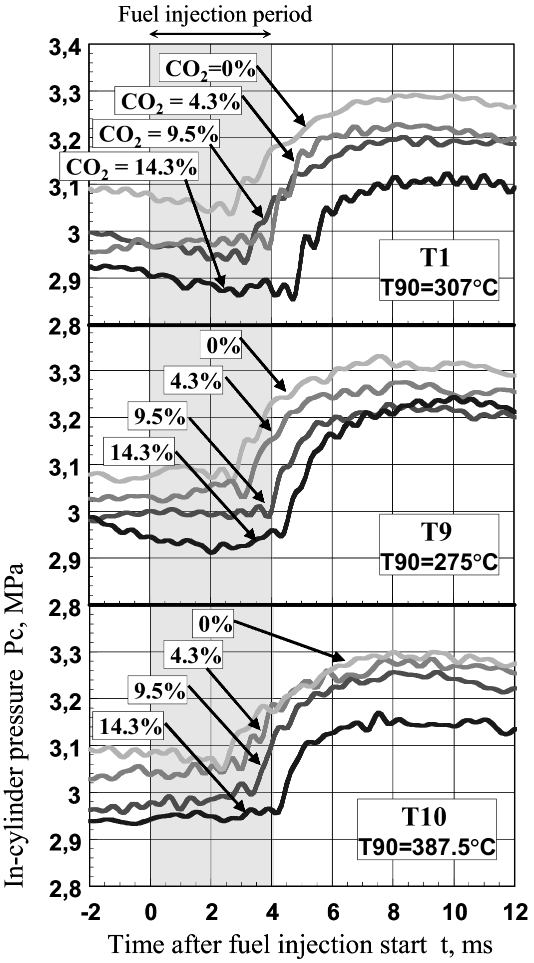

Fig. 9. *In-cylinder pressure histories*

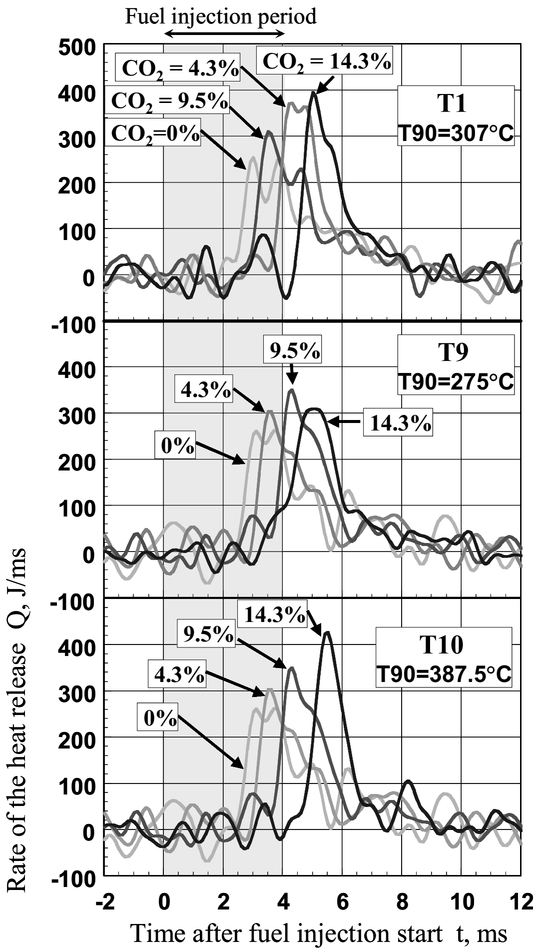

Fig. 10. *Rate of the heat-release-time histories*

the changed composition of the combustion air and could be associated with the increase of the specific heat of such a mixture.

Figure 10 shows the rate-of-heat-release (RHR) diagrams for all the test conditions and the test fuels. With the increase of the CO_2 concentration in the intake charge the high peaks of the RHR increase and are delayed. This is caused by the increased ignition delay, which means that at the time of the ignition there is more fuel available in the cylinder, well mixed, and with a faster burning rate after the ignition.

Figure 11 shows the relationships between the ignition delays, the luminous-flame appearance times, the luminous-flame periods and the combustion periods with characteristic times. The ignition-delay periods are longer with the increase of CO_2 concentrations. This is caused by the decrease of O_2 concentrations in the intake charge as well as the decrease of the intake gas temperature and pressure at the moment of the diesel-fuel injection. This fact makes the periods of fuel/gas-mixture preparation longer. The luminous-flame appearance times (the start of soot radiation) follow the same trend as the ignition delay periods. The luminous-flame periods and combustion periods decrease with the increase of the CO_2 concentration in the intake charge. This could be due to a prolonged ignition delay, the decrease of the O_2 concentrations from 21% to 18%, the lower in-cylinder temperatures and pressures, which all contribute to incomplete combustion.

Figure 12 shows an example of two-dimensional images of the flame temperature and the KL value distribution inside the diesel-fuel spray flame determined by the two-color method. In the case of CO_2=14.3%, due to the low luminosity of the flame, the two-color method was not applicable.

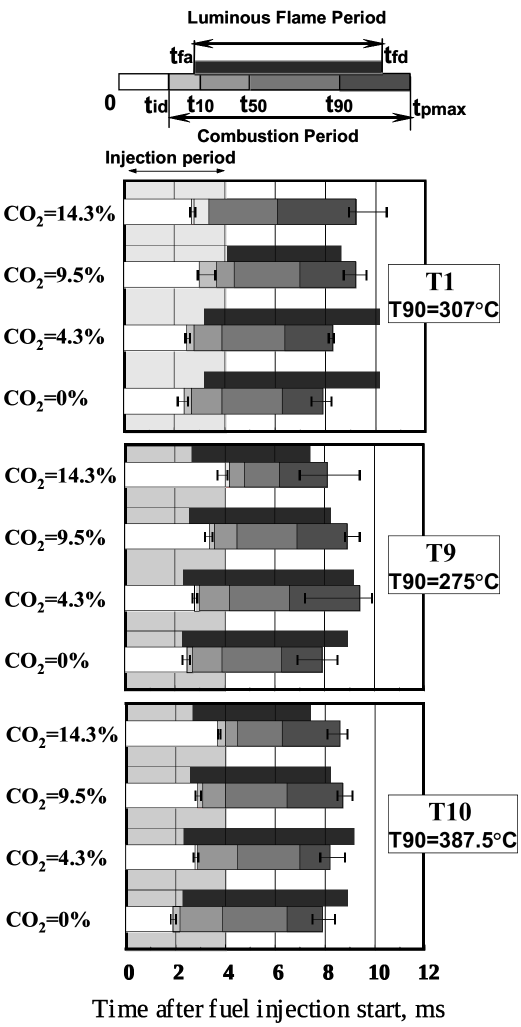

Fig. 11. *Ignition delays, characteristic combustion periods and luminous-flame periods*

Figure 13 (at the end of the paper) shows the time histories of the luminous-flame area and the flame-temperature distribution inside the fuel-spray flames. The flame temperatures obtained from the image analysis using the two-color method were hierarchies at 100K intervals, starting from 1750K. There are decreases in the luminous-flame areas and in the high-temperature areas with the increase of the CO_2 concentrations in the intake charge.

Figure 13 also shows the area-averaged flame temperature, which is defined by the ratio of $\Sigma A_i T_i$ / ΣA_i, in which T_i is the median value of each hierarchy, A_i is the area having temperature T_i, and ΣA_i is the total flame area. The maximum values of this temperature decrease with the increase of the CO_2 concentration in the intake charge. This decrease is more

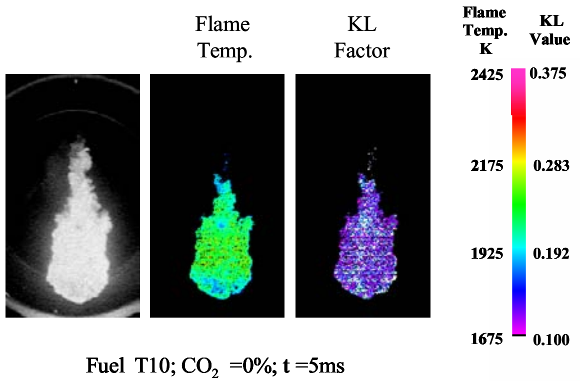

Fig. 12. *Examples of direct photograph images of luminous fuel spray flame, temperature and KL factor distribution in the fuel spray flame*

obvious for CO_2 concentrations of 4.3% and higher. This decrease is a consequence of the O_2 concentration decrease in the combustion chamber and the increase of the inert gases, the decrease of the intake-charge temperatures and the pressures at the time of the fuel injection as well as during the whole combustion period. Regarding the T90 distillation temperature of the diesel fuel, there is a decrease in the maximum area-averaged flame temperature as well as the duration of high temperatures with a decrease of the T90 distillation temperature in the cases of CO_2=0% and CO_2=9.5%. In the case of CO_2=4.3% there is no significant difference in the maximum area-averaged flame temperatures as well as in the duration of the high temperatures.

Figure 14 shows the time history of the area-integrated KL value. The KL value is a multiple of the absorption coefficient K, which is nearly proportional to the soot-particle number density in the flame (Beers law) and the optical path length L in the soot region. The KL value is an index of the total number of soot particles along the optical path. The area-integrated KL value $\Sigma A_i(KL)_i$ was defined as the product of the median value of each hierarchy $(KL)_i$ and its area, A_i.

With the increase of the CO_2 concentration in the intake charge, soot starts forming later due to increased ignition delays. The maximum area-integrated KL values decrease with the increase of the CO_2 concentration. It was expected that there would be more soot formed with the increase of CO_2 concentration due to a lower O_2 concentration. Lower values of the area-integrated KL value with the increase of CO_2 concentration could be the result of a more homogeneous mixture at the time of the ignition due to more time being available for mixture

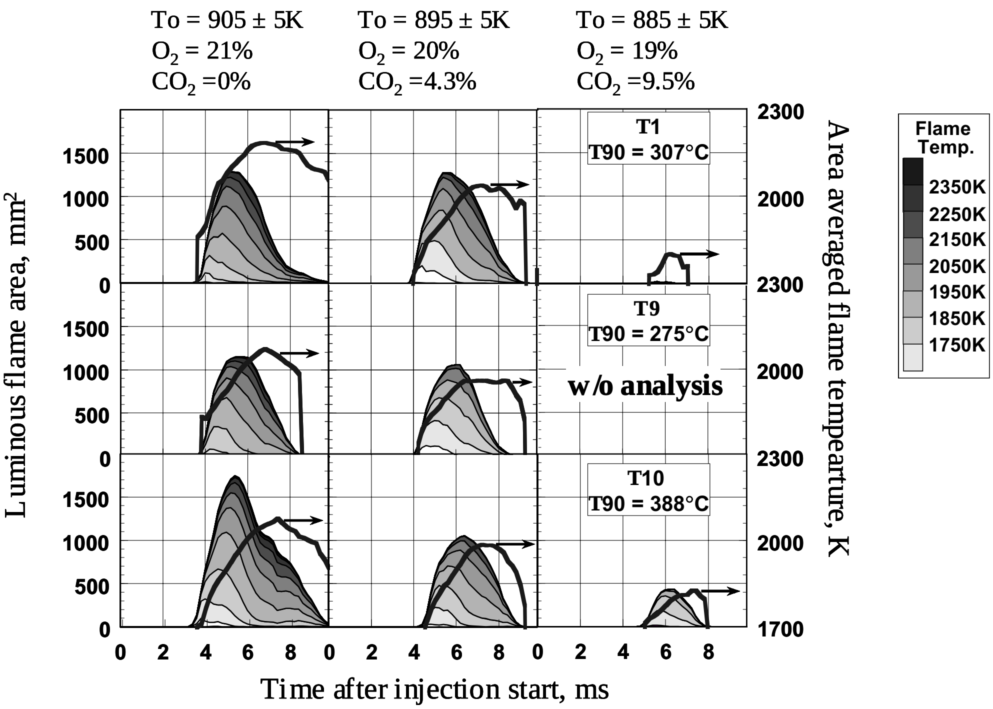

Fig. 13. *Time histories of temperature distribution inside diesel fuel spray flame and of area averaged flame temperature*

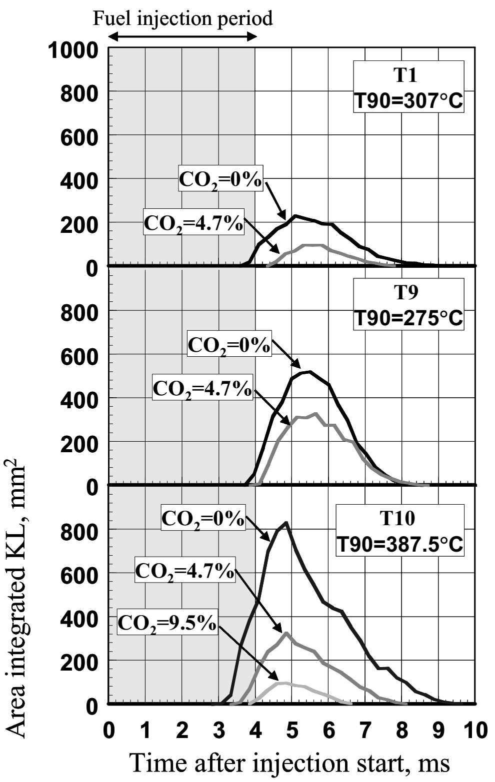

Fig. 14. *Time history of the area-integrated KL values*

preparation, due to lower temperatures inside combustion chamber at the time of the ignition, as well during the whole combustion period, and due to the fact that there is still enough air in such a big combustion chamber, which supports soot oxidation. Iida SAE950213 and Mitchell SAE932798 published similar results. The period of the KL existence decreases with the increase of CO_2 concentration in the intake charge, except for the fuel T9 with the lowest T90 distillation temperature. The KL existence period could be related to the soot exhaust emissions from a real diesel engine. By lowering the intake-gas temperature it is possible to use higher EGR rates, which will significantly lower NOx and, at the same time, not influence significantly the soot-formation and soot-extinction periods. Regarding the effect of the fuel on soot formation and emission, for cases of CO_2=0% and 9.5%, the soot-extinction periods decrease with the decrease of the T90 distillation temperature. For the case of CO_2=4.3%, there is a slight influence of the T90 distillation temperature on the soot-formation and soot-existence periods. This means that by using this CO_2 concentration there is a possibility to use heavier fuels for the same soot exhaust emission.

3 CONCLUSION

In this study exhaust gas recirculation (EGR) was simulated by the introduction of carbon dioxide (CO_2) into the intake air for four different concentrations, 0%, 4.3%, 9.5%, and 14.3%, using three diesel fuels with different T90 distillation temperatures of 275ºC, 307ºC, and 387.5ºC, in order to determine the influence on the nitrogen oxide (NOx) and soot formation inside the combustion chamber of a rapid compression machine (RCM).

The main conclusions from this study are as follows:

- Maximum flame temperature (NOx formation) decreases with CO_2 concentration increase in the intake charge.
- Soot formation and existence periods decrease with CO_2 concentration increase in the intake charge.
- The fuel with the lowest T90 distillation temperature, T9, showed a good soot-NOx trade-off in the case without any CO_2 addition to the intake charge.
- The fuel with the highest T90 distillation temperature, T10, showed a good soot-NOx trade-off in the case of CO_2=4.3% in the intake charge.

4 REFERENCES

[1] K.Mitchell (2000) Effects of fuel properties and source on emission from five different heavy duty Diesel engines, *SAE Paper No. 2000-01-2890*.

[2] N.Ladommatos, S.M.Abdelhalim, H.Zhao and Z.Hu (1996) The dilution, chemical and thermal effects of exhaust gas recirculation on Diesel engine emission – Part1: Effects of reducing inlet charge Oxygen, *SAE Paper No. 961165*.

[3] D. Nikolic, K. Wakimoto, S. Takahashi and N. Iida (2001) Effect of nozzle diameter and EGR ratio on the flame temperature and soot formation for various fuels, *SAE Paper No. 2001-01-1939*.

[4] D.L.Mitchell, J.A.Pinson and T.A.Litzinger (1993) The effects of simulated EGR via intake air dilution on combustion in an optically accessible DI Diesel engine, *SAE Paper No. 932798*.

[5] N.Ladommatos, S.M.Abdelhalim, H.Zhao and Z.Hu (1996) The dilution, chemical and thermal effects of exhaust gas recirculation on Diesel engine emission – Part2: Effects of Carbon Dioxide, *SAE Paper No. 961167*.

[6] N.Iida (1996) Surrounding gas effects on soot formation and extinction – Observations of Diesel spray combustion using a rapid compression machine, *SAE Paper No. 960603.*

[7] S.Ropke, G.W.Schweimer and T.S.Strauss. NOx formation in Diesel engines for various fuels and intake gases, *SAE Paper No. 950213.*

[8] A.M.Kreso, J.H.Johnson, L.D.Gratz, S.T.Bagley and D.G.Leddy (1998) A study of the effects of exhaust gas recirculation on heavy duty Diesel engine emissions, *SAE Paper No. 981422.*

[9] K.Nakakita, S.Takasu, H.Ban, T.Ogawa, H.Naruse, Y.Tsukasaki and L.I.Yeh (1998) Effect of hydrocarbon molecular on Diesel exhaust emissions – Part 1: Comparison of combustion and exhaust emission characteristics among representative Diesel fuels, *SAE Paper No. 982494.*

[10] N.Miyamoto, H. Ogawa, M.Shibuya, K.Arai, and O.Esmilaire (1994) Influence of the Hydrocarbon fuels on Diesel exhaust emissions, *SAE Paper No. 940676.*

[11] M.Tamanouchi, H.Morihisa, S.Yamada, J.Iida, T.Sasaki and H.Sue (1997) Effects of fuel properties on exhaust emissions for Diesel engines with and without oxidation catalyst and high pressure injection, S*AE Paper No. 970758.*

[12] W.S.Neill, W. L.Chippior, O.L.Gulder, J.Cooley, E.K.Richardson, K.Mitchell and C.Fairbridge (2000) Influence of fuel aromatics type on the particulate matter and NOx emissions of a H.D. Diesel engine, S*AE Paper No. 2000-01-1856.*

[13] K.Tsurutani, Y.Takei, Y. Fujimoto, J. Matsudaira and M. Kumamoto (1995). The effects of fuel properties and oxygenates on Diesel exhaust emissions, *SAE Paper No. 952349.*

[14] Consignment research report concerning influence of Diesel engine technology and fuel technology on exhaust emission, *Petroleum Energy Center* PEC-1999JC-25 (1999).

Authors' Addresses: Prof. Dr. Danilo Nikolić
Doc. Dr. Radoje Vujadinović
University of Montenegro
Cetinjski put bb
81000 Podgorica, Montenegro
dannikol@cg.yu

Prof. Dr. Norimasa Iida
KEIO University
3-14-1 Hiyoshi, Kohoku-ku
Yokohama 223-8522, Japan
iida@sd.keio.ac.jp

Prejeto:
Received: 13.3.2006

Sprejeto:
Accepted: 25.10.2006

Odprto za diskusijo: 1 leto
Open for discussion: 1 year

Strokovna literatura - Professional Literature

Ocene knjig - Book Reviews

Dušan Ješić
MERNA TEHNIKA
Zal.: Mašinski fakultet, Banja Luka, 2004
393 strani, 487 slik, format 17 × 23,8 cm

Nenehni razvoj znanosti, tehnike in tehnologije, razvoj novih kakovostnejših materialov in izdelkov terjajo razvoj novih metod in tehnik merjenja, merilno tehniko pa postavljajo kot posebno znanstveno panogo, ki obsega zelo široka in prepletena znanja. Zavedajoč se vseh razsežnosti problematike merilne tehnike avtor pričujočo knjigo, ki je pisana kot učbenik za študente strojništva, razdeli pogojno na štiri celote: osnove merjenja, merjenje geometrijskih veličin, merjenje temperature in hidromehanskih veličin ter merjenje hrupa in vibracij. Bolj podrobno pa je knjiga razdeljena na 19 poglavij, katerih vsebina je podana slikovno izredno pregledno in strokovno prepričljivo brez posebnih poglobljenih teoretičnih izvajanj in analiz.

1. Osnove merjenja: Obravnava uvod v metrologijo, nadzor kakovosti pri izdelavi izdelkov, osnove tehničnega merjenja ter klasifikacijo in izbiromerilnih in nadzornih instrumentov.
2. Merilni sistemi in zaznavala: Zajema osnove, naloge, klasifikacijo ter strukturo merilnih sistemov. Podaja podrobno delitev in opis vseh vrst zaznaval, ki se dandanes uporabljajo v merilni tehniki.
3. Industrijska merila za dolžine: Obravnava enonamenska merila (merilne kladice) in večnamenska merila.
4. Optična merilna tehnika: Podaja ABBE-jev merilnik dolžin, merilne stroje in merilne mikroskope.
5. Interferentna merilna tehnika: Obravnava problematiko merjenja z ravnim vzporednim steklom, svetlobne interferometre ter laserske merilne sisteme.
6. Merjenje in nadzor kotov, konusov in nagibov: Podaja primerjalne metode merjenja in nadzora ter trigonometrične in goniometrične metode merjenja kotov.
7. Merjenje in nadzor navojev: Obravnava nadzor navojev in problematiko merjenja značilnih parametrov navojev.
8. Merjenje in nadzor zobnikov: Zajema osnove in napake posameznih metod nadzora zobnikov, zahteven nadzor zobnikov, merjenje specifičnih parametrov profila ozobij, nadzor sledi nošenja ter nadzor šumnosti zobnikov.
9. Nadzor makrogeometrije površin: Definira makrogeometrična odstopanja površin, metode nadzora oblike, lege ter ravnosti površin.
10. Nadzor mikrogeometrije - hrapavosti površin: Poudarek je na parametrih hrapavosti, na kakovostnih (primerjalnih) ter kolikostnih (brezdotikalnih ali dotikalnih) metodah.
11. Koordinatni merilni stroji (KMS): Zajema osnovne pojme, načelo delovanja in področja uporabe, programiranje KMS, strukturo in klasifikacijo KMS ter smeri razvoja na področju KMS.
12. Avtomatizacija merjenja in nadzora: Definirani so dejavni in posredni merilni sistemi, pnevmatski in fotoelektrični merilni sistemi, merilno-nadzorni roboti, prilagodljivi metrološki sistemi (moduli, celice, središča in postaje).
13. Merjenje temperature: Posebej obdelane vsebine, ki obravnavajo razteznostne plinske, manometrske ter bimetalne termometre. Večji poudarek je na popisu električnih merilnih zaznaval ali termometrov, kakor so uporovni termometri, termopari, sevalni ali optični termometri. Prikazane so posebnosti in omejitve pripadajočih merilnih metod.
14. Merjenje tlaka: Obsega kratek pregled temeljnih pojmov in njihovih definicij, kapljevinske merilnike tlaka, batne manometre, tlačne tehtnice, manometre z elastičnimi elementi ter kratek popis posebnih merilnih metod merjenja tlaka.
15. Merjenje količine in gostote: Zajema podpoglavja o: določanju in merjenju prostornin trdnih teles, kapljevin in plinov, merjenje višine gladin kapljevin, merjenje mase in gostote trdnih teles, kapljevin ter plinov. Pri tem so na kratko podane posebnosti posameznih merilnih metod.
16. Merenje hitrosti in pretoka tekočin: Podane so osnove za: standardizirane merilne metode za umerjanje merilnikov pretoka; merilnike prostorninskega toka kapljevin in plinov; turbinske merilnike prostorninskega toka;

merjenje pretoka in hitrosti tekočin po dušilnih metodah; induktivne merilnike pretoka: rotametre; merilnike krajevnih hitrosti toka tekočin (anemometre, LDA, Pitot-Prandtlovo merilno sondo); merjenje prostorninskega toka kapljevin v odprtih pretočnih kanalih ter kratek oris nekaterih sodobnih za merjenje pretoka, npr.: ultrazvočni, vrtinčni in termični merilni postopki.

17. Merjenje vizkoznosti: Kratek pregled uveljavljenih merilnikov ter merilnih metod za merjenje viskoznosti.
18. Merjenje vlažnosti: Pregled izbranih merilnih metod za merjenje vlažnosti plinastih in sipkih ali prašnatih snovi. Posebej so na kratko popisane tehnike določanja ali merjenja vlažnosti, ki temeljijo na rosiščni higrometriji, psihrometriji ter kapacitivni higrometriji.
19. Merjenje hrupa in vibracij: Nekatere teoretične osnove s področja tehnične akustike in dinamike nihanja, ki se nanašajo na merjenje hrupa ter vibracij.

Knjiga naj bi bila namenjena ne samo študentom strojništva temveč tudi strokovnjakom v praksi za lažje spoznavanje in razumevanje merilne tehnike ter razvoja na področju merilnih naprav in sistemov, ki se uporabljajo tako v kovinsko-predelovalni industriji kakor tudi v tehniki postopkov in storitvenih dejavnostih.

prof. dr. Mirko Soković
prof. dr. Ivo Bajsić

Osebne vesti - Personal Events

Zoisovo priznanje za pomembne dosežke na področju strojništva in tribologije

Doktor Mitjan Kalin je izredni profesor na Fakulteti za strojništvo Univerze v Ljubljani. V fakultetnem Centru za tribologijo in tehnično diagnostiko, ki je pomembna raziskovalna enota predvsem v mednarodnem prostoru, raziskuje pojave mehanskega trenja. Posebej pomembna so njegova raziskovanja triboloških pojavov na področju biomedicine. Raziskoval je pojave obrabe naravnih zob zaradi obrabe hidroksiapatita, ki je poglavitna sestavina zobne sklenine. Ugotovil je, da se obraba zob poveča tudi do 20-krat, če se pojavijo že manjša odstopanja od idealno poliranih površin. Pojav je popisal z ustreznim mehanizmom obrabe, v katerega je vključil tudi tribokemijske pojave, to je kemijske spremembe, ki spremljajo trenje in obrabo.

Z različnimi tribološkimi sistemi je doktor Kalin v raziskavah dokazoval potrebo po poglobljenem razumevanju pojavov. Zato je razvil mehanizme mejnih nano-filmov na primerih mazanja keramike z vodo. Tribološki mehanizmi, ki jih je raziskal, so pomembna podlaga za oblikovanje mejnih filmov keramičnih materialov v stikih s kovinskimi kompoziti pri izjemnih temperaturah. Raziskuje tribološki mehanizem trdih DLC prevlek po mazanju z olji. Ugotovil je, da ni mogoče doseči želene "inertnosti" dodatkov v oljih tribološkega sistema, in dokazal, da tudi v tem primeru prihaja do značilnega tribokemijskega pojava.

V zadnjih treh letih je profesor Mitjan Kalin objavil kar 15 člankov v mednarodnih revijah, tri sestavke v monografijah ter bil soavtor dveh ameriških patentov, nadgrajenih iz slovenskih. Njegovo mednarodno vpetost dokazujeta tudi citiranost objavljenih del ter sodelovanje pri soorganiziranju mednarodnih konferenc v ZDA in več evropskih državah.

Puhovo priznanje za izume in razvojne dosežke na področju laserskih sistemov za tridimenzionalno merjenje oblike teles

Raziskovalci Fakultete za strojništvo Univerze v Ljubljani: dr. Matija Jezeršek, dr. Drago Bračun in izr. prof. dr. Janez Diaci so razvili več izvirnih optičnih merilnih sistemov, ki na principu aktivne triangulacije zaznavajo in merijo obliko poljubnih teles. Tovrstne naprave v podjetju Alpina omogočajo izdelavo obutve, prilagojene kupcu. V podjetju Goodyear laserski sistemi dinamično testirajo gumijaste izdelke in zračne vzmeti. V Kliničnem centru zdravnikom omogočajo spremljati celjenje kožnih razjed. Laserske sisteme so uporabili tudi pri nadzoru varilnih postopkov in ugotavljanju stopnje obrabe elektrodnih konic pri uporovnem točkovnem varjenju. Slovenski laserski sistemi za trirazsežno merjenje oblik telesa se v primerjavi z evropskimi odlikujejo s hitrostjo, natančnostjo, enostavnostjo uporabe in nizko ceno. Dr. Matija Jezeršek, dr. Drago Bračun in prof. dr. Janez Diaci so svoje razvojne dosežke predstavili tudi v obliki člankov, referatov, patentov in patentnih prijav.

Puhovo priznanje za izume in razvojne dosežke na področju numeričnega modeliranja materialov in procesov

Raziskovalno in razvojno delo profesorja Božidarja Šarlerja, zaposlenega na Univerzi v Novi Gorici, obsega posodobitev kontinuirnega ulivanja aluminijevih zlitin in jekel ter informatizacijo livnih naprav. Optimizacijo značilnosti postopkov je dosegel z vključitvijo zaznaval in simulacijskih sistemov v proizvodne postopke. S tem se je izboljšala kakovost obstoječih izdelkov, povečala storilnost livnih naprav, pospešil razvoj izdelkov, zmanjšal izmet in povečala varnost postopkov. Te uporabne dosežke, vrhunske tudi v mednarodnem merilu, je profesor Šarler prenesel v podjetja Acroni, Štore Steel, Impol in Talum. Profesor Šarler sodeluje v številnih evropskih projektih. Posebej ga odlikuje dejstvo, da je v evropske projekte uspel vključiti tudi slovenska podjetja. Z objavljenimi članki, vabljenimi predavanji in članstvom v uredniških odborih revij pa izstopa tudi po znanstveni odličnosti.

Častni doktorat znanosti prof.dr. Manfredu Geigerju - dolgoletnemu članu mednarodnega svetovalnega odbora Strojniškega vestnika

Univerza v Ljubljani vsak prvi teden v decembru proglasi za svoj teden, kajti tretjega decembra leta 1919 je bilo na novoustanovljeni Univerzi v Ljubljani opravljeno prvo predavanje. V tem tednu se na sedežu Univerze pa tudi pri njenih članicah zvrsti veliko dogodkov, med katerimi vsekakor zaseda prvo mesto svečana seja Senata Univerze v Ljubljani, kajti tedaj so proglašeni tudi njeni novi častni doktorji znanosti.

Med letošnjima nagrajencema je tudi profesor doktor Manfred Geiger z Univerze Erlangen - Nürnberg. Častni doktor prve slovenske univerze je leta 1974 doktoriral na Tehniški univerzi v Stuttgartu pri profesorju Langeju, enemu od soustanoviteljev nove znanstvene panoge plastomehanskih postopkov. Leta 1977 je dr. Geiger odšel v industrijo, v podjetju Trumpf je bil odgovoren za razvoj laserskega stroja za razrez pločevin, kar mu vsi priznavajo kot inovacijo v svetovnem merilu. Dr. Geiger je bil nato glavni vodja razvoja in raziskav pri podjetju PEBRA, kjer so pod njegovim vodstvom razvili prve z vlakni ojačane plastične dele za avtomobilske karoserije.

Profesor Geiger je leta 1982 prešel v akademske vode ko je bil od Univerze Erlangen-Nürnberg povabljen in pooblaščen za ustanovitev nove Katedre za izdelovalne tehnologije. Katedra je danes v Nemčiji pa tudi v svetu priznana kot ena od vodilnih pedagoških in znanstveno-raziskovalnih institucij za svoje področje. Katedra ima trenutno 59 raziskovalcev in tehniškega osebja in okoli 55 študentov v dopolnilnem delovnem razmerju.

Med najpomembnejše merljive uspehe profesorja bi lahko našteli:

- Njegova skrb za znanstveni podmladek in raziskovalno delo se kaže v 89 doktorskih disertacijah.
- Profesor Geiger je ustanovitelj treh podjetij oziroma tehnoloških centrov: Bayerisches Laser-zentrum, Erlanger Lasertechnik in Laserequipment, kjer dela skupaj okoli 80 raziskovalcev.

Profesor Geiger je prve stike s Fakulteto za strojništvo navezal že kot doktorand leta 1965, ko se je na Tehniški univerzi v Stuttgartu srečal s tedanjim docentom Francem Golograncem, ki je na tej šoli prav tako pripravljal svojo doktorsko disertacijo. Naslednja leta se je to sodelovanje in prijateljevanje razširilo še na tedanjega asistenta Karla Kuzmana, ki je na tej ustanovi občasno pomagal docentu Golograncu pri eksperimentalnem delu pri disertaciji. Ko je docent Gologranc promoviral pri prof. Langeju, so se stiki ohranjali s pogostimi obiski v obe smeri, pri katerih so slovenski partnerji pridobivali dragocene informacije o smereh razvoja preoblikovalnih tehnologij.

Večletni prijateljski stiki so se še okrepili, ko je dr. Geiger postal profesor na Univerzi v Erlangenu. Med najpomembnejša dokazila o nesebični pomoči prof. dr. Geigerja pri razvoju nove znanstveno-raziskovalne panoge na Fakulteti za strojništvo bi lahko navedli:

- Koordinator TEMPUS-Projekta "Advanced Manufacturing Technology, Engineering Economy an CIM-Oriented Techniques in Metal forming" 1991 - 1994;
- Član mednarodnega svetovalnega odbora Strojniškega vestnika (več ko 10 let);
- Pooblaščenec in koordinator Pogodbe o sodelavi med Univerzama Erlangen in Ljubljana;
- Darilo laserskega obdelovalnega sistema Katedri

za izdelovalne tehnologije in sisteme, Fakultete za strojništvo v Ljubljani;
- Bivanja do- in podiplomskih študentov, raziskovalcev v Erlangenu (nekaj mesecev, leto in več): Tomaž Pepelnjak, Andrej Horvat, Igor Komel, Uroš Flere, Edvard Govekar, Karl Kuzman;
- Profesor Geiger je skupaj z raziskovalci FS predstavil 17 del v uglednih revijah ali znanstvenih srečanjih.

Področje sinergij bi bilo mogoče tisto, s katerim bi najbolje predstavili profesorjev lik. Ne išče sinergij le med tehnološkimi procesi, še bolj pomembne so sinergije med ljudmi, in to: med raziskovalci iz akademske sfere ter strokovnjaki iz industrijskega okolja, sinergije med mladimi in starimi, med predstavniki različnih narodov, med predstavniki različnih kultur.

To priznanje ni bilo le priznanje učitelju, temveč je pokazalo, kako zna najstarejša slovenska Univerza ceniti ljudi, ki so toliko svoje energije in znanja vložili v napredek več sinergijsko povezanih znanstvenih tehniških panog in hkrati ta znanja uspešno prenesli v gospodarska okolja z vrhunsko tehnologijo.

prof. dr. Karl Kuzman
dekan Fakultete za strojništvo

Prof. dr. Viljem Kralj - petinsedemdesetletnik

Dne 31.7.2006 je dopolnil 75 let dr. mag. Viljem Kralj, univ. dipl. inž. elektrotehnike, upokojeni redni profesor Fakultete za strojništvo Univerze v Ljubljani. Rodil se je v Dugem Ratu pri Splitu, kot prvi od petih otrok materi Zlati in očetu Rudolfu, kjer je oče delal pri izgradnji tovarne karbida, ki jo je gradila francoska delniška družba Le Dalmatien d.d. v sodelovanju s prav tako francoskim podjetjem L'Air Liquide.

Ko otroška igrivost še ni prerasla v fantovske podvige, so očeta že čakale nove službene zadolžitve. Takrat se je družina Kraljevih preselila v Novi Sad, od koder pa jih je 1941 leta madžarska okupacijska oblast izgnala. Izgon se je končal v Mariboru, kjer si je oče našel zaposlitev v tamkajšnjih Železniških delavnicah.

Podobno kakor mladostno odraščanje je bilo pestro in bogato tudi šolanje. Osnovno šolo je začel obiskovati v Novem Sadu, nadaljeval in končal pa jo je v Mariboru, kjer je dokončal tudi pet razredov klasične gimnazije, maturiral pa je na Srednji hidrometeorološki šoli v Beogradu. Po maturi se je zaposlil kot klimatolog in sinoptik na Hidrometeorološkem zavodu SR Slovenije v Ljubljani, in se leta 1950 vpisal na Naravoslovno matematično fakulteto ter 23.1.1957 na Tehniški fakulteti diplomiral iz elektrotehnike - šibki tok.

Prva inženirska zaposlitev je bila v tovarni Telekomunikacije v Ljubljani, kjer je sodeloval pri razvoju električnih elementov in sistemov ter bil vodja merilnice. Leta 1959 ga je življenjska pot privedla na novoustanovljeni Zavod za varjenje (danes Institut za varilstvo), kjer se je dejavno vključil v strokovno-razvojno, znanstveno-raziskovalno in pedagoško delo. Od tod je leta 1962 bil preko ASTEF (francoske fundacije za tehnično pomoč državam v razvoju) poslan tudi na varilsko specializacijo v Paris.

Kot raziskovalec in vodja raziskav je delal na razvoju varilnih strojev in naprav ter opreme za varjenje, tako za zavod kot tudi za druga podjetja. Na tem mestu je težko predstaviti vse dosežke tega oddelka, navedimo le najodmevnejše: plazemski rezalnik PR-100, naprava za plazemsko mikro varjenje PV-20, naprava za plamensko rezanje z ročnim, magnetnim ali fotoelektronskim vodenjem, naprava za avtomatsko privarjanje v proizvodnji malih kompresorjev v tovarni Iskra v Kranju, sistem za avtomatizirano vodenje varilne proge pri uporovnem varjenju streh avtobusov v Avtomontaži, v Ljubljani. Razvil je napravi za obločno varjenje v zaščiti nevtralnih plinov TIGVAR in MIGVAR. Za novo ustanovljeno podjetje VARSTROJ v Lendavi so takrat na Zavodu pripravili tehnično dokumentacijo za industrijsko proizvodnjo domala celotnega proizvodnega programa strojev in naprav: prenosni varilni transformator za obločno varjenje tipa Furlan, stroj za uporovno varjenje Furlan TT 1 in TT 2, ob tem pa še povsem na novo razvili stroj za sočelno obžigalno varjenje ter namizno izvedbo stroja za plamensko rezanje. Rezultati tega razvojno-raziskovalnega dela so bili predstavljeni tudi širši strokovni javnosti doma in po svetu, ob rednih prispevkih v strokovnem glasilu Varilna tehnika tudi v berlinskem Schweißtechnik, pa tudi v strokovnem glasilu vsesovjetskega inštituta za znanost in tehniko, pri Akademiji nauk SSSR, kjer je bil podan skrajšan prikaz njegovega referata z naslovom "Ekonomska primerjava plazemskega varjenja z različnimi plini in plinskimi mešanicami", ki ga je pred tem predstavil na Mednarodnem posvetovanju o toplotnem rezanju v Halleju, NDR (Ekspres informacije-Svarka, Moskva 1973/No. 39, str. 26-28).

Že med zaposlitvijo na Zavodu za varjenje je na Fakulteti za elektrotehniko opravil podiplomski magistrski študij s področja avtomatike in ga 1969 uspešno končal. Začete raziskave in spoznanja je poglobil in razširil v doktorski disertaciji z naslovom: Raziskave gibov roke človeka elektrovarilca pri ročnem obločnem varjenju z metodami biokibernetike, ki jo je izdelal pod mentorstvom akademika prof. dr. Alojza Vodovnika in somentorstvom akademika prof. dr. Ludvika Gyergyeka in jo 1973 leta tudi uspešno zagovarjal. Rezultati raziskav na tem področju so bili resnično svetovno odmevni. Prvič je bil namreč popisan in izmerjen gib varilčeve roke, narejena avto in križna korelacija med gibom varilčeve roke in varilnimi parametri, dokazana je bila uporaba varilčevega otipa, zastavljene so bile raziskave za študij kinematike paličaste elektrode. Rezultati teh raziskav so bili predstavljeni na več Letnih skupščinah Mednarodnega instituta za varjenje IIS/IIW, v študijski skupini za fiziko obloka št. 212 in objavljeni v več znanstvenih člankih na domačih in mednarodnih konferencah ter recenziranih strokovnih revijah. Z gotovostjo se lahko trdi, da če je slovenska in jugoslovanska varilska stroka v čem dosegla svetovni vrh, ga je prav gotovo z rezultati raziskav s področja biokibernetike varilca. Teze in zamisli teh raziskav so bile namreč sprejete tudi v raziskovalni program pri IIS/IIW. V 80 letih so bile te raziskave eno od temeljnih področij za raziskovalne programe v komisiji II-B- za obločno varjenje.

Prof. Kralj je kot habilitiran docent prišel na Fakulteto za strojništvo leta 1975, v času izredne rasti gospodarstva, velikega povpraševanja po inženirskih kadrih, med njimi tudi po takšnih z varilsko usmeritvijo, ki so jo prav v tistem času udejanjali na Fakulteti za strojništvo. Tu je bil aprila 1979 izvoljen za izrednega profesorja in junija 1984 za rednega profesorja.

Ob že uvedenih vsebinah predavanj in laboratorijskih vaj za predmete Varjenje, Tehnika spajanja in Varilska tehnologija, je zaoral ledino pri uvedbi predavanj in laboratorijskih vaj za ostale varilske predmete: Varilni stroji in naprave, Oprema za varilne procese in varstvo pri delu, ter Fizikalno-kemijske osnove varilnih procesov (skupaj s prof. Prosencem). Tako je leta 1985, ob uvedbi nove visokošolske usmeritve na Fakulteti za strojništvo v Ljubljani, prvič v Sloveniji bil uveden redni univerzitetni študij varjenja. V okviru podiplomskega študija pa je pripravil program predavanj za Posebne načine toplotnega varjenja in rezanja, ki sta ga s pokojnim profesorjem Francem Roethlom zaokrožila v predmet Posebni načini obdelave. Ob neposrednem pedagoškem delu ne gre prezreti njegovega mentorstva številnim diplomantom na vseh stopnjah in različnih programih dodiplomskega in podiplomskega študija. Če se odmisli listo z Zavoda, se je samo na Fakulteti za strojništvo nabralo zajetno številko preko 300 mentorstev. Ena od temeljnih značilnosti njegovega dela s kolegi kot s študenti je bila in ostaja izjemna neposrednost, odprtost in strokovna verodostojnost.

Kar opazen del vsebinsko bogatih in strokovno poglobljenih predavanj je predstavil tudi v izdanih učbenikih: Kontrola brez porušitve in Novejši varilni postopki, oboje Zavod za varjenje, 1959; Varjenje v zaščiti CO_2 (soavtor z Ivanom Limplom), Društvo za varilno tehniko Slovenije, 1971; Točkovno uporovno varjenje (poglavje: Stroji in naprave za uporovno točkovno varjenje), Institut za varilstvo, 1992; Krautov strojniški priročnik (dodano na novo napisano poglavje o varjenju), Littera picta. Kot eden od dveh predstavnikov Jugoslavije (med 30-imi iz celotnega sveta) je sodeloval pri pripravi knjige Physics of welding (je tudi naveden), ki jo je v izdaji Mednarodnega Instituta za varjenje, 1984 založil Pergamon Press.

Na področju znanstvene raziskovalne dejavnosti v mednarodnih okvirih izstopajo njegovi prispevki pri Mednarodnem Institutu za varjenje. Od leta 1959, ko je kot opazovalec prvič sodeloval na 12. letni skupščini IIW-ja, pa do 56. letne skupščine 2001 v Ljubljani, je deloval v domala vseh komisijah kot ekspert, imenovani delegat ali delegat Jugoslavije oz. Slovenije. Bil je član Organizacijskega odbora in član Upravnega odbora v Mednarodnem inštitutu za varjenje in tam predstavil preko 30. znanstvenih dokumentov. Na javni seji 47. letne skupščine Mednarodnega inštituta za varjenje leta 1982 v Ljubljani je sopredsedoval bloku predavanj z naslovom "Value of the new Welding Processes in Respect of Energy, Economy and Technology" in imel sam predavanje z naslovom "Welding and Allied Processes". Za udeležence te Letne skupščine je bil, skupaj s pokojnim doc. dr. Andrejem Grželjem in podpisanima, tudi eden od organizatorjev in vodičev ogleda laboratorijev na Fakulteti za strojništvo.

Znanstvenoraziskovalno delo na Fakulteti za strojništvo je bilo usmerjeno predvsem v temeljne raziskave varjenja v okviru večletnih raziskovalnih projektov, ki so bili financirani s strani Raziskovalne skupnosti Slovenije, oziroma Ministrstva za znanost.

Te raziskave se lahko strne v tri zaokrožene sklope, in sicer: Študij varilnih procesov, njihove dinamike in matematično modeliranje ročnega obločnega varjenja. Študij kinematike paličaste taljive elektrode pri obločnem varjenju in Študij varjenja in navarjanja z dvojno in trojno elektrodo pod praškom in v zaščitnih plinih.

Na tem mestu je nemogoče zajeti vsega njegovega družbenega delovanja. Na Zavodu za varjenje je bil član in predsednik Sveta, ter član Upravnega odbora, Znanstvenega sveta in Odbora za razvoj in raziskave. Na Fakulteti za strojništvo je bil član in predsednik Odbora za znanstveno raziskovalno delo in Odbora za vzgojno-izobraževalno delo, ter član Odbora za koordinacijo v samoupravni interesni skupnosti RSS. V letih 1988 do 1993 je bil predsednik Katedre za tehnologijo materialov med leti 1990 in 1996 vodja Laboratorija za varjenje in med leti 1991 in 1993 prodekan za pedagoško delo.

Pri starosti 65 let, z izpolnjenimi 40 leti delovne dobe, se je septembra 1996, po tedaj veljavnem zakonu upokojil, ohranil pa je stike tako s Fakulteto za strojništvo kot z Institutom za varilstvo. Na Fakulteti za strojništvo je še zmeraj udeležen kot mentor ali somentor v dodiplomskem in podiplomskem študiju, na Institutu za varilstvo pa kot predavatelj na tečajih specialističnega programa IWE/IWT, z mednarodno priznanimi diplomami.

Od leta 1976 je častni član Društva za varilno tehniko Slovenije. Za zasluge pri razvoju varilne tehnike je dobil pisno priznanje Društva za varilno tehniko SR Slovenije, za sodelovanje na strokovnem področju je leta 1984 prejel tudi pisno priznanje Društva za tehniku zavarivanja Hrvatske. Za dolgoletno sodelovanje pri razvoju družine varilnih izvorov mu je bilo podeljeno posebno priznanje s strani Iskre - Industrije za avtomatiko.

Če se znanstveno-raziskovalnemu in izobraževalno vzgojnemu opusu dodajo njegove obče človeške dobrine: široko splošno izobraženost, znanje tujih jezikov (ob tekočem znanju srbohrvaščine in nemščine še znanje ruščine, angleščine in francoščine), poštenost in doslednost pri delu, ugotavljamo, da njegov prispevek (še) ni bil ustrezno umeščen. Vendar: "Tisto kar je vredno, s časom pridobiva na vrednosti, kar ni vredno z vsakim dnem izgublja na svoji vrednosti".

Ob kar visokem življenjskem jubileju, se prijatelji in sodelavci s hvaležnostjo spominjamo slavljenca ter mu želimo predvsem trdnega zdravja, saj za zdravo-razumsko skeptičnost in hkrati optimizem in vedrino zna najbolje poskrbeti kar sam.

prof.dr. Viktor Prosenc
doc.dr. Ivan Polajnar

Doktorata in diplome - Doctor's and Diploma Degrees

DOKTORATA

Na Fakulteti za strojništvo Univerze v Mariboru sta z uspehom zagovarjala svoji doktorski disertaciji:

dne *14. novembra 2006*: **mag. Aleš Belšak**, z naslovom: "Časovno-frekvenčna analiza stanja zobniških gonil";

dne *17. novembra 2006*: **mag. Bojan Vohar**, z naslovom: "Optimizacija manipulatorja z upoštevanjem elastičnih deformacij".

S tem sta navedena kandidata dosegla akademsko stopnjo doktorja znanosti.

DIPLOMIRALI SO

Na Fakulteti za strojništvo Univerze v Ljubljani so pridobili naziv univerzitetni diplomirani inženir strojništva:

dne *23. novembra 2006*: Miha BAZNIK, Gregor GRGIĆ, Uroš TRDAN, Luka ŽAGAR.

*

Na Fakulteti za strojništvo Univerze v Ljubljani so pridobili naziv diplomirani inženir strojništva:

dne *9. novembra 2006*: Matija JEREB, Blaž KOREN, Damjan PIRNAR, Ivan SIMONIČ, Matej ŽEŽE;

dne *10. novembra 2006*: Rajko ARKAR, Tomaž DREMELJ, Aleš KLINAR, Darko ROGELJ, Janez ŠKERL, Rok VOZEL;

dne *13. novembra 2006*: Franc PERKO, Jure RAJŠELJ, Matej STAVANJA, Marko UMEK.

Na Fakulteti za strojništvo Univerze v Mariboru so pridobili naziv diplomirani inženir strojništva:

dne *30. novembra 2006*: Danijel CAJNKO, Bine ČARE, Roland GOMBOŠI, Ermin LUJINOVIĆ, Tomaž OBAD.

Vsebina 2006 - Contents 2006

Navodila avtorjem - Instructions for Authors

Članki morajo vsebovati:
- naslov, povzetek, besedilo članka in podnaslove slik v slovenskem in angleškem jeziku,
- dvojezične preglednice in slike (diagrami, risbe ali fotografije),
- seznam literature in
- podatke o avtorjih.

Strojniški vestnik izhaja od leta 1992 v dveh jezikih, tj. v slovenščini in angleščini, zato je obvezen prevod v angleščino. Obe besedili morata biti strokovno in jezikovno med seboj usklajeni. Članki naj bodo kratki in naj obsegajo približno 8 strani. Izjemoma so strokovni članki, na željo avtorja, lahko tudi samo v slovenščini, vsebovati pa morajo angleški povzetek.

Za članke iz tujine (v primeru, da so vsi avtorji tujci) morajo prevod v slovenščino priskrbeti avtorji. Prevajanje lahko proti plačilu organizira uredništvo. Če je članek ocenjen kot znanstveni, je lahko objavljen tudi samo v angleščini s slovenskim povzetkom, ki ga pripravi uredništvo.

Papers submitted for publication should comprise:
- Title, Abstract, Main Body of Text and Figure Captions in Slovene and English,
- Bilingual Tables and Figures (graphs, drawings or photographs),
- List of references and
- Information about the authors.

Since 1992, the Journal of Mechanical Engineering has been published bilingually, in Slovenian and English. The two texts must be compatible both in terms of technical content and language. Papers should be as short as possible and should on average comprise 8 pages. In exceptional cases, at the request of the authors, speciality papers may be written only in Slovene, but must include an English abstract.

For papers from abroad (in case that none of authors is Slovene) authors should provide Slovenian translation. Translation could be organised by editorial, but the authors have to pay for it. If the paper is reviewed as scientific, it can be published only in English language with Slovenian abstract, that is prepared by the editorial board.

VSEBINA ČLANKA

Članek naj bo napisan v naslednji obliki:
- Naslov, ki primerno opisuje vsebino članka.
- Povzetek, ki naj bo skrajšana oblika članka in naj ne presega 250 besed. Povzetek mora vsebovati osnove, jedro in cilje raziskave, uporabljeno metodologijo dela,povzetek rezulatov in osnovne sklepe.
- Uvod, v katerem naj bo pregled novejšega stanja in zadostne informacije za razumevanje ter pregled rezultatov dela, predstavljenih v članku.
- Teorija.
- Eksperimentalni del, ki naj vsebuje podatke o postavitvi preskusa in metode, uporabljene pri pridobitvi rezultatov.
- Rezultati, ki naj bodo jasno prikazani, po potrebi v obliki slik in preglednic.
- Razprava, v kateri naj bodo prikazane povezave in posplošitve, uporabljene za pridobitev rezultatov. Prikazana naj bo tudi pomembnost rezultatov in primerjava s poprej objavljenimi deli. (Zaradi narave posameznih raziskav so lahko rezultati in razprava, za jasnost in preprostejše bralčevo razumevanje, združeni v eno poglavje.)
- Sklepi, v katerih naj bo prikazan en ali več sklepov, ki izhajajo iz rezultatov in razprave.
- Literatura, ki mora biti v besedilu oštevilčena zaporedno in označena z oglatimi oklepaji [1] ter na koncu članka zbrana v seznamu literature. Vse opombe naj bodo označene z uporabo dvignjene številke[1].

THE FORMAT OF THE PAPER

The paper should be written in the following format:
- A Title, which adequately describes the content of the paper.
- An Abstract, which should be viewed as a mini version of the paper and should not exceed 250 words. The Abstract should state the principal objectives and the scope of the investigation, the methodology employed, summarize the results and state the principal conclusions.
- An Introduction, which should provide a review of recent literature and sufficient background information to allow the results of the paper to be understood and evaluated.
- A Theory
- An Experimental section, which should provide details of the experimental set-up and the methods used for obtaining the results.
- A Results section, which should clearly and concisely present the data using figures and tables where appropriate.
- A Discussion section, which should describe the relationships and generalisations shown by the results and discuss the significance of the results making comparisons with previously published work. (Because of the nature of some studies it may be appropriate to combine the Results and Discussion sections into a single section to improve the clarity and make it easier for the reader.)
- Conclusions, which should present one or more conclusions that have been drawn from the results and subsequent discussion.
- References, which must be numbered consecutively in the text using square brackets [1] and collected together in a reference list at the end of the paper. Any footnotes should be indicated by the use of a superscript[1].

OBLIKA ČLANKA

Besedilo članka naj bo pripravljeno v urejevalnilku Microsoft Word. Članek nam dostavite v elektronski obliki.

Ne uporabljajte urejevalnika LaTeX, saj program, s katerim pripravljamo Strojniški vestnik, ne uporablja njegovega formata.

Enačbe naj bodo v besedilu postavljene v ločene vrstice in na desnem robu označene s tekočo številko v okroglih oklepajih

THE LAYOUT OF THE TEXT

Texts should be written in Microsoft Word format. Paper must be submitted in electronic version.

Do not use a LaTeX text editor, since this is not compatible with the publishing procedure of the Journal of Mechanical Engineering.

Equations should be on a separate line in the main body of the text and marked on the right-hand side of the page with numbers in round brackets.

Enote in okrajšave

V besedilu, preglednicah in slikah uporabljajte le standardne označbe in okrajšave SI. Simbole fizikalnih veličin v besedilu pišite poševno (kurzivno), (npr. *v, T, n* itn.). Simbole enot, ki sestojijo iz črk, pa pokončno (npr. ms^{-1}, K, min, mm itn.).

Vse okrajšave naj bodo, ko se prvič pojavijo, napisane v celoti v **slovenskem jeziku**, npr. časovno spremenljiva geometrija (ČSG).

Slike

Slike morajo biti zaporedno oštevilčene in označene, v besedilu in podnaslovu, kot sl. 1, sl. 2 itn. Posnete naj bodo v ločljivosti, primerni za tisk, v kateremkoli od razširjenih formatov, npr. BMP, JPG, GIF. Diagrami in risbe morajo biti pripravljeni v vektorskem formatu.

Pri označevanju osi v diagramih, kadar je le mogoče, uporabite označbe veličin (npr. *t, v, m* itn.), da ni potrebno dvojezično označevanje. V diagramih z več krivuljami, mora biti vsaka krivulja označena. Pomen oznake mora biti pojasnjen v podnapisu slike.

Vse označbe na slikah morajo biti dvojezične.

Preglednice

Preglednice morajo biti zaporedno oštevilčene in označene, v besedilu in podnaslovu, kot preglednica 1, preglednica 2 itn. V preglednicah ne uporabljajte izpisanih imen veličin, ampak samo ustrezne simbole, da se izognemo dvojezični podvojitvi imen. K fizikalnim veličinam, npr. *t* (pisano poševno), pripišite enote (pisano pokončno) v novo vrsto brez oklepajev.

Vsi podnaslovi preglednic morajo biti dvojezični.

Seznam literature

Vsa literatura mora biti navedena v seznamu na koncu članka v prikazani obliki po vrsti za revije, zbornike in knjige:

[1] A. Wagner, I. Bajsić, M. Fajdiga (2004) Measurement of the surface-temperature field in a fog lamp using resistance-based temperature detectors, *Stroj. vestn.* 2(2004), pp. 72-79.

[2] Vesenjak, M., Ren Z. (2003) Dinamična simulacija deformiranja cestne varnostne ograje pri naletu vozila. *Kuhljevi dnevi '03*, Zreče, 25.-26. september 2003.

[3] Muhs, D. et al. (2003) Roloff/Matek Maschinenelemente – Tabellen, 16. Auflage. *Vieweg Verlag*, Wiesbaden.

Podatki o avtorjih

Članku priložite tudi podatke o avtorjih: imena, nazive, popolne poštne naslove in naslove elektronske pošte.

SPREJEM ČLANKOV IN AVTORSKE PRAVICE

Uredništvo Strojniškega vestnika si pridržuje pravico do odločanja o sprejemu članka za objavo, strokovno oceno recenzentov in morebitnem predlogu za krajšanje ali izpopolnitev ter terminološke in jezikovne korekture.

Avtor mora predložiti pisno izjavo, da je besedilo njegovo izvirno delo in ni bilo v dani obliki še nikjer objavljeno. Z objavo preidejo avtorske pravice na Strojniški vestnik. Pri morebitnih kasnejših objavah mora biti SV naveden kot vir.

Units and abbreviations

Only standard SI symbols and abbreviations should be used in the text, tables and figures. Symbols for physical quantities in the text should be written in italics (e.g. *v, T, n,* etc.). Symbols for units that consist of letters should be in plain text (e.g. ms^{-1}, K, min, mm, etc.).

All abbreviations should be spelt out in full on first appearance, e.g., variable time geometry (VTG).

Figures

Figures must be cited in consecutive numerical order in the text and referred to in both the text and the caption as Fig. 1, Fig. 2, etc. Pictures may be saved in resolution good enough for printing in any common format, e.g. BMP, GIF, JPG. However, graphs and line drawings sholud be prepared as vector images.

When labelling axes, physical quantities, e.g. *t, v, m,* etc. should be used whenever possible to minimise the need to label the axes in two languages. Multi-curve graphs should have individual curves marked with a symbol, the meaning of the symbol should be explained in the figure caption.

All figure captions must be bilingual.

Tables

Tables must be cited in consecutive numerical order in the text and referred to in both the text and the caption as Table 1, Table 2, etc. The use of names for quantities in tables should be avoided if possible: corresponding symbols are preferred to minimise the need to use both Slovenian and English names. In addition to the physical quantity, e.g. *t* (in italics), units (normal text), should be added in new line without brackets.

All table captions must be bilingual.

The list of references

References should be collected at the end of the paper in the following styles for journals, proceedings and books, respectively:

[1] A. Wagner, I. Bajsić, M. Fajdiga (2004) Measurement of the surface-temperature field in a fog lamp using resistance-based temperature detectors, *Stroj. vestn.* 2(2004), pp. 72-79.

[2] Vesenjak, M., Ren Z. (2003) Dinamična simulacija deformiranja cestne varnostne ograje pri naletu vozila. *Kuhljevi dnevi '03*, Zreče, 25.-26. september 2003.

[3] Muhs, D. et al. (2003) Roloff/Matek Maschinenelemente – Tabellen, 16. Auflage. *Vieweg Verlag*, Wiesbaden.

Author information

The information about the authors should be enclosed with the paper: names, complete postal and e-mail addresses.

ACCEPTANCE OF PAPERS AND COPYRIGHT

The Editorial Committee of the Journal of Mechanical Engineering reserves the right to decide whether a paper is acceptable for publication, obtain professional reviews for submitted papers, and if necessary, require changes to the content, length or language.

Authors must also enclose a written statement that the paper is original unpublished work, and not under consideration for publication elsewhere. On publication, copyright for the paper shall pass to the Journal of Mechanical Engineering. The JME must be stated as a source in all later publications.